Context Aware Body Regulation of Redundant Robots

Von der
Carl-Friedrich-Gauß-Fakultät
der Technischen Universität Carolo-Wilhelmina zu Braunschweig

zur Erlangung des Grades eines

Doktoringenieurs (Dr.-Ing.)

genehmigte Dissertation

von
Pouya Mohammadi
geboren am 12.11.1983
in Ghom, Iran

Eingereicht am: 22. Oktober 2019
Disputation am: 19. Dezember 2019
1. Referent: Prof. Dr. Jochen Steil
2. Referent: Prof. Dr. Darwin Caldwell

2019

Abstract

The past few decades have seen a new trend in robotics towards more complex hardware systems: The classical six degrees of freedom manipulators' dominance has been challenged by the rise of seven degrees of freedom redundant robots. Similarly, with increased availability of humanoid robots in academic research, roboticists have gained access to highly dexterous platforms with multiple kinematic chains capable of undertaking multiple tasks simultaneously. The execution of lower-priority tasks, however, are often done in task/scenario specific fashion. Consequently, these systems are not scalable and slight changes in the application often implies re-engineering the entire control system and deployment which impedes the development process over time.

This thesis introduces an alternative systematic method of addressing the secondary tasks and redundancy resolution called, *context aware body regulation*. *Contexts* consist of one or multiple tasks, however, unlike the conventional definitions, the tasks within a context are not rigidly defined and maintain some level of abstraction. For instance, following a particular trajectory constitutes a concrete task while performing a Cartesian motion with the end-effector represents an abstraction of the same task and is more appropriate for context formulation. Furthermore, contexts are often made up of multiple abstract tasks that collectively describe a reoccurring situation. *Body regulation* is an umbrella term for a collection of schemes for addressing the robots' redundancy when a particular context occurs. These schemes include impedance adaptation, postural regulation, joint space redundancy resolution, contact exploitation, etc.

By adhering to task abstractions, modularity and separation of concerns principle, context aware body regulation offers several advantages over traditional methods. Most notably among them are reusability, scalability and composability of contexts and body regulation schemes. These three fundamental concerns are realized by in-depth study and thorough mathematical analysis of contexts and regulation strategies; and are practically implemented by a component based software architecture that complements the theoretical aspects. Real world robotic experiments empirically validate the proposed approach with state of the art humanoid platforms, redundant manipulators and in user studies.

The thesis studies four contexts and several respective body regulations. Their selection is motivated by two considerations. Firstly, these contexts present real applications and frequently occurring situations. Secondly, they reveal important aspects and implications of the proposed paradigm of context aware body regulation. The implementations likewise, demonstrate reusability, scalability and composability of contexts and body regulations when formulated at proper level.

The findings of the thesis are applicable to any redundant manipulator and humanoid, and allow them to be used in real world applications. The proposed methodology presents an alternative approach for the control of robots and offers a new perspective for future deployment of robotic solutions.

Zusammenfassung

In den letzten Jahrzehnten gab es einen neuen Trend in der Robotik hin zu immer komplexeren Systemen: Klassische Roboterarme mit sechs Freiheitsgraden weichen zunehmend den neuen und flexibleren Manipulatoren mit sieben Gelenken. Ebenso stehen der Forschung mit den neuartigen Humanoiden inzwischen auch hoch-redundante Roboterplattformen mit mehreren kinematischen Ketten zur Verfügung. Diese überaus flexiblen und komplexen Roboter-Kinematiken ermöglichen generell das gleichzeitige Verfolgen mehrerer priorisierter Bewegungsaufgaben. Die Steuerung der weniger wichtigen Aufgaben erfolgt jedoch oft anwendungsspezifisch, was die Skalierung hin zu generellen Kontexten erschwert. Selbst kleine Änderungen in der Anwendung bewirken oft schon, dass große Teile der Robotersteuerung überarbeitet werden müssen, was wiederum den gesamten Entwicklungsprozess behindert.

Diese Dissertation stellt eine alternative, systematische Methode vor um die Redundanz neuer komplexer Robotersysteme zu bewältigen und vielfältige, priorisierte Bewegungsaufgaben parallel zu steuern: Die so genannte *Kontextsensitive Körperregulierung*. Darin bestehen *Kontexte* aus einer oder mehreren Bewegungsaufgaben. Anders als in konventionellen Anwendungen sind die Aufgaben nicht fest definiert und beinhalten eine gewisse Abstraktion. Beispielsweise stellt das Folgen einer bestimmten Trajektorie eine sehr konkrete Bewegungsaufgabe dar, während die Ausführung einer Kartesischen Bewegung mit dem Endeffektor eine Abstraktion darstellt und damit für die Kontextformulierung besser geeignet ist. Kontexte setzen sich oft aus mehreren solcher abstrakten Aufgaben zusammen und beschreiben kollektiv eine sich wiederholende Situation. Die vorgestellte *Körperregulierung* umfasst eine Sammlung von Schemata, welche die kinematische Redundanz adressieren, wenn ein bestimmter Kontext auftritt. Dazu gehören Impedanz-Adaptierung, Haltungs-Regelung, Redundanzauflösung im Gelenkwinkelraum, Ausnutzen von Kontakten und viele mehr.

Die Kontextsensitive Körperregulierung verwendet unter anderem Aufgabenabstraktion, -modularität und das Prinzip der verteilten Verantwortlichkeit. Dadurch ergeben sich vielfältige Vorteile gegenüber traditionellen Methoden: Wiederverwendbarkeit, Skalierbarkeit, sowie Komponierbarkeit von Konzepten. Diese drei fundamentalen Eigenschaften werden in der vorliegenden Arbeit theoretisch mittels gründlicher mathematischer Analyse aufgezeigt und praktisch mittels einer auf Komponenten basierenden Softwarearchitektur realisiert. Empirische Experimente mit modernen, redundanten Manipulatoren und Humanoiden validieren den vorgeschlagenen Ansatz in Benutzerstudien.

Beispielhaft werden dazu in dieser Dissertation konkret vier Kontexte und mehrere Körperregulierungen behandelt. Die Auswahl ist durch zwei wesentliche Beobachtungen motiviert: Erstens präsentieren diese Konzepte reale Anwendungen und sich regelmäßig

wiederholende Situationen. Und zweitens offenbaren diese Konzepte wichtige Aspekte und Implikationen des vorgestellten Paradigmas. Entsprechend demonstrieren die konkreten Implementierungen auf grundlegende Weise Wiederverwendbarkeit, Skalierbarkeit und Komponierbarkeit von Konzepten.

Die Ergebnisse dieser Dissertation lassen sich auf beliebige redundante Manipulatoren oder Humanoide Roboter anwenden und befähigen diese damit zu Anwendungen in realen Umgebungen außerhalb des Labors. Die hier vorgestellte Methode zur Regelung von Robotern stellt damit eine neue Perspektive für die zukünftige Entwicklung von robotischen Lösungen dar.

Acknowledgment

I genuinely consider myself lucky and privileged to have the nicest and finest people surrounding me in my professional and personal circles.

First and foremost, I am most grateful to Prof. Dr. Jochen Steil, my supervisor, who has not only been an exceptional teacher and professor but also a great mentor. His leadership has been instrumental in carrying out my work and his personal motto of "do good science" has guided me in conducting my research. Likewise, I should thank all my professors in Italy and Iran who built the foundation. I shall remain in debt to all of you.

I also have to acknowledge my co-authors for their helps in conducting the research and publishing the papers that back this thesis. Engaging with these excellent colleagues *and* friends, I have learned a lot. I look forward working with you again.

I would like to mention the nameless individual who contribute to open source projects as well. Those who write and edit Wikipedia articles; those who publish their code without any expectation; those who develop finest pieces of software, without which, this thesis would have remained a concept only. You are the pioneers of open knowledge sharing and I salute you.

Last but most certainly not least, my most sincere gratitude goes to my family. My father Hamidreza, my mother Soraya, my sister Parisa, my brothers Babak and Mohammad, and of course my friend, partner, and amazing wife Michela Manetti. Your patience, your support, your kindness and your love has always had my back. You are the reason for everything I was able to do and achieve. Thank you all.

October 21, 2019
Pouya Mohammadi

Contents

List of Figures

List of Tables

List of Acronyms and Abbreviations

Notation	Description
BR	Body Regulation
CA	Context Aware
CABR	Context Aware Body Regulation
CBSE	Component-Based Software Engineering
CoM	Center of Mass
DoF	Degrees of Freedom
EE	End-Effector
HAL	Hardware Abstraction Layer
IDDP	Intra Domain Datagram Protocol
iHQP	Inequality Hierarchical Quadratic Programming
LKC	Lower Kinematic Chain
LWR	Light Weight Robot
NRT	Non Real-Time
OCL	Orocos Component Library
pHRI	Physical Human Robot Interaction
QP	Quadratic Programming
RSB	Robotics Service Bus
RT	Real-Time
RTT	Real-Time-Toolkit
SoT	Stack of Tasks
SRDF	Semantic Robot Description Format
SVD	Singular Value Decomposition
UKC	Upper Kinematic Chain
URDF	Unified Robot Description Format
VR	Virtual Reality
w.r.t.	With Respect To
WPG	Walking Pattern Generator
ZMP	Zero Moment Point

Symbols, conventions and nomenclature

Description	**Example**
Matrices are shown in upright boldface roman	$\mathbf{J}$
Vectors are presented in italic boldface	$\boldsymbol{q}$
Scalars are in italic	α
Normalized vectors and matrices dented with $\hat{}$	$\hat{\boldsymbol{n}}$
A '$\bullet$' denotes anonymous, any, or for all values	see below
Dot product $\langle , \rangle$	$\langle \bullet, \bullet \rangle$
Cross product ($\times$)	$(\bullet \times \bullet)$
Related to upper/lower kinematic chains with under/over bars	$\underline{\boldsymbol{\tau}} / \bar{\boldsymbol{\tau}}$
An asterisk superscript denotes 'desired'	$\dot{\boldsymbol{x}}^*$
The symbol '+' in a superscript stands for the pseudo-inverse	$\mathbf{J}^+$
Tasks with upright T	$\mathrm{T}_i \coloneqq [\![\mathbf{J}_i, \dot{\boldsymbol{x}}_i]\!]$
Constraints with upright C	$\mathrm{C}_i \coloneqq [\![\mathbf{A}_i, \boldsymbol{b}_i]\!]$
Slanted superscript $\bullet^T$ is the transpose	$\boldsymbol{q} = [0, 0, 0]^T$
Equations are referred to by parentheses	(2.28)
Figures, tables, chapters, and sections without brackets	figure 2.2

1 Introduction

In the last couple of decades a new trend in robotic research has emerged. The classical 6-Degrees of Freedom (DoF) articulated arms' dominance has been challenged by the rise of 7-DoF redundant robots. Although this movement was initially occurring in academia, with the advent of physical human robot interaction, even the industry sector has started to adopt the new technology.

This paradigm shift is not only influenced by the number of degrees of freedom. The new robots are often light-weighted and equipped with accurate force/torque sensors that are integrated in their actuators, allowing them to interact with their environment or the human counterparts[1]. The Physical Human Robot Interaction (pHRI) field has been made possible thanks to these advancements in the design and production of light-weight, torque controlled redundant robots, alongside advances in software engineering and control.

Similarly, the humanoid robotics community was involved in advancing the state of the art of bipedal platforms. Research groups and companies have been developing a diverse range of humanoids and making significant progress over several decades. Special to this thesis is the COMAN family of robots by the Italian Institute of Technology which has gone through many iterations and upgrades resulting in COMAN+ (see figure 1.1c).

The evolution of robotic research towards redundant robots has created new challenges and raised new research questions: A 7-DoF manipulator can position and orient its End-Effector (EE) at any point in its reachable workspace in infinite configurations. In general, for an n-DoF robot performing an m-dimensional task, where $n > m$, there are $\infty^{(n-m)}$ ways to perform the designated task. This property can be exploited to achieve secondary objectives while performing the primary task. For instance, minimum effort solution among the infinite number of possible solutions minimizes the overall actuator torques and energy expenditure. Alternatively, it is possible to use the redundancy to avoid obstacles or to aim for other criteria.

Similar questions need to be addressed for humanoids, however, at a much higher level of complexity. A humanoid with multiple kinematic chains (e.g., arms, legs, waist, neck) can undertake multiple tasks simultaneously. Consequently, the range of possible strategies to exploit the redundancy is wider and oftentimes tertiary, quaternary and even more objectives have to be considered. Addressing the lower order tasks in humanoids not only includes all the standard manipulator approaches, but also many notions that

[1] In this work humans are not considered as part of "the surrounding environment". The main reason for this distinction is that interacting with humans and the environment demands vastly different considerations and delicacies, most notably the safety and the margin of tolerance in case of critical errors.

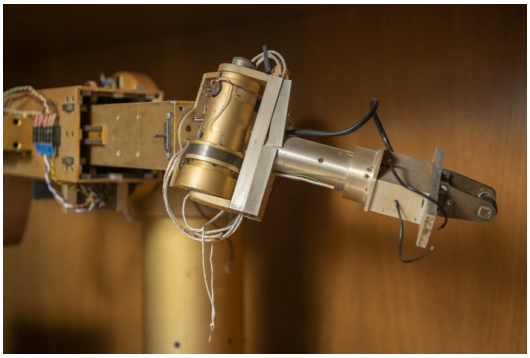

(a) Stanford arm

(b) Kuka LWR-4+

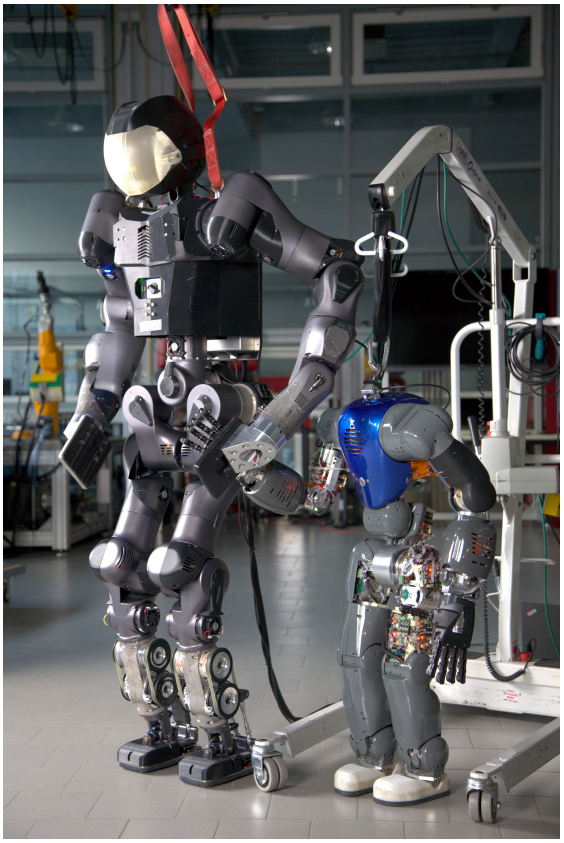

(c) COMAN+ and COMAN

Figure 1.1: From the prototypic Stanford arm (a) to light weighted redundant Kuka LWR-4+ (b) and to the state of the art humanoids COMAN+ (c-left) and COMAN (c-right), the trend in modern era of robotics points towards redundant, compliant and torque controlled robots that are capable of interacting with the environment and human counterparts while performing multiple tasks.

are specific to legged floating-base platforms, some of which rather hard to quantify (e.g., human-likeness).

Different strategies and approaches to exploit the redundancy of the robots are gathered under the umbrella term Body Regulation (BR) in this thesis. The common way of performing body regulation is usually application and task specific. That is, given a specific robot designated for a specific task, the BR is conducted based on such a task considering the characteristics of the given robot. The first issue with this approach is its scalability: the handling of secondary tasks has to be done from the scratch, should the application change slightly or the platform replaced. Furthermore, since the body regulation is tailored to a specific situation it cannot be reused in different scenarios, which in turn increases the development time and cost.

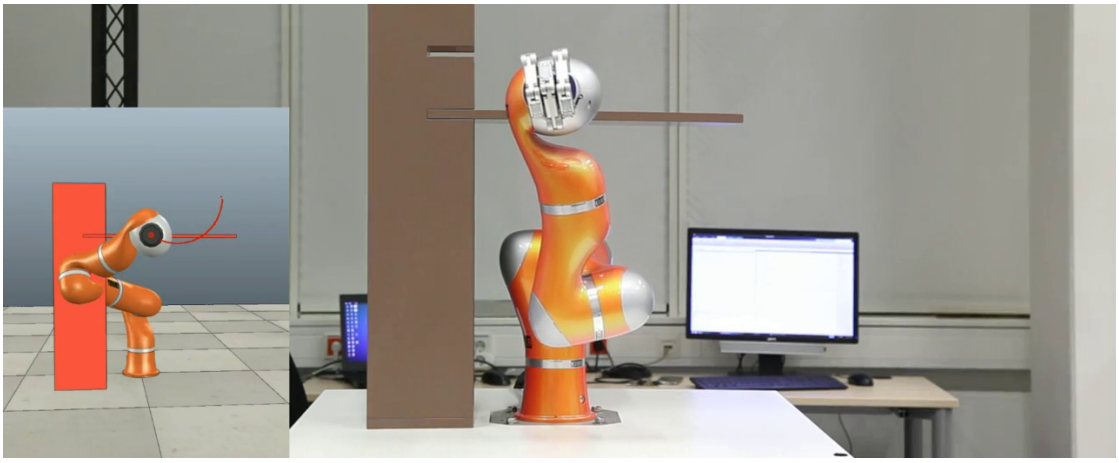

Figure 1.2: *Critical Handling* of redundancy of the robot. Without suitable body reconfiguration the execution of the task is impossible due to collision with the vertical stand as shown in the simulated frame. Note that both the robot and simulation perform the same end-effector task starting from identical configurations.

As the current trends in robotics strongly favor redundant robots and humanoids with capabilities to interact with the environment and human counterparts, the classical mindset of (lack of systematic) body regulation can no longer serve the needs of roboticists. The ability to achieve secondary objectives offers vast potential and tapping into suitable body regulation allows roboticists and system designers to achieve goals that are impossible, or intimidatingly difficult otherwise. Additionally, improper administration of body regulation could potentially jeopardize the execution of primary tasks.

1.1 Secondary Tasks Have Primary Significance

While working with a humanoid or another redundant robot, three situations arise frequently when the roboticists attempt to handle the redundancy:

1. **Critical Handling:** address the most critical situation such as collision avoidance. This is often the case when the robot offers only one degree of redundancy.

2. **Null Handling:** not address the redundancy. In this case the robot assumes a particular configuration depending on the setup and/or implementation.

3. **Adaptive Handling:** orchestrate and coordinate the execution of multiple different secondary task. This class occurs often when dealing with humanoids. It contrasts the *Critical Handling* in that there is a certain freedom and adaptivity to control the redundancy.

Critical Handling of redundancy for body regulation is often —but not always— about collision avoidance. In figure 1.2 for instance, the robot is reconfigured in order to avoid

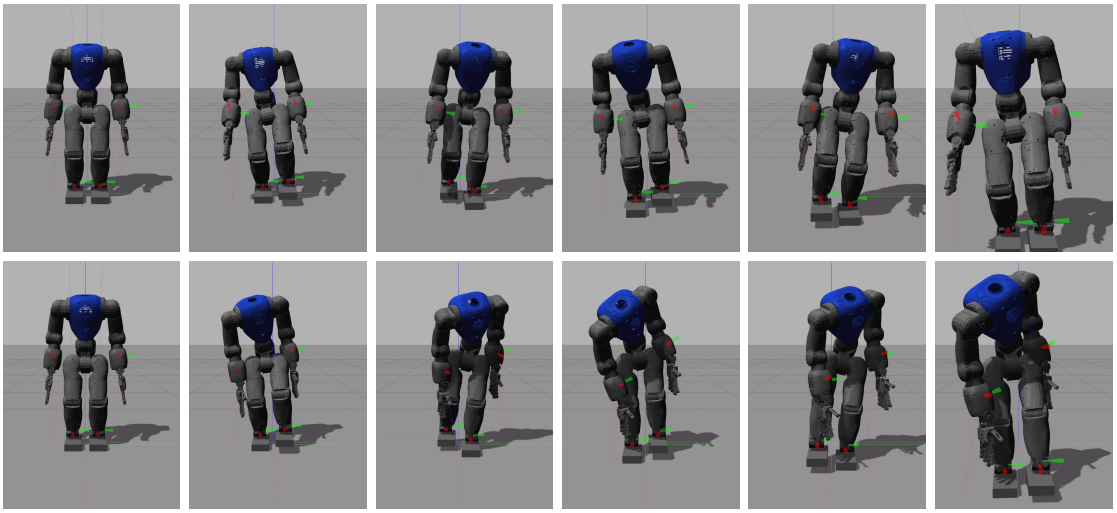

Figure 1.3: *Null Handling* of redundancy: Sequence of a simple implementation of steps with naive joint space redundancy resolution for the waist is shown at the top row. Bottom: the same walking implementation without any body regulation.

collision with the vertical bar and consequently finishes the task. Another case where resolving the redundancy becomes critical, is when actuators' velocity capacities are insufficient to undertake the task. Through body regulation, it is possible to assume a configuration with better joint-space to task-space velocity transmission factors. Alternatively, the transmission ratios between the joint space torques and end-effector wrenches can be considered as the body regulation metric. These cases are extensively studied in the upcoming chapters. At first glance, it might seem that these situations, due to their forced nature that often requires a single form of body regulation, cannot benefit from the context aware body regulation methodology. However, even if there is only one way to regulate the body, there are still good reasons to consider a more systematic process of body regulation.

Opting for *Null Handling* makes the system susceptible to overlooked mathematical subtleties, scenario parameterization, numerical errors or perhaps an unhealthy mixture thereof. Sometimes it is easy to identify or predict the impact of these factors. Nevertheless, there are cases where these inconspicuous factors result in robot behaviors that are unwanted, unexpected or detrimental to the execution of the main task. Figure 1.3 depicts an example of the effects of such factors where the robot performs a sequence of simple steps. Note the unnatural body posture as a consequence of leaving the redundancy unhandled. This case is discussed in more detail later in section 4.2. This example shows that consequences of *Null Handling* could be unexpected. In general, leaving the redundancy uncontrolled should almost always be avoided, with very few exceptions (e.g., extremely limited computational resources) and even in those exceptional situations, the behavior of the robot should be predictable and known in advance.

Adaptive Handling is the most frequent case and appears often in two situations. In the first case, there is no critical demand for body regulation and the primary task can be achieved regardless. The redundancy is resolved by body regulation schemes that best serves the task, or by assigning a neutral joint space configuration. In the second case, the target platform offers several degrees or forms of redundancy, hence, the developers have multiple options for their choice of body regulation and depending on the nature of the primary task (e.g., walking) one or more BR among the possibilities is (are) adopted. In the latter case, however, it is necessary to orchestrate the collaboration and coordination of multiple secondary or tertiary tasks. Usually humanoids fall in the second category.

Despite their names, secondary or lower priority tasks are sometimes equally important and must be handled with care. Leaving the redundancies of a robot uncontrolled, or governing them without rigorous attention to details, at best results in unnatural or unwanted motions and at worst could completely jeopardizes the execution of the primary task. The dire consequences of improper handling of the redundancies, alongside the shortcomings of traditional methods call for a novel and systematic approach for body regulation of humanoids and redundant robots.

1.2 Context Aware Body Regulation

In computer science, *context awareness* is the notion that machines should sense and act based on the environment or the context they are functioning within, and adapt their behavior accordingly [1]. This concept was originally introduced in mobile communication and defined criteria for a context aware agent, i.e., a context aware agent should be able to react based on the location of use, the nearby users, host and accessible devices. While the term context awareness has entered other disciplines, it is mostly present in computer science and its fields such as network engineering, satellite communication, etc.

Despite the fact that robots are capable of *sensing* and *acting* (even more so than computers in the literal meaning of those two words), the context awareness in robotics has been barely touched. Location awareness, which complements context awareness, is mentioned in [2]. In [3], the robots are considered in a context aware system, however, in that work context awareness is defined in the classical computer science domain and robots are merely actors (agents). This thesis, similarly, does not try to implement context awareness to the full extent of the original definition. Instead, it borrows the term and the idea of context awareness —rather loosely— from computer science to serve its needs.

In this thesis, contexts refer to common and reoccurring situations, and are formed by one or multiple tasks defined at suitable abstraction levels. This notion can be conveyed through an example: following a trajectory with the tip of the right arm is a rigidly defined task. Following a geometric path (without any timing law) with the EE of the right arm is a less concrete definition of the first task. Performing a Cartesian task with the end-effector of a kinematic chain is an abstraction of the task. The level of abstraction in this formulation is dictated by the desired range of applicability of the context to different scenarios. That is to say, contexts should present and be applicable to reoccurring

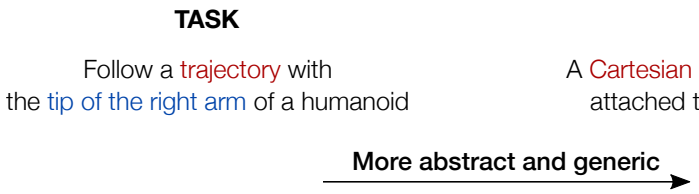

Figure 1.4: Context are more abstract, generalized concepts that present concrete tasks. Moving towards a less rigid definition of a task facilitates reusability of body regulations.

situations and the level of abstraction of constituting tasks control this property. Ideally, a context should represent multiple applications of similar nature. A humanoid standing still while maintaining its dynamic balance and performing Cartesian tasks with its kinematic chains, is an example of a context that adheres to these conditions. In terms of applicability, this illustrative context presents scenarios/situations like throwing an object, a hammering task, single/bi-manual manipulation, etc. Note that the context mentions "Cartesian task" with no specificity towards torque or velocity control (cf. figure 1.4).

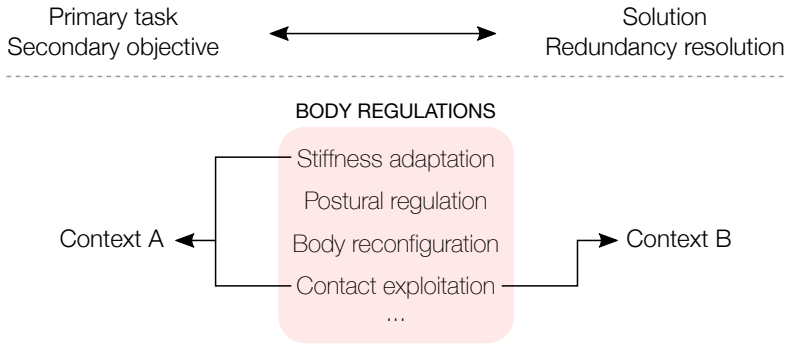

Figure 1.5: In the common way of solving the 'primary task'/'secondary tasks', the 'solution'/'redundancy resolution' often have a 1-to-1 relationship (top). On the contrary, context aware body regulation offers an n-to-n (n can be 1 as well) alternative, thanks to the abstract definition of context and reusability of body regulations.

Body regulation is a collective term for different schemes (see figure 1.5) to handle the redundancy when a particular context arises. A non-exhaustive list includes schemes such as body reconfiguration for different cost functions, stiffness adaptation, contact exploitation, joint space redundancy resolution, etc. Body regulation not only should take into account the tasks within the context, but it also should consider the synergies among the tasks, hardware specifications, and possibly more contributing factors. In the previous example, a possible BR scheme for the context is a generic stack of tasks with robot and context specific constraints, which accepts a variety of desired Cartesian inputs for the kinematic chains. Such stacks of tasks, are internally composed of other more specific body regulation schemes for kinematic chains or for the whole body.

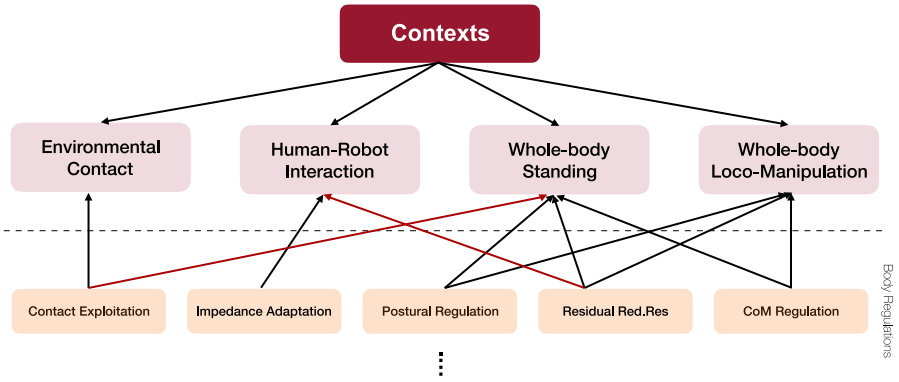

Figure 1.6: Exemplary contexts and body regulations: each of these contexts embody multiple potential applications and tasks. Different body regulations forming a catalog, can be applied to different contexts. Note that ideally it should be possible to treat individual kinematic chains of a kinematic tree (e.g., the arms of a humanoid) as a whole robot. For instance, contact exploitation or residual redundancy resolution should be applicable to a whole robot, or to a sequence of joints regarded as a robot (red arrows). This concern is resolved by "kinematic chain abstraction" concept and is detailed throughout the thesis.

Context aware body regulation consists of three major steps;

1. **Context identification:** Contexts should be formalized over different domains and at different operational levels. Overtime, they construct a catalogue of different contexts that robotic platforms will face in diverse scenarios (cf. figure 1.6).

2. **Body regulation planning:** In parallel, suitable body regulation schemes should be derived and planned. Similar to the context, they form a directory of body regulations. Note that contexts and body regulations do not form a one-to-one relationship. Instead, a particular BR scheme can be applicable to multiple contexts and a context can benefit from multiple body regulations simultaneously.

3. **Execution and deployment:** More geared towards software engineering, this step imposes requirements for which the context aware body regulation should be implemented, deployed and executed. This crucial step is an attempt to distance the proposed paradigm from the tailored approaches towards a more methodical, systematic and scalable scheme at the implementation level.

The three stages of Context Aware Body Regulation (CABR) are tightly interconnected and complementary to each other. That is, how a context is defined directly impacts the body regulation strategy and its deployment. Hence the granularity level of context identification is paramount to all other steps and to the applicability of the method as a whole. Defining the "correct" granularity level is complicated and in many disciplines has remained a topic of debate. Therefore, rather than seeking the answer to the granularity level question, discussed contexts are selected at different granularity levels which highlight some features and nuances of the body regulation in the bigger picture.

1.3 Contribution, Scope and Outline

This these makes multiple contributions. Firstly, it puts forward the notion of contexts in terms of abstract tasks and analyzes them in the scope of realistic reoccurring robotic situations. Secondly, several body regulations for the introduced contexts are studied, analyzed and derived, and in the process new findings are revealed. The derived body regulations, furthermore, are not only applicable to other contexts beyond those discussed in the thesis, but they are also useful outside the context aware body regulation approach. These contexts and regulation schemes are discussed in the scope of real world applications with theoretical and empirical contributions. Additionally, by adhering to context abstractions, and by following principles of modularity and separation of concerns in deriving body regulation schemes, CABR offers several key features that make robotic systems more robust and facilitate the development process. This thesis is an effort in addressing different aspects of the proposed paradigm and revealing its features in a reasonable scope that includes multiple contexts, body regulations, and robotic platforms. From a larger perspective, the thesis endorses a methodical alternative to the traditional techniques of addressing the robots' redundancy. Furthermore, this thesis contributes to and benefits from an accompanying component based software architecture that practically implements these theoretical aspects.

To achieve its goals, this thesis studies four contexts. Starting from a simple setup in chapter 2, the first context looks at the case where the robot is in contact with the environment and is exerting some end-effector wrenches. Accordingly, the reaction forces from the environment are applied to the robot and get dissipated through its body. This state in which the robot and the environment are in contact and exchanging forces while remaining in static equilibrium outlines the first context. A candidate BR for this context is to exploit a second contact so that part of the reaction forces is absorbed through the second contact point, thus, the overall required actuator torques are reduced. This context also demonstrates that seemingly simple situations could have unexpected hidden implications which body regulation studies can reveal.

Chapter 3 contains the second context aware body regulation case. Here the robot is interacting with a human counterpart in one of the most common situations in pHRI, i.e., co-manipulation and kinesthetic guidance. Considering human factors such as ergonomy, the body regulation materializes as impedance adaptation to improve the overall human comfort. This case is selected to demonstrate that human factors could be one of the relevant aspects of context aware body regulation. Furthermore, it exhibits the applicability of body regulations among different contexts.

Scaling up from manipulators to humanoids, chapter 4 investigates the body regulation of humanoids. The analysis are conducted in the scope of a whole-body context where the humanoid stands still but performs multiple tasks with its kinematic chains (this is indeed the previously noted example). Similar to the previous cases, this context is chosen to highlight some characteristics of the humanoids body regulation. Firstly, it illustrate the tight relationship between CABR and the stack of tasks scheme. Secondly,

and perhaps more importantly, it shed some light on several desirable properties of context aware body regulation.

The body regulation for a humanoid's whole-body is a multi-objective practice. There is the overall posture that contributes to human-likeness of the motion. At the same time, controlling the robot's posture should not impede the execution of other tasks, rather, a composed BR scheme contributes to the task execution. Furthermore, same regulation approaches can be reused. Kinematically (in topology, not dimension), the COMAN's arm is not different from a Kuka LWR-4+, hence, the ability to reuse one's body regulation for the other is both reasonable and desirable.

Developing reliable and robust robotic solutions demands scarce resources such as development time, expert knowledge, financial means and a wide variety of assets. Context aware body regulation is an attempt to mediate some of these challenges, however, without proper implementation it immediately converges to the classical approaches that it tries to distinguish itself from them in the first place. To this end, the identification and analysis of the contexts and body regulations are performed with the aim to maximize the following objectives;

1. **Reusability:** regulation strategies should be reusable in different situations and contexts.

2. **Scalability:** the definition of a context or regulation should be such that it can be scaled to accommodate more complex situations.

3. **Composability:** certain regulatory approaches should be able to be aggregated in order to form composite schemes.

These objectives which are paramount in software engineering are addressed by a component based software architecture that complements context aware body regulation. The details of the architecture, as well as some of its key features are presented in chapter 5.

With the theoretical aspect in place and provided a suitable software architecture, chapter 6 explores two comprehensive examples of humanoids context aware body regulation. These two examples show the three aforementioned desirable features alongside other advantages of the method. First, the whole-body standing context introduced previously is used in a real world application with important implications for the general public. It is then scaled up to present another context to demonstrate reusability of body regulation among the context and highlight the effectiveness of the accompanying component based software architecture.

Finally, the thesis is concluded with some remarks on the direction for the future research, and certain open challenges and possible shortcomings alongside potential solutions for them. In the final chapter, further possible context and body regulations as well as a short discussion on the composability are put forward. Furthermore, some thoughts regarding the steps towards [semi-]automatic body regulation are presented.

1.4 On the Existing Literature and Background Knowledge

It is a common convention for theses to deliver a review of the existing works in the literature after the introduction. This thesis, however, follows a different structure dictated by its nature. The contexts and body regulations studied throughout the dissertation —even though *seemingly* irrelevant to each other— are conceptually tightly related. However, within the existing works they are often treated as single individual methods. Consequently, if they were to be addressed in an isolated chapter of this thesis, they would look scattered, unfocused and out of context. Instead, a small introduction alongside related works is provided whenever a new context is put forward. The aim is to make a better reading experience, and at the same time by addressing the similar approaches within the context, allowing the readers to compare them more vividly.

As for the background knowledge, similar approach is followed. The technical details and related mathematics is provided when needed, and similar equations are revisited if required later. In particular, the body regulation for humanoids heavily relies on the inequality hierarchical quadratic programming and the stack of task schemes. These notions are discussed in the containing chapter. One exception is the closely related concepts of kinematic and dynamic manipulability of mechanisms, and the velocity and force transmission factors. These concepts are fundamental to several body regulation schemes. Although they are well established and roboticists are acquainted with them, a gentle refresher is provided in the following for the sake of completeness.

1.5 A Gentle Reminder on Manipulability and Transmission Factors

The manipulability of robotic mechanisms is a concept introduced in [4] and [5]. Since then, it has been one of the most important assets in robotic research. Manipulability is a quantitative measure that describes robots' manipulating ability in positioning and orienting their end-effectors. Although it is a relatively well discussed concept in the literature, providing a brief explanation could facilitate the interpretation of discussions.

While carrying out a task, humans tend to articulate their arms or whole-body such that they maximize their dexterity for that task. When writing, the elbow is at a comfortable angle which allows generating velocities in all directions with small efforts. Instead, when pushing on a surface, humans often fully stretch their arm towards the direction of the push, increasing their force application capabilities. Analogous to the robots, the arm in these examples is reconfigured to increase its manipulability.

1.5.1 Velocity Manipulability

Consider an n-DoF robot and its generalized coordinates $\boldsymbol{q}$ with $\boldsymbol{q} \in \mathbb{R}^n$, operating in $\mathbb{R}^m$ Cartesian space. The Jacobian matrix, $\mathbf{J}$, expresses a mapping between the joint and

the task spaces by

$$\dot{\boldsymbol{x}} = \mathbf{J}\dot{\boldsymbol{q}} \tag{1.1}$$

where $\dot{\boldsymbol{x}} \in \mathbb{R}^m$ are the Cartesian velocities. The Singular Value Decomposition (SVD) [6] of $\mathbf{J}$ is expressed as

$$\begin{aligned}
\mathbf{J} &= \mathbf{U}\boldsymbol{\Sigma}\mathbf{V}^*, \\
\mathbf{U} &= [\boldsymbol{u}_1, \boldsymbol{u}_2, \ldots, \boldsymbol{u}_m], \\
\mathbf{V} &= [\boldsymbol{v}_1, \boldsymbol{v}_2, \ldots, \boldsymbol{v}_n], \\
\boldsymbol{\Sigma} &= [\mathrm{diag}(\sigma_1, \ldots, \sigma_m)|0] = \left[\begin{array}{cccc|c} \sigma_1 & & & & \\ & \sigma_2 & & & \\ & & \ddots & & 0 \\ & & & \sigma_m & \end{array}\right]
\end{aligned} \tag{1.2}$$

where $\mathbf{U}$ and $\mathbf{V}$ are $m \times m$ and $n \times n$ unitary matrices. $\boldsymbol{\Sigma}$ is an $m \times n$ diagonal matrix with $\sigma_1 \geq \sigma_2 \geq \ldots \geq \sigma_m \geq 0$. The matrix $\mathbf{V}^*$ is the conjugate transpose of $\mathbf{V}$ (since the Jacobian in this context contains no complex entries, the conjugate transpose reduces to normal transpose). The columns of $\mathbf{U}$ and $\mathbf{V}^*$ $(\boldsymbol{u}_i, \boldsymbol{v}_i)$ are orthonormal vectors called left and right singular vectors respectively.

The singular value decomposition of the Jacobian can be interpreted geometrically as follows: if the space of all possible joint velocities is expressed as a unit hypersphere such that

$$\|\dot{\boldsymbol{q}}\|^2 = \sum_{i=1}^{n} \dot{\boldsymbol{q}}_i^2 \leq 1 \tag{1.3}$$

then the SVD of the Jacobian maps such a hypersphere into an ellipsoid, henceforth the *manipulability ellipsoid*. This mapping can be described as

$$\dot{\boldsymbol{q}}^T\dot{\boldsymbol{q}} \leq 1 \rightarrow \dot{\boldsymbol{x}}^T(\mathbf{J}\mathbf{J}^T)^+\dot{\boldsymbol{x}} \leq 1 \tag{1.4}$$

where the + super-script denotes the pseudo-inverse operation. Figure 1.7 extends on this notion further. The principle axes of this ellipsoid are defined by the singular values and the left singular vectors of the Jacobian as $\sigma_1\boldsymbol{u}_1, \sigma_2\boldsymbol{u}_2, \ldots \sigma_m\boldsymbol{u}_m$. Figure 1.8 shows the manipulability ellipsoid of a simplified planar robot in multiple configurations. Note that when the Jacobian is rank deficient, the smallest singular value $\sigma_m = 0$ and the ellipsoid collapses.

The dexterity can be seen from two perspectives; i) as directions w.r.t. the axes of the ellipsoid toward which the robot has better or worse joint-space to Cartesian-space transmission; ii) the volume of the manipulability ellipsoid. The volume describes the manipulability as an overall scalar quantity. It is calculated according to [4] as:

$$\begin{aligned}
v &= c_v \cdot \prod_{i=1}^{m} \sigma_i, \\
c_v &= \begin{cases} (2\pi)^{m/2} \cdot (2 \cdot 4 \cdots m)^{-1}, & \text{if } m \text{ is even,} \\ 2(2\pi)^{(m-1)/2} \cdot (1 \cdot 3 \cdots m)^{-1}, & \text{if } m \text{ is odd.} \end{cases}
\end{aligned} \tag{1.5}$$

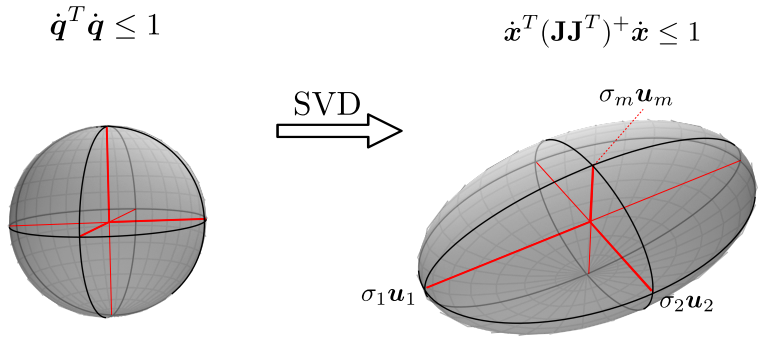

Figure 1.7: Mapping between the joint space and the Cartesian space velocities as a mapping between a unit hypersphere and an ellipsoid.

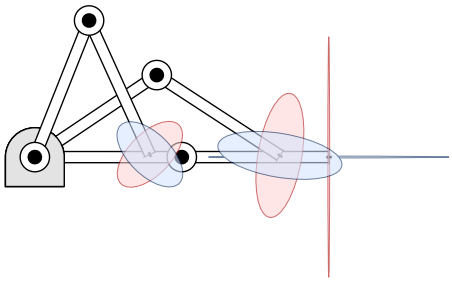

Figure 1.8: Velocity (red) and force (blue) manipulability ellipsoids of a simple planar robot. Note the orthogonal nature of velocity and force transmissions in identical configurations.

If the mechanism is not redundant (i.e., $n = m$) the equation (1.5) simplifies to

$$v = \sqrt{\det(\mathbf{J}\mathbf{J}^T)} = \sqrt{\det(\mathbf{J}) \cdot \det(\mathbf{J}^T)} = |\det(\mathbf{J})| \tag{1.6}$$

1.5.2 Force Ellipsoid

Mapping the joint velocities hypersphere to an ellipsoid can be extended to joint torques and end-effector wrenches. With reference to equation (1.4), the force ellipsoid mapping is described as

$$\boldsymbol{\tau}^T\boldsymbol{\tau} \leq 1 \rightarrow \boldsymbol{F}^T(\mathbf{J}\mathbf{J}^T)\boldsymbol{F} \leq 1 \tag{1.7}$$

and its volume as

$$v = \sqrt{\det(\mathbf{J}\mathbf{J}^T)^{-1}} \tag{1.8}$$

where $\boldsymbol{\tau}$ and $\boldsymbol{F}$ are actuator torques and end-effector generalized forces respectively. Force ellipsoids, as seen in figure 1.8, are orthogonal to the velocity ellipsoids. Postures or configurations that have high torque to force transmission factors, suffer from low velocity transmission and vice versa.

This refresher ends by making two side remarks. The force manipulability discussed here assumes instantaneous motions. To compute the full dynamic manipulability [5], [7] it is necessary to consider the effects of inertial, centrifugal, coriolis and gravity (fictitious)

forces. Secondly, the assumption made in 1.7 considering a unit hyper-sphere of torques, is a conservative assumption. That is, in reality actuator torques constitute a n-polytope and its mapping creates a m-parallelepiped [8], [9]. The polytope approach has remained mostly theoretical since it is computationally demanding. For the purposes of CABR, however, these assumptions introduce no shortcomings.

As a final remark, it should be mentioned that it is necessary to treat the linear and angular parts of the Jacobian separately when using it for manipulability calculations [10]. Alternatively when *only* the forces (excluding the torques, not the full wrenches) or linear velocities are required, then the three rows of the Jacobian related to linear motion should be used for the SVD and the following computations.

2 Environmental Contact Context and Its Body Regulation

Humans have a natural tendency to establish contact with their surrounding regularly for a variety of purposes; to localize themselves, to maintain their balance, or to boost their psychological factors when negotiating through an uncomfortable pathway. From a mechanical point of view, all these cases are in fact the exploitation of *secondary* contacts by hands since humans have one or both feet on the grounds at all times (the feet contacts are considered as the primary/main/base contacts here).

In robotics, however, more effort has been devoted to reacting to environmental contacts and avoiding detrimental ones than to actively utilizing contacts to enhance robot capabilities. Therefore, secondary contacts have been exploited rarely. Consider physical interactions of robots with inanimate objects in the environment. Three types of contacts can be categorized, namely detrimental, neutral, and beneficial contacts.

Detrimental contacts, a.k.a. collisions, are undesired and potentially cause damage to the robot and/or the environment. They are by far the most considered case in industrial robotics and decades of research have been dedicated to avoid such contacts, whether the obstacles are stationary (e.g., [12]–[14]) or moving [15]. Most of the works in this group related to this thesis revolve around pHRI. For instance in [16], upon entrance of the human within the robot's workspace, the robot's redundancy is employed to avoid collisions while the task execution is continued as much as possible.

Neutral contacts occur in grasping [17] and manipulation [18], as well as in assembly scenarios [19]. Common contact control schemes allow robots to exert necessary wrenches onto objects in the environment and react to external forces. Impedance, admittance, and hybrid control (e.g., [20]–[22]) are among the common methods of handling the neutral contacts.

Beneficial contacts are predominantly present in the humanoids field where they are exploited to boost the robots' stability margin by holding on to [23], or by merely touching the surrounding objects [24]. Outside of the humanoids field, these contact situations have remained untouched for the most parts. To take advantage of beneficial secondary contacts for redundant manipulators, it is necessary to have suitable body regulation which enhances robot's performance in desired criteria.

Using the human analogy once more, there is another motivation that drives humans when touching their surrounding, i.e., to enhance their capability to apply forces. Fig-

The findings of this chapter are supported by [11]. Special thanks go to Daniel Kubus for his invaluable contribution to the writing and analysis of that work.

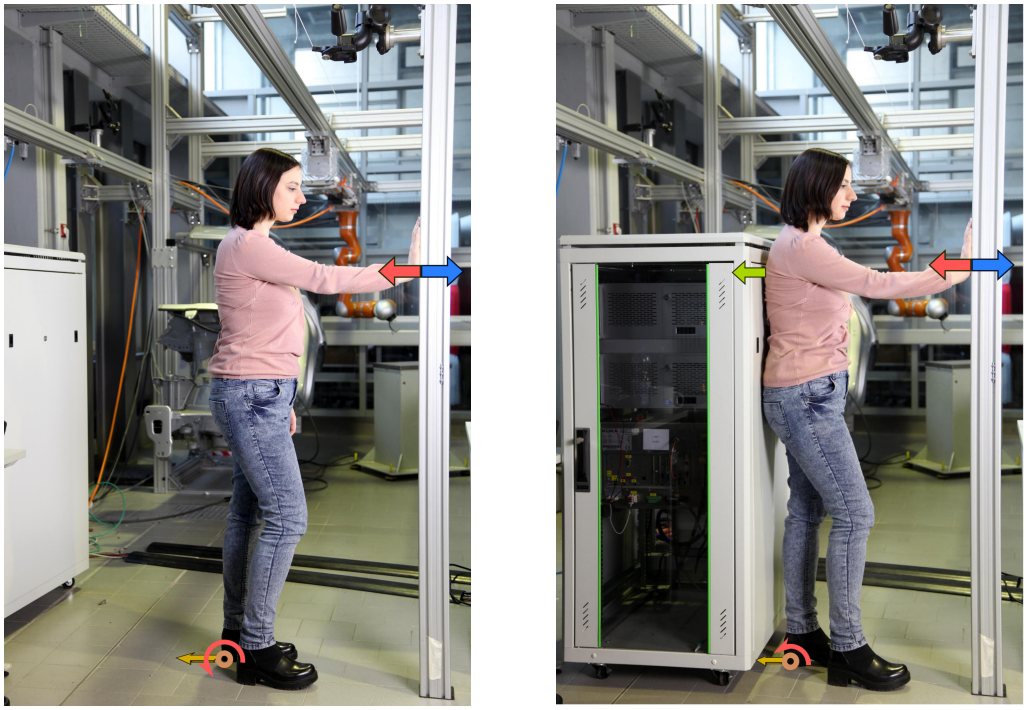

Figure 2.1: Humans naturally tend to exploit secondary contacts for better stability or minimized effort when applying forces. Left: The reaction forces resulting from the end-effector forces propagate through the entire body and generate a wrench at the ground contact. Right: The same reaction forces at the contact location require less effort of the lower part of the body to be compensated as part of them (green arrow) are absorbed by the secondary contact.

ure 2.1 depicts two cases of pushing an object, once freestanding and once while leaning on a surface. Note how part of the reaction forces are channeled to the secondary contact point hence, the load on the ankles is reduced.

Most robots nowadays come with a dynamic model and if not, acceptable models can be identified [25], reverse engineered [26] and improved upon [27]. As a result, the dynamic interaction with the surrounding is feasible and new applications exploiting new robots and leveraging on force/torque control schemes are emerging rapidly. A context that presents the situation where the robot is in contact with the environment is motivated similarly. Such a context encapsulates applications such as polishing and drilling. For applications where the robot is exerting considerable amount of force on the environment (e.g., the drilling task), one form of body regulation is through body reconfiguration to improve joint space to Cartesian space transmission factors. Alternatively, it is possible to exploit a second contact in the same fashion as humans do. Establishing secondary contacts with the goal of increasing maximum applicable end-effector forces is the core idea of body regulation for the environmental contact context.

2.1 Problem Statement

Consider an m-DoF manipulator with the task of exerting a desired contact force $\boldsymbol{f}_e$ by its end-effector at a given pose[1]. The robot may establish a second contact between points p_c and p_l where p_c belongs to a set of contact surfaces in the workspace and p_l is a point on the surfaces of the links. The point p_l splits the robot into two sub chains, namely, Lower Kinematic Chain (LKC) and Upper Kinematic Chain (UKC) whose Jacobians are denoted by $\underline{\mathbf{J}}$ and $\bar{\mathbf{J}}$. The static contact between p_c and p_l is governed by Coulomb friction with a known or measurable coefficient of friction μ_s and it is assumed that the end-effector force lie within the friction cone.

Let $\boldsymbol{\tau}_c$ and $\boldsymbol{\tau}$ denote the actuator forces with and without secondary contact. Assuming a static equilibrium, smooth contact surfaces which can locally be approximated by planes, and negligible elasticity at the contact point, the actuator torques in both cases can be compared as a torque ratio

$$r_\Phi = \frac{\|\boldsymbol{\tau}_c\|}{\|\boldsymbol{\tau}\|}. \tag{2.1}$$

Note that the 2-norm in (2.1) is ill-defined for joints of mixed type as it was shown in [28], hence tailored norms have to be used if the mechanism has prismatic joint.

Considering identical configurations with and without the second contact, it would be tempting to assume that $0 < r_\Phi \leq 1$ holds. That is, with contact the performance is better, or at worst the same as no contact situation. However, throughout this chapter it is revealed, both mathematically and empirically, that based on the configuration and physical and geometric characteristics of the contact, it is indeed possible to face situations where $r_\Phi \gg 1$. In this thesis, these counter intuitive secondary contacts are labeled as disadvantageous contacts.

2.2 Forces Acting on the Robot

In the following section the propagation of forces through the partial kinematic chains, the forces at the secondary contact, and the actuator forces $\underline{\boldsymbol{\tau}_c}$ of the LKC required to balance static forces for a general environment contact without the secondary contact are compared. Lastly, disadvantageous secondary contacts are illustrated and quantitative expressions as well as bounds for the resulting actuator forces are derived.

2.2.1 Forces at the Secondary Contact

At a *single end-effector contact*, reaction forces $\boldsymbol{f}_r$ resulting from the robot's wrenches propagate through the kinematic chain from the end-effector to the base. Therefore, $\boldsymbol{f}_r$ occurs at each link all the way to the base. That is to say, any partial chain consisting of joints '0 to j' (denoted by ${}^0\bullet_j$) is generating equivalent force:

$$\forall j \in [6, m], m \geq 6 : \left({}^0\mathbf{J}_j^T\right)^+ \cdot {}^0\boldsymbol{\tau}_j = \boldsymbol{f}_r. \tag{2.2}$$

[1] $\boldsymbol{f}_e$ is in fact a "generalized force" or in this case a wrench. Instead of "generalized actuator forces and torques" the term "actuator forces" is used for brevity.

Equation (2.2) implies that every virtual kinematic chain has to exert a counter-force $\boldsymbol{f}_e$ compensating $\boldsymbol{f}_r$ at each virtual end-effector. Let $\boldsymbol{f}_e = -\boldsymbol{f}_r$ denote the force to be provided at the corresponding virtual end-effector to keep the robot at equilibrium. Consider also a workspace surface that is defined by a normal vector $\hat{\boldsymbol{n}}$, and is in rigid point contact with some link i ($0 < i < m + 1$) of the robot. Figure 2.2 demonstrates forces and their orthogonal components at the point of secondary contact.

Having established the secondary contact while ensuring a static equilibrium, $\boldsymbol{f}_r$ propagating through the UKC is exerted on to the contact surface. Now take the force $\boldsymbol{f}_c$ which has to be provided by LKC to compensate the effect of $\boldsymbol{f}_r$. Since the robot is in equilibrium, the $\boldsymbol{f}_o$ component of $\boldsymbol{f}_r$ orthogonal to the surface is fully absorbed by the second contact. Therefore, $\boldsymbol{f}_c$ is the counter-force to the vector sum of the projection of $\boldsymbol{f}_r$ on to the contact surface ($\boldsymbol{f}_p$) and the static friction force $\boldsymbol{f}_{fr}$ which opposes $\boldsymbol{f}_p$. Finally, comparing to the no-contact case (recall $\boldsymbol{f}_e = -\boldsymbol{f}_r$), $\boldsymbol{f}_c$ instead of $\boldsymbol{f}_e$ has to be provided at each link of the LKC while $\boldsymbol{f}_e$ has to be provided at each link of the UKC, that is to say, the force balance is not disturbed by the secondary contact.

The projection of $\boldsymbol{f}_r$ on to the contact plane specified by $\hat{\boldsymbol{n}}$ is given by

$$\boldsymbol{f}_p = (\hat{\boldsymbol{n}} \times \boldsymbol{f}_r) \times \hat{\boldsymbol{n}} \tag{2.3}$$

$$= \left\langle \boldsymbol{f}_r, \hat{\boldsymbol{f}}_p \right\rangle \hat{\boldsymbol{f}}_p, \tag{2.4}$$

where $\hat{\boldsymbol{f}}_p = \boldsymbol{f}_p \left\| \boldsymbol{f}_p \right\|^{-1}$, and '$\langle \bullet, \bullet \rangle$' and '$\times$' denote the dot and the cross products respectively. Assuming a Coulomb friction mode, the magnitude of the friction force due to $\boldsymbol{f}_r$ is given its projection on to the contact surface denoted by the normal vector $\hat{\boldsymbol{n}}$, scaled by the friction coefficient μ_s. Direction of this force opposes that of $\boldsymbol{f}_p$. The friction force can be written as $\boldsymbol{f}_{fr} = -\mu_s \langle \boldsymbol{f}_r, \hat{\boldsymbol{n}} \rangle \hat{\boldsymbol{f}}_p$ and the total static force to be compensated, namely $\boldsymbol{f}_c$, amounts to

$$\boldsymbol{f}_c = -\left[\boldsymbol{f}_p + \boldsymbol{f}_{fr} \right] = -\left[\left\langle \boldsymbol{f}_r, \hat{\boldsymbol{f}}_p \right\rangle - \mu_s \langle \boldsymbol{f}_r, \hat{\boldsymbol{n}} \rangle \right] \hat{\boldsymbol{f}}_p. \tag{2.5}$$

The force $\boldsymbol{f}_c$ determines the required generalized actuator forces (i.e., torques for an only revolute joint robot) in the lower kinematic chain with secondary contact. This can be compared to the case without secondary contact which quantifies the ratio between the two cases, therefore, bounds on the required actuator forces can be derived.

2.2.2 Actuator Forces with and without Secondary Contact

Consider the endormorphism $\phi : T \to T$ from and to the vector space $T = \mathrm{col}(\mathbf{J}^T)$ of actuator forces, where $\mathrm{col}(\bullet)$ denotes the column space of a matrix. The endormorphism ϕ relates the static actuator forces $\underline{\boldsymbol{\tau}}$ required without secondary contact to those $\underline{\boldsymbol{\tau}}_c$ required with secondary contact (recall that $\underline{\boldsymbol{\tau}}$ are actuator forces of the LKC). The composition of ϕ can be characterized with four linear maps represented by the following matrices:

$$\underline{\boldsymbol{\tau}} \xrightarrow{\underline{\mathbf{J}}^{+T}} \boldsymbol{f}_e \xrightarrow{\mathbf{P}_\perp} \boldsymbol{f}_p \xrightarrow{\boldsymbol{\Gamma}} \boldsymbol{f}_c \xrightarrow{\underline{\mathbf{J}}^{T}} \underline{\boldsymbol{\tau}}_c, \tag{2.6}$$

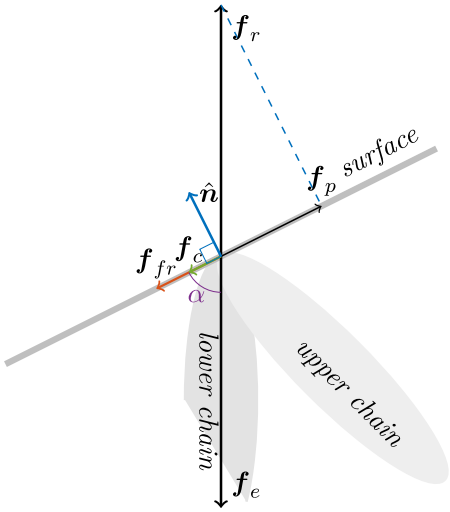

Figure 2.2: Sketch of a planar secondary contact and acting forces. Link i of the LKC (darker ellipse) exerts the force $\boldsymbol{f}_r$ onto the contact surface. In the non-contact case, $\boldsymbol{f}_e$ has to be provided by the LKC to compensate $\boldsymbol{f}_r$. $\boldsymbol{f}_p$ denotes the orthogonal projection of $\boldsymbol{f}_r$ onto the contact surface. $\boldsymbol{f}_{fr}$ denotes the opposing static friction force and $\boldsymbol{f}_c$ the force to be provided by the LKC after establishing the secondary contact. $\hat{\boldsymbol{n}}$ indicates the surface normal of the contact surface and α the angle between $\boldsymbol{f}_e$ and the contact plane.

where $\mathbf{P}_\perp$ denotes the orthogonal projection of the force $\boldsymbol{f}_e$ on to the contact surface. The mapping $\boldsymbol{\Gamma}$ represent the relationship between projected forces at the secondary contact and the required compensation forces. This mapping is quantified later in this section.

The endormorphism ϕ can be written as the following matrix product:

$$\boldsymbol{\Phi} = \underline{\mathbf{J}}^T \boldsymbol{\Gamma} \mathbf{P}_\perp \underline{\mathbf{J}}^{+T}. \tag{2.7}$$

The orthogonal projection on to $\hat{\boldsymbol{n}}$ is defined by projection matrix

$$\mathbf{P}_\parallel = \hat{\boldsymbol{n}}\hat{\boldsymbol{n}}^T, \tag{2.8}$$

and the projection on to the contact plane orthogonal to $\hat{\boldsymbol{n}}$ is given by

$$\mathbf{P}_\perp = \mathbf{I} - \hat{\boldsymbol{n}}\hat{\boldsymbol{n}}^T. \tag{2.9}$$

Assuming isotropic friction[29] characteristics[2] at the contact point, $\boldsymbol{\Gamma}$ can be expressed by a scalar parameter γ as $\boldsymbol{\Gamma} = \gamma\mathbf{I}$. Considering $\boldsymbol{f}_e = -\boldsymbol{f}_r$ and using (2.3) and (2.6),

[2] A side remark on isotropic friction assumption: while considering an anisotropic friction model seems more comprehensive, in reality there are two reason to opt for isotropic alternative. Firstly, neglecting the imperfections on the contact surface, the materials that a robot could potentially touch are often isotropic such as hard metals. Furthermore anisotropic materials such as wood often have elasticity that cannot be neglected. Secondly, isotropic friction provides certain mathematical conveniences which are exploited here without loss of generality.

equations (2.4),(2.5) can be respectively rewritten as

$$\mathbf{P}_{\perp}\boldsymbol{f}_e = \left\langle \boldsymbol{f}_e, \hat{\boldsymbol{f}}_p \right\rangle \hat{\boldsymbol{f}}_p \tag{2.10}$$

$$\boldsymbol{f}_c = \boldsymbol{\Gamma}\mathbf{P}_{\perp}\boldsymbol{f}_e. \tag{2.11}$$

Using (2.5) and (2.10) the following can be deduced

$$\begin{aligned} \boldsymbol{f}_c &= \mathbf{P}_{\perp}\boldsymbol{f}_e - \mu_s \frac{\langle \boldsymbol{f}_e, \hat{\boldsymbol{n}} \rangle}{\left\langle \boldsymbol{f}_e, \hat{\boldsymbol{f}}_p \right\rangle} \mathbf{P}_{\perp}\boldsymbol{f}_e \\ &= \left(1 - \mu_s \frac{\left\langle \hat{\boldsymbol{f}}_e, \hat{\boldsymbol{n}} \right\rangle}{\left\langle \hat{\boldsymbol{f}}_e, \hat{\boldsymbol{f}}_p \right\rangle}\right)\mathbf{P}_{\perp}\boldsymbol{f}_e = \left(1 - \mu_s \frac{\sin(\alpha)}{\cos(\alpha)}\right)\mathbf{P}_{\perp}\boldsymbol{f}_e, \end{aligned} \tag{2.12}$$

where α is the angle of attack according to figure 2.2. Hence

$$\boldsymbol{\Gamma} = \gamma\mathbf{I} = \left(1 - \mu_s \frac{\left\langle \hat{\boldsymbol{f}}_e, \hat{\boldsymbol{n}} \right\rangle}{\left\langle \hat{\boldsymbol{f}}_e, \hat{\boldsymbol{f}}_p \right\rangle}\right)\mathbf{I} = \left(1 - \mu_s \frac{\sin(\alpha)}{\cos(\alpha)}\right)\mathbf{I}. \tag{2.13}$$

Equation (2.13) expresses a diagonal matrix scaled by a factor $\gamma = 1 - \mu_s \tan(\alpha)$.

For any $\mu_s > (\cos(\alpha)\sin(\alpha))^{-1}$ the magnitude of the static friction force $\boldsymbol{f}_{fr} = -\mu_s \langle \boldsymbol{f}_r, \hat{\boldsymbol{n}} \rangle \hat{\boldsymbol{f}}_p$ opposing $\boldsymbol{f}_p$ would exceed $\boldsymbol{f}_p$ itself. This in fact means for any $\mu_s > (\cos(\alpha)\sin(\alpha))^{-1}$, $\boldsymbol{f}_e$ lies inside the friction cone, thus, the static friction force $\boldsymbol{f}_{fr}$ *fully* compensates $\boldsymbol{f}_p$ —hence $\boldsymbol{f}_c = 0$ holds. However, in this case γ is physically ill-defined. To address this issue γ and Γ are modified to consider this physical limit:

$$\gamma = \begin{cases} 1 - \mu_s \tan(\alpha) & \mu_s \leq (\cos(\alpha)\sin(\alpha))^{-1} \\ 0 & \mu_s > (\cos(\alpha)\sin(\alpha))^{-1}. \end{cases} \tag{2.14}$$

Note that the non-standard condition $\mu_s > (\cos(\alpha)\sin(\alpha))^{-1}$ results from consideration of α as the angle between the contact plane and the applied force. Utilizing (2.9) the linear map $\boldsymbol{\Phi}$ relating the actuator forces of the LKC in case of no secondary contact to those in case of a secondary contact can be written as

$$\boldsymbol{\Phi} = \gamma \underline{\mathbf{J}}^T \mathbf{P}_{\perp} \underline{\mathbf{J}}^{+T} \tag{2.15}$$

$$= \gamma\mathbf{I} - \gamma \underbrace{\underline{\mathbf{J}}^T \hat{\boldsymbol{n}}\hat{\boldsymbol{n}}^T \underline{\mathbf{J}}^{+T}}_{\Theta} \tag{2.16}$$

$$= \gamma\left(\mathbf{I} - \boldsymbol{\Theta}\right). \tag{2.17}$$

The above three equations reveal the mapping that characterize the required torques with secondary contact $\underline{\boldsymbol{\tau}}_c$

$$\underline{\boldsymbol{\tau}}_c = \boldsymbol{\Phi}\underline{\boldsymbol{\tau}} = \gamma\left(\underline{\boldsymbol{\tau}} - \boldsymbol{\Theta}\underline{\boldsymbol{\tau}}\right). \tag{2.18}$$

Denote $\underline{\boldsymbol{\tau}}' = \boldsymbol{\Theta}\underline{\boldsymbol{\tau}}$ from (2.18). The torques $\underline{\boldsymbol{\tau}}'$ can be expressed in terms of the left and right singular vectors, and the singular values of the Jacobian, as shown in (2.27). The derivation of $\underline{\boldsymbol{\tau}}'$ is presented from equation (2.19) to (2.27) in the following:

Let $\underline{\mathbf{J}} = \mathbf{U}\boldsymbol{\Sigma}\mathbf{V}^T$ denote the SVD of the Jacobian, let $\hat{\boldsymbol{u}}_\bullet$ and $\hat{\boldsymbol{v}}_\bullet$ denote the left and the right singular vectors respectively, and take n as the dimension of the task space hence the number of rows of $\underline{\mathbf{J}}$. Hence,

$$\underline{\mathbf{J}}^T = \mathbf{V}\boldsymbol{\Sigma}^T\mathbf{U}^T, \tag{2.19}$$

$$\underline{\mathbf{J}}^{+T} = \mathbf{U}\boldsymbol{\Sigma}^{+T}\mathbf{V}^T. \tag{2.20}$$

Using orthogonality of the singular vectors $\underline{\mathbf{J}}^{+\mathbf{T}}\underline{\boldsymbol{\tau}}$ is written as

$$\underline{\mathbf{J}}^{+\mathbf{T}}\underline{\boldsymbol{\tau}} = \mathbf{U}\boldsymbol{\Sigma}^{+T}\mathbf{V}^T \sum_{i=1}^{n} \langle \underline{\boldsymbol{\tau}}, \boldsymbol{v}_i \rangle \, \boldsymbol{v}_i \tag{2.21}$$

$$\underline{\mathbf{J}}^{+\mathbf{T}}\underline{\boldsymbol{\tau}} = \mathbf{U} \sum_{i=1}^{n} \sigma_i^{-1} \langle \underline{\boldsymbol{\tau}}, \hat{\boldsymbol{v}}_i \rangle \, \hat{\boldsymbol{e}}_i = \sum_{i=1}^{n} \sigma_i^{-1} \langle \underline{\boldsymbol{\tau}}, \hat{\boldsymbol{v}}_i \rangle \, \hat{\boldsymbol{u}}_i, \tag{2.22}$$

and from (2.8) $\hat{\boldsymbol{n}}\hat{\boldsymbol{n}}^T\underline{\mathbf{J}}^{+\mathbf{T}}\underline{\boldsymbol{\tau}}$ as

$$\hat{\boldsymbol{n}}\hat{\boldsymbol{n}}^T\underline{\mathbf{J}}^{+\mathbf{T}}\underline{\boldsymbol{\tau}} = \sum_{i=1}^{n} \sigma_i^{-1} \langle \underline{\boldsymbol{\tau}}, \hat{\boldsymbol{v}}_i \rangle \langle \hat{\boldsymbol{n}}, \hat{\boldsymbol{u}}_i \rangle \, \hat{\boldsymbol{n}}. \tag{2.23}$$

Writing $\hat{\boldsymbol{n}}$ in terms of $\boldsymbol{u}_i, i \in \{1, ..., n\}$, i.e., $\hat{\boldsymbol{n}} = \sum_{j=1}^{n} \langle \hat{\boldsymbol{n}}, \hat{\boldsymbol{u}}_j \rangle \, \hat{\boldsymbol{u}}_j$ (2.23) yields

$$\hat{\boldsymbol{n}}\hat{\boldsymbol{n}}^T\underline{\mathbf{J}}^{+\mathbf{T}}\underline{\boldsymbol{\tau}} = \sum_{i=1}^{n} \sigma_i^{-1} \langle \underline{\boldsymbol{\tau}}, \hat{\boldsymbol{v}}_i \rangle \langle \hat{\boldsymbol{n}}, \hat{\boldsymbol{u}}_i \rangle \sum_{j=1}^{n} \langle \hat{\boldsymbol{n}}, \hat{\boldsymbol{u}}_j \rangle \, \hat{\boldsymbol{u}}_j. \tag{2.24}$$

With $\underline{\mathbf{J}}^T$ from (2.19) and $\boldsymbol{\Theta}$ from (2.15), $\boldsymbol{\Theta}_{\underline{\boldsymbol{\tau}}}$ is deduced as

$$\boldsymbol{\Theta}_{\underline{\boldsymbol{\tau}}} = \underline{\mathbf{J}}^T\hat{\boldsymbol{n}}\hat{\boldsymbol{n}}^T\underline{\mathbf{J}}^{+T}\underline{\boldsymbol{\tau}} \tag{2.25}$$

$$= \mathbf{V}\boldsymbol{\Sigma}^T \sum_{i=1}^{n}\sum_{j=1}^{n} \sigma_i^{-1} \langle \underline{\boldsymbol{\tau}}, \hat{\boldsymbol{v}}_i \rangle \langle \hat{\boldsymbol{n}}, \hat{\boldsymbol{u}}_i \rangle \langle \hat{\boldsymbol{n}}, \hat{\boldsymbol{u}}_j \rangle \, \hat{\boldsymbol{v}}_j \tag{2.26}$$

finally yielding

$$\underline{\boldsymbol{\tau}}' = \sum_{i=1}^{n}\sum_{j=1}^{n} \frac{\sigma_j}{\sigma_i} \langle \underline{\boldsymbol{\tau}}, \hat{\boldsymbol{v}}_i \rangle \langle \hat{\boldsymbol{n}}, \hat{\boldsymbol{u}}_i \rangle \langle \hat{\boldsymbol{n}}, \hat{\boldsymbol{u}}_j \rangle \, \hat{\boldsymbol{v}}_j. \tag{2.27}$$

Putting (2.18) and (2.27) together the required actuator forces with secondary contact, namely $\underline{\boldsymbol{\tau}}_c$, can be related to those forces $\underline{\boldsymbol{\tau}}_c$ without secondary contact

$$\underline{\boldsymbol{\tau}}_c = \gamma \left(\underline{\boldsymbol{\tau}} - \sum_{i=1}^{n}\sum_{j=1}^{n} \frac{\sigma_j}{\sigma_i} \langle \underline{\boldsymbol{\tau}}, \hat{\boldsymbol{v}}_i \rangle \langle \hat{\boldsymbol{n}}, \hat{\boldsymbol{u}}_i \rangle \langle \hat{\boldsymbol{n}}, \hat{\boldsymbol{u}}_j \rangle \, \hat{\boldsymbol{v}}_j \right). \tag{2.28}$$

In (2.28), the dependency of $\underline{\boldsymbol{\tau}}_c$ on the singular values $\sigma_\bullet$ of $\underline{\mathbf{J}}$ and hence the configuration of the LKC as well as on the contact geometry and friction characteristics given by $\hat{\boldsymbol{n}}$ and γ becomes apparent. Equation (2.28) constitutes the foundation for selecting optimal

environment contacts in terms of actuator force reduction. It can be exploited in an optimization problem as the cost function to find best contact strategy.

Given the geometric and physical characteristics of the secondary contact point, the body regulation in this context can be derived by exploiting these findings with the goal to minimize the overall actuator forces. Comparing this form of BR to the non-systematic approaches, it becomes apparent that at best, part of the robot's potential is remained unused, however, at worst choosing a secondary contact point naively, could have negative consequences. That is, choosing an improper second contact, the actuator torques in some case can in fact increase. Such improper contacts are called *disadvantageous secondary contacts* and are detailed in the following.

2.2.3 Disadvantageous Secondary Contacts

It is possible that $\mathbf{\Phi}$ becomes a no contraction mapping [30], should certain conditions arise, i.e.,

$$\exists \boldsymbol{q} : \|\underline{\boldsymbol{\tau}}_c\| = \|\mathbf{\Phi}\underline{\boldsymbol{\tau}}\| > \|\underline{\boldsymbol{\tau}}\|\,. \tag{2.29}$$

This circumstance constitutes secondary contacts that indeed result in higher actuator forces compared to identical configuration but without a secondary contact. The condition for which the (2.29) holds can be derived based on the Eigendecomposition of the Gram matrix $\mathbf{G} = \underline{\mathbf{J}}\underline{\mathbf{J}}^T$.

Letting $\underline{\boldsymbol{\tau}} = \|\tau\|\,\hat{\boldsymbol{v}}_{i_0}$ coincide with the right singular vector $\hat{\boldsymbol{v}}_{i_0}$ in (2.27) yields

$$\underline{\boldsymbol{\tau}}' = \|\underline{\boldsymbol{\tau}}\| \sum_{i=1}^{n}\sum_{j=1}^{n} \frac{\sigma_j}{\sigma_i} \langle \hat{\boldsymbol{v}}_{i_0}, \hat{\boldsymbol{v}}_i \rangle \langle \hat{\boldsymbol{n}}, \hat{\boldsymbol{u}}_i \rangle \langle \hat{\boldsymbol{n}}, \hat{\boldsymbol{u}}_j \rangle \hat{\boldsymbol{v}}_j. \tag{2.30}$$

If the contact surface is selected such that $\hat{\boldsymbol{n}}$ is any linear combination of two singular vectors ($\hat{\boldsymbol{n}} = -\sin(\alpha)\hat{\boldsymbol{u}}_{i_0} + \cos(\alpha)\hat{\boldsymbol{u}}_{j_0}$), by substituting the expression of $\hat{\boldsymbol{n}}$ into (2.30) and exploiting the orthogonality properties of the singular vectors $\hat{\boldsymbol{u}}_\bullet$ and $\hat{\boldsymbol{v}}_\bullet$, only two contributions in the sums do not vanish, that are, $i = i_0, j \in \{i_0, j_0\}$. Accordingly $\underline{\boldsymbol{\tau}}'$ in (2.27) can be expressed as

$$\underline{\boldsymbol{\tau}}' = -\sin(\alpha)\,\|\underline{\boldsymbol{\tau}}\| \left[-\sin(\alpha)\hat{\boldsymbol{v}}_{i_0} + \cos(\alpha)\sigma_{i_0}^{-1}\sigma_{j_0}\hat{\boldsymbol{v}}_{j_0}\right]. \tag{2.31}$$

Regarding $\mathbf{\Phi}$ from (2.15) and (2.16), and its derived form from (2.28), $\underline{\boldsymbol{\tau}}_c = \mathbf{\Phi}\underline{\boldsymbol{\tau}}$ and its norm $\|\underline{\boldsymbol{\tau}}_c\|$ yield

$$\underline{\boldsymbol{\tau}}_c = \gamma\,\|\underline{\boldsymbol{\tau}}\| \left[\left[1 - \sin^2(\alpha)\right]\hat{\boldsymbol{v}}_{i_0} + \sin(\alpha)\cos(\alpha)\sigma_{i_0}^{-1}\sigma_{j_0}\hat{\boldsymbol{v}}_{j_0}\right] \tag{2.32}$$

$$\|\underline{\boldsymbol{\tau}}_c\| = \gamma\sqrt{\left[1 - \sin^2(\alpha)\right]^2 + \left[\sin(\alpha)\cos(\alpha)\sigma_{i_0}^{-1}\sigma_{j_0}\right]^2}\,\|\underline{\boldsymbol{\tau}}\|\,. \tag{2.33}$$

Given that $\sigma_\bullet^2 = \lambda_\bullet$, computing $\frac{\|\underline{\boldsymbol{\tau}}_c\|^2}{\|\underline{\boldsymbol{\tau}}\|^2}$ finally results in the inequality:

$$\frac{\lambda_j}{\lambda_i} > \frac{1 - \cos^2(\alpha)\left[\cos(\alpha) - \mu_s\sin(\alpha)\right]^2}{\sin^2(\alpha)\left[\cos(\alpha) - \mu_s\sin(\alpha)\right]^2}. \tag{2.34}$$

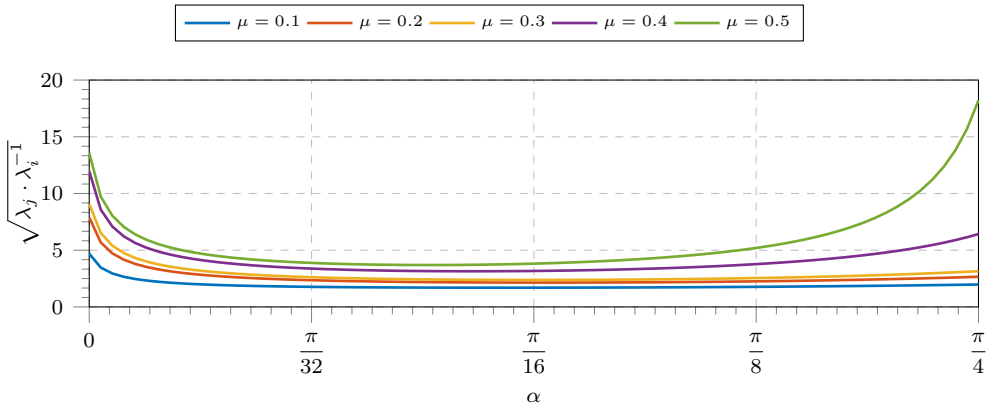

Figure 2.3: Ratios of singular values of $\underline{\mathbf{J}}$ for which $\|\underline{\boldsymbol{\tau}}_c\|^2 = \|\underline{\boldsymbol{\tau}}\|^2$ holds over contact angle $\alpha \in [0, \ldots, \frac{\pi}{4}]$. The higher μ_s, the higher is the required ratio of the eigenvalues for the secondary contact to become disadvantageous.

Inequality (2.34) defines the condition for which a secondary contact becomes disadvantageous. Figure 2.3 shows the ratios of square roots $\sqrt{\lambda_j \lambda_i^{-1}} = \sigma_j \sigma_i^{-1}$ of eigenvalues of $\mathbf{G}$, i.e., singular values $\sigma_\bullet$ of $\underline{\mathbf{J}}$, for which $\|\underline{\boldsymbol{\tau}}_c\|^2 = \|\underline{\boldsymbol{\tau}}\|^2$. Ratios are shown over $\alpha \in [0, \ldots, \frac{\pi}{4}]$ for different friction coefficients μ_s. Depending on μ_s and α, the secondary contact can become disadvantageous, i.e., $\|\underline{\boldsymbol{\tau}}_c\|^2 > \|\underline{\boldsymbol{\tau}}\|^2$.

2.2.4 Bounds on the Actuator Force Ratios

Among the goals of CABR is the ability to systematically assess the quality of body regulation in a well defined context *before* committing to the said regulatory scheme. To this end, it is helpful to estimate the bounds of the torque ratios if the robot establishes the second contact.

Recall (2.1) as the ratio between the actuator torques with and without the secondary contact:

$$r_\Phi = \frac{\|\boldsymbol{\tau}_c\|}{\|\boldsymbol{\tau}\|}. \tag{2.1 revisited}$$

Exploiting definition of $\underline{\boldsymbol{\tau}}'$ from (2.27) once again, a general condition on the torque norms with and without secondary contact can be derived. Take the ratio r_Θ

$$r_\Theta = \frac{\|\underline{\boldsymbol{\tau}}'\|}{\|\underline{\boldsymbol{\tau}}\|} = \left\| \sum_{i=1}^{n} \sum_{j=1}^{n} \langle \hat{\underline{\boldsymbol{\tau}}}, \hat{\boldsymbol{v}}_i \rangle \langle \hat{\boldsymbol{n}}, \hat{\boldsymbol{u}}_i \rangle \langle \hat{\boldsymbol{n}}, \hat{\boldsymbol{u}}_j \rangle \frac{\sigma_j}{\sigma_i} \hat{\boldsymbol{v}}_j \right\| \tag{2.35}$$

and its square as

$$r_\Theta^2 = \left\| \sum_{i=1}^{n} \sum_{j=1}^{n} \langle \hat{\underline{\boldsymbol{\tau}}}, \hat{\boldsymbol{v}}_i \rangle \langle \hat{\boldsymbol{n}}, \hat{\boldsymbol{u}}_i \rangle \langle \hat{\boldsymbol{n}}, \hat{\boldsymbol{u}}_j \rangle \frac{\sigma_j}{\sigma_i} \hat{\boldsymbol{v}}_j \right\|^2. \tag{2.36}$$

By rearranging the terms in (2.36) and employing the orthogonality properties of $\boldsymbol{v}_\bullet$ the following are acquired

$$r_\Theta^2 = \left\| \sum_{j=1}^{n} \sigma_j \langle \hat{\boldsymbol{n}}, \hat{\boldsymbol{u}}_j \rangle \hat{\boldsymbol{v}}_j \sum_{i=1}^{n} \frac{\langle \hat{\underline{\boldsymbol{t}}}, \hat{\boldsymbol{v}}_i \rangle \langle \hat{\boldsymbol{n}}, \hat{\boldsymbol{u}}_i \rangle}{\sigma_i} \right\|^2 \tag{2.37}$$

$$= \sum_{j=1}^{n} \sigma_j^2 \langle \hat{\boldsymbol{n}}, \hat{\boldsymbol{u}}_j \rangle^2 \left[\sum_{i=1}^{n} \frac{\langle \hat{\underline{\boldsymbol{t}}}, \hat{\boldsymbol{v}}_i \rangle \langle \hat{\boldsymbol{n}}, \hat{\boldsymbol{u}}_i \rangle}{\sigma_i} \right]^2 . \tag{2.38}$$

Orthonormality of the left and right singular vectors from SVD gives $\|\hat{\boldsymbol{n}}\| = \|\hat{\boldsymbol{u}}_\bullet\| = 1$. Furthermore, $\sum_{i=1}^{n} \langle \hat{\boldsymbol{n}}, \hat{\boldsymbol{u}}_i \rangle^2 = 1$ holds for the norm of the projections of $\hat{\boldsymbol{n}}$ along the $\hat{\boldsymbol{u}}_i$; same applies to $\langle \hat{\underline{\boldsymbol{t}}}, \hat{\boldsymbol{v}}_i \rangle$. Substitute $\langle \hat{\boldsymbol{n}}, \hat{\boldsymbol{u}}_\bullet \rangle$ by $\nu_\bullet$ and $\langle \hat{\underline{\boldsymbol{t}}}, \hat{\boldsymbol{v}}_\bullet \rangle$ by $\delta_\bullet$ in r_Θ^2, bearing in mind the constraints $\sum_{i=1}^{n} \nu_i^2 = 1$ and $\sum_{i=1}^{n} \delta_i^2 = 1$. This simplifies (2.38) to

$$r_\Theta^2 = \sum_{j=1}^{n} \sigma_j^2 \nu_j^2 \left[\sum_{i=1}^{n} \frac{\delta_i \nu_i}{\sigma_i} \right]^2 . \tag{2.39}$$

It is safe to assume that singular vectors $\sigma_\bullet$ are strictly fixed (since the configuration is remained unchanged) and monotonically decreasing (properties of SVD), i.e., $\sigma_1 \geq \sigma_2 \geq \ldots \geq \sigma_n$. In this case, the upper bound can be shown to depend only on σ_1 and σ_n, hence $\delta_i, \nu_i = 0 \; \forall i \in \{2, \ldots, n-1\}$. Furthermore, $\nu_1 = \nu_n = \frac{1}{\sqrt{2}}$ can be inferred. Substituting $\delta_n = \sqrt{1 - \delta_1^2}$ finally gives (2.40) and algebraic solution of the resulting expression define the bounds on r_Θ in (2.41). In a hypothetical isotropic SVD case [31], i.e., $\sigma_1 = \sigma_2 = \ldots = \sigma_n$, actuator force transmission is identical in all task-space directions, hence $0 \leq r_\Theta \leq 1$

$$r_\Theta^2 = \frac{1}{8} \left(\sigma_1^2 + \sigma_n^2 \right) \left(\frac{\delta_1 \sqrt{2}}{\sigma_1} + \frac{\sqrt{1 - \delta_1^2}\sqrt{2}}{\sigma_n} \right)^2 \tag{2.40}$$

$$0 \leq r_\Theta \leq \frac{1}{2} \left(\frac{\sigma_1}{\sigma_n} + \frac{\sigma_n}{\sigma_1} \right) . \tag{2.41}$$

Considering the entire map ϕ, using the ratio r_Φ (cf. (2.1)) and exploiting the triangle inequality for vector spaces (e.g., [32])

$$\exists r_\Phi : r_\Phi \geq \gamma(r_{\Theta_{max}} - 1), \nexists r_\Phi : r_\Phi \geq \gamma(r_{\Theta_{max}} + 1). \tag{2.42}$$

If $\boldsymbol{f}_r$ is fully absorbed by the environment contact, no actuator force is required and hence $r_\Phi \geq 0$. Therefore,

$$0 \leq r_\Phi \leq \gamma \left(\frac{1}{2} \left(\frac{\sigma_1}{\sigma_n} + \frac{\sigma_n}{\sigma_1} \right) + 1 \right) . \tag{2.43}$$

$\gamma \in [0, 1]$ depends on the contact angle α and the friction coefficient μ_s whereas σ_1 and σ_n depend solely on the configuration of the LKC. When the LKC approaches a singularity, $r_{\Theta_{max}}$ and consequently r_Φ tends to infinity. That is to say, the closer the LKC is to a singularity, the more disadvantageous a secondary contact can become.

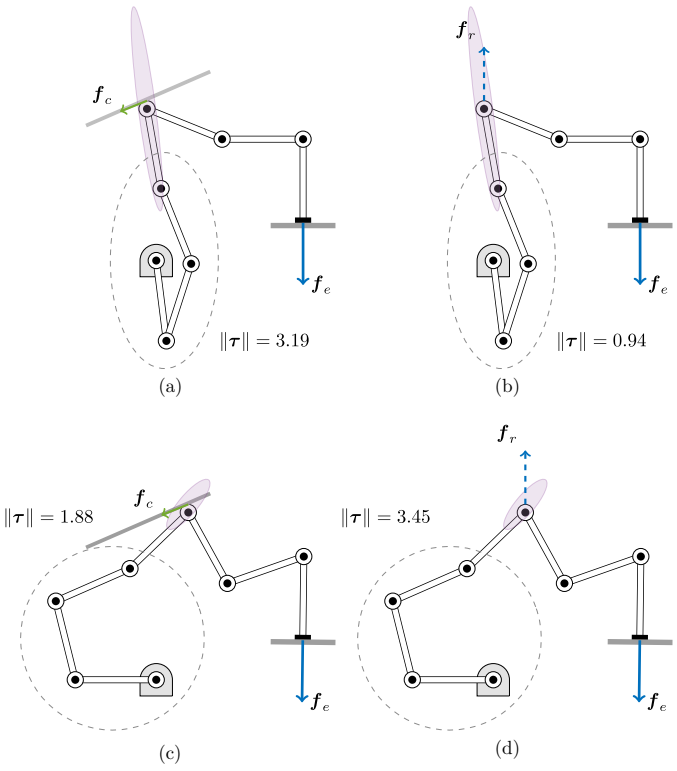

Figure 2.4: EE forces $\boldsymbol{f}_e$, resulting reaction forces f_r at link i with and without secondary contact as well as total norm $\|\boldsymbol{\tau}\|$ of actuator torques. (a): Disadvantageous secondary contact. More torque than in (b) is required when establishing the secondary contact. Exerting $\boldsymbol{f_c}$ in the direction of the contact surface requires higher $\|\boldsymbol{\tau}\|$ than exerting $\boldsymbol{f}_e$ in the direction opposing the reaction force $\boldsymbol{f}_r$. This increase in torques is due to the significantly lower force transmission factor of LKC in the direction of $\boldsymbol{f}_c$ compared to that in the direction of $\boldsymbol{f_e}$ as indicated by the force ellipsoid. (c): Advantageous secondary contact. Applying $\boldsymbol{f}_c$ requires lower $\|\boldsymbol{\tau}\|$ than exerting $\boldsymbol{f_e}$ in the non-contact case (d). Here, the decrease in $\|\boldsymbol{\tau}\|$ is not only due to part of the reaction force $\boldsymbol{f}_r$ being absorbed by the environment but also by an improved force transmission factor.

2.3 Discussion of the Analysis

By providing intuitive example alongside some discussion, the major findings of the previous section can be put into perspective.

2.3.1 Interpretation in Terms of Force Transmission Factors

Recall from section 1.5 that the singular values of the Jacobian can be interpreted as velocity transmission factors from configuration space to task space along the direction of their associated singular vectors. Likewise, their inverses can be regarded as force transmission factors [33]. To ensure dimensional consistency of the transmission factor [28], only revolute joints and pure forces are considered in the discussion.

Employing a secondary contact scales and projects the force $\boldsymbol{f}_r$ exerted by the lower partial chain onto the contact surface changing its direction and scaling its magnitude. If the force $\boldsymbol{f}_r$ required without secondary contact points along a task-space direction of high force transmission but the force $\boldsymbol{f}_c$ in case of the secondary contact points along a direction of significantly lower force transmission, the necessary actuator forces will increase and the contact may become disadvantageous depending on the ratio of the involved singular values and the contact's physical and geometric properties. Figure. 2.4

illustrates this observation by showing the changes in the required actuator forces for an advantageous and a disadvantageous secondary contact.

2.3.2 Contact Location and Redundancy

In order to select the secondary contact reasonably in terms of actuator force reduction, the position and orientation of the secondary contact surface as well as the exploitation of potential kinematic redundancy in the lower partial chain of the manipulator are essential.

Secondary contacts closer to the end-effector allow EE contact forces to be absorbed into the environment at links with higher indices, thus, *potentially* resulting in a greater overall actuator force reduction as more joints benefit from the secondary contact.

As the force applied at the secondary contact is ideally independent of the configuration of the lower partial chain, its potential redundancy can be employed to reduce the required actuator forces by moving it into a configuration with a more favorable force transmission factor in the direction of $\boldsymbol{f}_c$. In this case, $\boldsymbol{\Phi}$ (cf. (2.7)) must be modified by considering the original and altered configurations $\underline{\boldsymbol{q}}_0$ and $\underline{\boldsymbol{q}}_1$ which results in

$$\boldsymbol{\Phi}' = \underline{\mathbf{J}}^T(\underline{\boldsymbol{q}}_1)\boldsymbol{\Gamma}\mathbf{P}_\perp\underline{\mathbf{J}}^{+T}(\underline{\boldsymbol{q}}_0). \tag{2.44}$$

2.3.3 Gravity

Let $\boldsymbol{\tau}_g$ denote the actuator forces required to compensate gravity. Gravity has not been considered in the preceding sections for two reasons:

1. Secondary contacts only affect the actuator forces $\boldsymbol{\tau}_g$ if the angle $\beta = \sphericalangle(\hat{\boldsymbol{n}}, \boldsymbol{g})$ between the normal vector $\hat{\boldsymbol{n}}$ of the secondary contact surface and the gravity vector $\boldsymbol{g}$, is below $\beta = \frac{\pi}{2}$, and $\boldsymbol{f}_r$ has a component in the direction of the contact surface, i.e., $\sphericalangle(\hat{\boldsymbol{n}}, \boldsymbol{f}_r) < \frac{\pi}{2}$. Regarding the bounds derived in the previous sections, by reversing the direction of the EE force, this can always be assured.

2. Changes in $\boldsymbol{\tau}_g$ due to the secondary contact solely depend on the configuration $\bar{\boldsymbol{q}}$ of the upper partial chain but *not* on the applied EE forces and associated actuator forces. Only the actuator forces $\underline{\boldsymbol{\tau}}_g$ of the joints of the lower partial chain can be affected by the secondary contact. Assuming $\beta < \frac{\pi}{2}$, the actuator forces $\underline{\boldsymbol{\tau}}_g$ of the LKC are reduced as gravitational forces acting on the link which establishes the secondary contact and the proximal links are partially absorbed by the secondary contact, hence, they do not have to be compensated by the joints of the LKC.

Gravity can be considered in $\underline{\boldsymbol{\tau}}_c$ (cf. (2.28)) by

$$\underline{\boldsymbol{\tau}}_c = \boldsymbol{\Phi}\underline{\boldsymbol{\tau}} - \underline{\mathbf{J}}^T\boldsymbol{\Gamma}\mathbf{P}_\parallel\boldsymbol{f}_g(\bar{\boldsymbol{q}}) = \underline{\mathbf{J}}^T\boldsymbol{\Gamma}\left[\mathbf{P}_\perp\underline{\mathbf{J}}^{+T}\underline{\boldsymbol{\tau}} - \mathbf{P}_\parallel\boldsymbol{f}_g(\bar{\boldsymbol{q}})\right]. \tag{2.45}$$

$\boldsymbol{f}_g(\bar{\boldsymbol{q}})$ denotes the configuration-dependent gravitational force acting at the secondary contact due to the link masses of the upper partial chain and $\mathbf{P}_\parallel$ denotes the orthogonal projection on to $\hat{\boldsymbol{n}}$. Note that $\boldsymbol{f}_g(\bar{\boldsymbol{q}})$ depends only on the configuration of the upper partial chain while $\underline{\mathbf{J}}$ depends only on the configuration of the lower chain.

2.3.4 Compliant Environment Contact

Throughout the analysis of the body regulation in secondary contact context, static end-effector and support contacts were assumed. In the case of non-negligible environment compliance, the resulting static configuration of the lower partial chain with and without support contact cannot be considered roughly identical any longer. As the Jacobian of the lower partial chain $\underline{\mathbf{J}}(\underline{\boldsymbol{q}})$ is a continuous mapping in $\underline{\boldsymbol{q}}$, small changes in $\underline{\boldsymbol{q}}$ due to contact compliance will not significantly alter the singular values and vectors of $\underline{\mathbf{J}}(\underline{\boldsymbol{q}})$ and consequently the required actuator forces $\underline{\boldsymbol{\tau}}_c$ —unless, $\underline{\boldsymbol{q}}$ is close to a singular configuration. Changes in the singular values $\sigma_\bullet$ due to contact compliance can be considered in (2.44), by selecting $\underline{\boldsymbol{q}}_1$ to reflect the configuration change due to contact compliance.

2.4 Empirical Evaluation

To validate the mathematical analysis and their subsequent interpretations in the previous sections, empirical evaluations based on these findings were performed. These experiments were devised not only to validate the analysis, but also to entertain the notion of context aware body regulation and its implications in a realistic setup.

The experiment studies three cases of secondary contacts with identical robot configuration, namely, no contact; advantageous contact; and disadvantageous contact. A redundant 7-DoF Kuka LWR-4+ robot is employed, which exerts a force of up to $\boldsymbol{f}_e = 120N$ on to a sufficiently rigid surface with its end-effector. The surface of the EE in contact with the environment is small enough to be approximated by a point contact. The secondary contact to a planar aluminum surface ($\mu_{s,1} \approx 0.10 - 0.13$) is established on link 3. A 6-axis external force/torque sensor measures the exerted forces. The setup is depicted in figure 2.5.

Note the configuration of the lower chain and the pose of the contacts. This observation reinforces the argument regarding the force transmission ratio and how it is an indicator of secondary contacts qualities. The bottom right panel of figure 2.5, shows an advantageous contact as it absorbs almost all the reaction force, whereas the top image demonstrates a disadvantageous contact since it deflects the direction of the force to be compensated into a direction of lower force transmission of LKC. Indeed, the same high transmission ratio results in a disadvantageous contact if the singular vectors are not suitably oriented w.r.t. to the contact surface.

Figure. 2.6 shows recorded data from the robot and the mounted external sensor. These results empirically validate the provided mathematical analysis and proves that the intuitive assumption that every contact is at worst neutral, does not hold (in the environmental contact situations at least).

2.5 Conclusion

One of the goals of the thesis is deriving body regulation schemes that are usable standalone outside the CABR approach. The analysis and the results provided in this

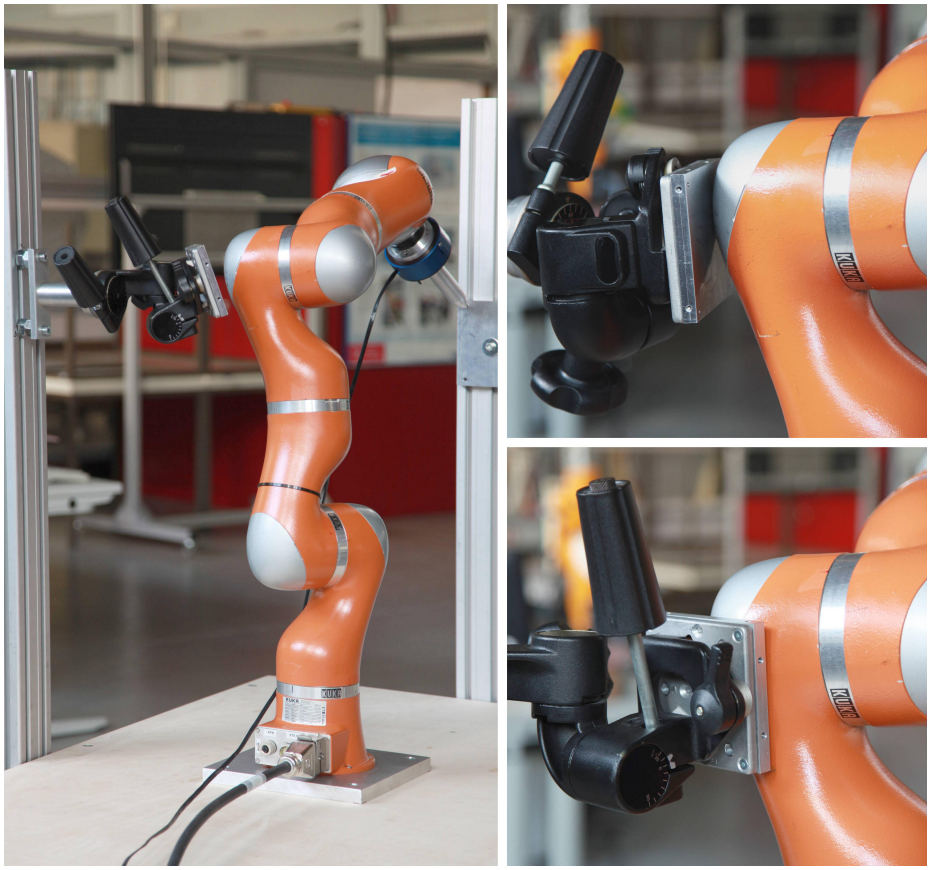

Figure 2.5: Left: Experimental setup with the robot equipped with an external force torque sensor exerting EE force. Right: Same robot configuration with advantageous (bottom) and disadvantageous (top) secondary contacts at the third link.

chapter can be studied from two distinct point of views accordingly. Firstly, the derived body regulation can be used in an optimization problem by exploiting (2.28) to find the best configuration in a secondary contact situation. Furthermore, the analysis of the bounds on the actuator torques provides the estimated gain for different contact surfaces. Secondly, these findings can be studied in the scope of the CABR.

As new applications with environment interactions emerge, the tendency towards establishing secondary contacts gets sharper as it offers new possibilities. With reference to the three phases outlined in section 1.2, actions like leaning and touching indicate a context and the mathematical analysis of this chapter outlines a suitable body regulation for such a context. The execution and deployment mechanisms that were used for the experimental evaluations are extensively discussed in chapter 5.

The mathematical analysis of this chapter also revealed an interesting phenomenon that was not visible at first sight. I.e., the body regulation analysis disproved the intuitive belief that any secondary contact which absorbs forces will also reduce required actuator

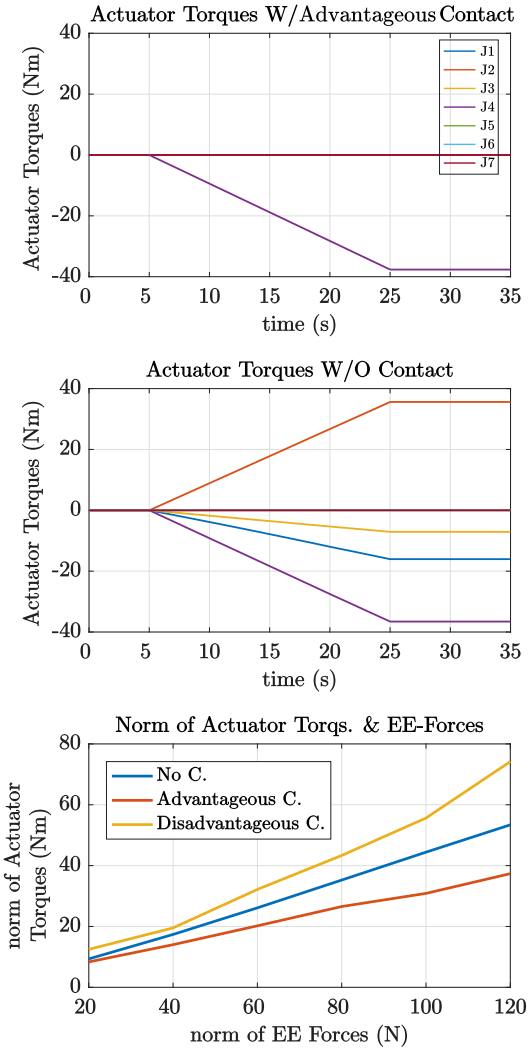

Figure 2.6: The two top figures compare time series of the applied actuator torques with no contact against an advantageous one. While the manipulator achieves the task in both cases, it requires considerably less torque when exploiting an advantageous secondary contact. In the non-contact case, three joints significantly contribute to the end-effector force, whereas in the contact case, joint 4 prominently provides the required torque.
The bottom figure depicts the norm of actuator torques and EE forces of three identical configurations with no contact as well as advantageous and disadvantageous contacts. The robot tracks a force ramp and exerts identical forces of up to $\|\boldsymbol{f}_e\| = 120N$ in all three cases. These results, validated by an external sensor, clearly demonstrate that choosing an unfavorable contact could cause up to nearly 100% increase in total actuator torques compared to an advantageous contact (red and yellow lines).

forces. This fact highlights further the importance of systematic study of secondary tasks and proves that dedicating time and effort in BR planning pays off.

The experimental results demonstrated that when secondary contacts are permissible, their exploitation should be considered to increase applicable forces, conserve energy, reduce tear and wear of the drives, and stabilize the robot. The results also suggest that establishing secondary contact in real applications is feasible and consequential to the execution of demanding tasks. Contact exploitation is also beneficial for the robots by extending their life span as their actuators are not saturated to their limits.

3 Impedance Adaptation as Body Regulation in pHRI Context

Among the defining properties of a context is the frequency at which it appears. That is, context should present reoccurring situations and not specific tasks or applications. With that in mind, one of the most reoccurring situations in robotics that suggests a context, is compliant interactions with humans. Although quite reoccurring, this definition does not necessarily fit into a clear frame. With finer granularity, consider a context where a robot and a human are in a kinesthetic-like interaction, performing collaborative tasks together. A common example is welding or application of sealant where the robot carries the load of the equipment while the human performs the complex manipulation task. This definition of the context complies with the abstraction criterion mentioned in the introduction. That is, a context is not a rigid task, rather, it conforms to a variety of contextually related situations.

In their classical setting, industrial robots have been isolated from humans by cages, light curtains, guards and other safety margins. With the advancements in hardware and control, however, new tendencies have emerge that point towards shared workspaces between humans and robots. In terms of hardware, new compliant platforms are capable of measuring interaction forces and torques more precisely. As for the controllers, impedance [20], [35], [36], admittance [37], and hybrid [38] controllers allow the robots to interact with their surroundings by measuring and controlling the interaction forces [39].

The progress in these fields lowered the barriers separating humans from robots and allowed humans to enter into robots' workspaces. Over the past two decades humans have been getting to a closer and closer proximity of the robots, leading to the important research field of physical human robot interaction. Interaction with humans has an extra critical requirement, and that is the humans' safety must be guaranteed. The safety problem can be viewed from two complementary perspectives, namely detecting human presence *and* reacting to that [40], [41].

Hence the significance of this context can be described as follows. Human-robot cooperation brings advantages regarding reduced programming time and cost, as well as facilitating tasks that otherwise would be too complicated to be programmed. On the less technical side, pHRI has also improved the image of robotic research in the eyes of the layperson, even if ever so slightly: robots are not here to steal occupations, but to help humans carrying out their arduous jobs. But perhaps above all, pHRI has the

The findings of this chapter are supported by multiple publications, most notably [34]. Special thanks go to Dr. Sugeeth Gopinathan for his contribution to the writing, conducting presented user study and the data analysis of those works.

potential of improving working conditions in the factories by creating systems that take into consideration the ergonomics, comfort and physical health of the workers. Such a goal can be achieved by considering human factors in industrial settings and assembly lines [42], by orienting work-pieces towards more comfortable human postures in welding scenarios [43], or by adapting the impedance characteristics of the robot, hence reducing the overall workers' effort [44]. By considering both the task and the human parameters, the body regulation for this context is outlined and planned in order to reduce the users' fatigue and consequently improve the task execution quality.

This form of BR is implemented as stiffness adaptation of the robot based on the *human*'s arms manipulability (cf. figure 3.1). Three manipulability based stiffness adaptation schemes for a Kuka LWR-4+ robot were devised. Each of the strategies attempt to approach ergonomics from a different angle. The three strategies are compared against each other along side a constant stiffness (*Null Handling*) adaptation as the baseline. To better evaluate the quality of BR in the rather delicate matter of human factors and ergonomics, the outcomes are validated in a user study consisting of 40 participants of varying expertise on two tasks with distinct interaction characteristics.

3.1 Adaptation Strategies

The design and implementation of the three stiffness adaptation strategies are motivated by two hypotheses:

H1. When the manipulability of the human arm is below a certain threshold, the task accuracy will decrease, hence the user needs more assistance.

H2. When the manipulability is high the human has more control over the task and the robot can be less stiff.

In essence, the robot's Cartesian stiffness is adjusted based on the manipulability measures of the human counterpart's arm. This section continues by presenting such adaptation mechanisms, their mathematical details, and what they offer to humans' ergonomics.

3.1.1 Scalar Adaptation

Perhaps the simplest, scalar adaptation (MANIP) sets the stiffness of the robot in all Cartesian directions equally. The manipulability of the human arm, $v = \sqrt{\det(\mathbf{J}\mathbf{J}^T)^{-1}}$, is mapped linearly to robot's stiffness k_s as

$$k_s = \left(\frac{k_{min} - k_{max}}{m_{max} - m_{min}} \right) \cdot v + k_{max} \tag{3.1}$$

where k_{min}, k_{max} are robot dependent minimum and maximum nominal stiffness. For the Kuka LWR-IV+ (see figure 3.3a) as an example, (k_{min}, k_{max}) are $(10, 5000N/m)$ and $(0.7, 300Nm/rad)$ in translation and rotational spaces respectively. The values of (m_{min}, m_{max}) are estimated minimum and maximum manipulability of the human counterpart obtained during an initial warm-up phase as described in figure 3.2.

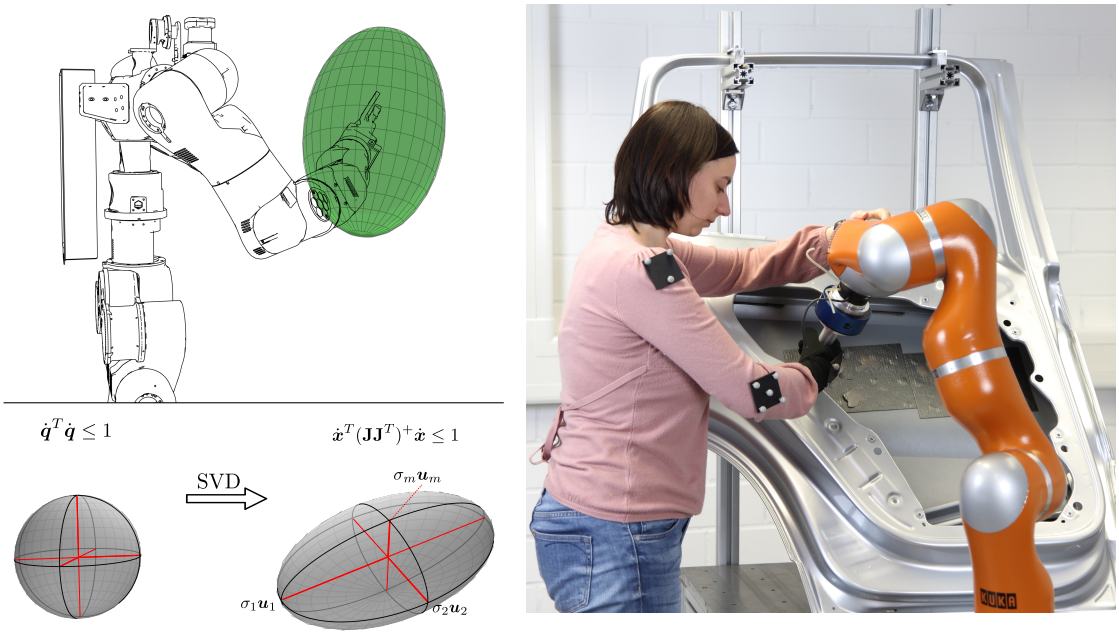

Figure 3.1: Modeling the human arm similar to a robot, it is possible to apply the same manipulability measure to it. Human arm is indeed vastly more complex in its biomechanics and dexterity, however, modeling it in this simple manner allows the administration of well established robotic techniques to it.

3.1.2 Directional Adaptation

Directional adaptation (XYZ) attempts to modify the stiffness by taking into consideration the principle axes of manipulability ellipsoid. The lengths of the manipulability ellipsoid axes are normalized and the stiffness of the robot in Cartesian space is varied in each axis independently

$$\boldsymbol{k}_s = \frac{\mathbf{U} \cdot \mathrm{diag}(\boldsymbol{\Sigma})}{\|\boldsymbol{\Sigma}\|_\infty} \cdot k_{max}. \tag{3.2}$$

In (3.2), $\mathbf{U}$ and $\boldsymbol{\Sigma}$ are the left singular vectors and singular values of the Jacobian (recall equation (1.2), page 11), and "diag" represent a vector consisting of the diagonal elements of the argument matrix.

3.1.3 Force Transmission Adaptation

Force transmission adaptation (FT) acts similar to the previous scheme, however, instead of considering the velocity transmission capabilities it considers the users' force transmission factors. Recall the omnidirectional mapping between the actuator generalized forces and Cartesian wrenches as

$$\boldsymbol{\tau}^T\boldsymbol{\tau} \leq 1 \rightarrow \boldsymbol{F}^T(\mathbf{J}\mathbf{J}^T)\boldsymbol{F} \leq 1. \tag{1.7 revisited}$$

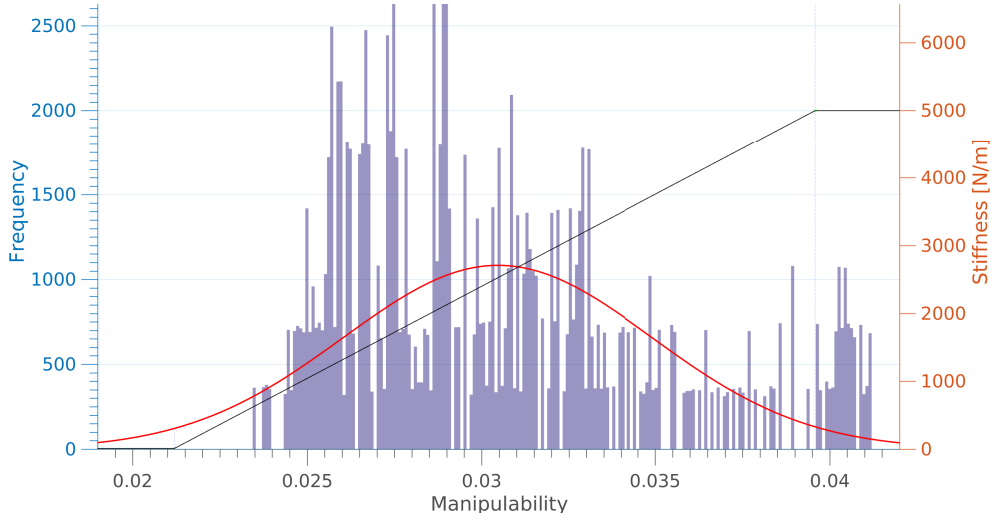

Figure 3.2: Calibration for each user base on the inverse normal distribution. The red line represents the manipulability distribution and the black lines represents the stiffness adaptation scheme gains. Using this data gathered during a warm-up phase, the manipulability at inverse normal probability distribution of 98% is chosen empirically as the manipulability limits.

This equation regards all the possible Cartesian generalized forces. To measure the force generation capabilities, namely 'ft', towards a specific Cartesian direction $\boldsymbol{\nu}$, from the (1.7) the following can be derived

$$ft = \left(\boldsymbol{\nu}^T \left(\mathbf{J}\mathbf{J}^T\right) \boldsymbol{\nu}\right)^{-1/2}. \tag{3.3}$$

Force transmission adaptation exploits (3.3) similar to scalar adaptation while considering users' force transmission factor by:

$$k_s = \left(\frac{k_{min} - k_{max}}{ft_{min} - ft_{max}}\right) \cdot ft + k_{min}. \tag{3.4}$$

Similarly, ft_{min} and ft_{max} are the human counterparts' capabilities to generate forces in different directions. They are collected similar to $m_{min/max}$ according to figure 3.2.

3.1.4 On Adaptation Strategies as Body Regulation Schemes

The rational for the scalar adaptation is that as the users' dexterity deteriorate (v converges to 0), their comfort, and therefore the task execution performance reduces. By adapting based on v an *overall* comfort level is provided to the user. This measure on the other hand, is rather naive as it does not take into account directions toward which the user suffers from low manipulability and treats them all equally. Directional adaptation is designed to overcome this shortcoming by adapting the stiffness anisotropically in different directions based on the users' manipulability ellipsoid. Force transmission adaptation

considers the force factors (instead of velocities) of the user in a similar fashion and in addition, it takes into account the kinematics of the task via the vector $\boldsymbol{\nu}$.

These strategies and hypotheses are evaluated empirically by conducting a user study and recording the performance of participants during execution of two tasks while the robot employed these adaptation schemes. Apart from these three adaptations, a constant stiffness (CONST) strategy was employed as the baseline. This scheme is in fact akin to the *Null Handling* body regulation.

3.2 User Study

The body regulation in this particular context has a hybrid nature that tries to accommodate the user comfort and simultaneously improve the task execution. While the implemented BR schemes can be easily evaluated for the task, the human aspects are not as easily measurable. Hence, a user study was designed to investigate the BR performance regarding the human factors, in both quantitative and qualitative aspects.

3.2.1 Study Design and Ethic Statement

The user study consisted of 40 participants. A within-subject design was used for comparing four control modes, where each participant interacts with the robot using all the four control modes. To prevent sequencing effects such as tiring or learning effects, the order of control modes were randomized for each user independently. The qualitative and quantitative performances of the participants were gathered through questioners and by the recorded robot and sensor data respectively.

The participants in the study were acquired through snowball sampling [45], following an initial advertisement. The ethics committee of the Bielefeld University approved the study as being ethically innocuous. All participants gave their written informed consent in accordance with Declaration of Helsinki.

3.2.2 Setup

The experimental setup is depicted in figure 3.3. A 7-DoF Kuka LWR-4+ equipped with a 6-axis force/torque sensor mounted at its end-effector was used as the platform. The robot is an active compliant robot and its built-in Cartesian impedance control was employed for the user study.

The manipulability of the users' arm was estimated by measuring their physical characteristics (height, and upper arm and forearm lengths) and assigning a 4-DoF virtual manipulator to it as depicted in figure 3.3a. Indeed an adequate representation of the human arm requires more degrees of freedom, however, considering i) the evaluation measures, ii) using only the linear part of the Jacobian, and iii) the nature of interactions and collaborative tasks, the naive 4-DoF model sufficed for the purposes of the user study.

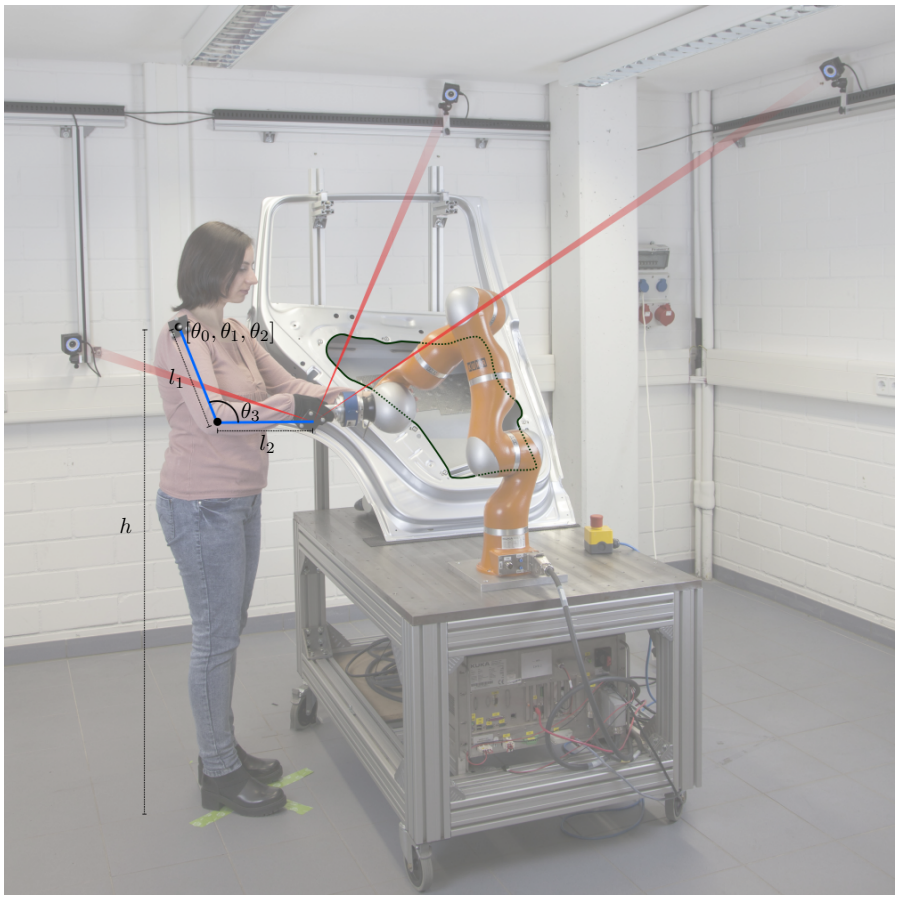

(a) Experimental setup of the user study: The user's arm was modeled as a 4-DoF shoulder-elbow manipulator with link lengths l_1 and l_2 which were measured before the task phase. Reflective markers attached to the shoulder, elbow, and wrist were tracked by a tracking system and the Jacobian of the arm was computed in terms of the human arm configuration $[\theta_1, \theta_2, \theta_3, \theta_4]$. Afterwards, the SVD of the Jacobian was used to govern the stiffness of the robot according to the three stiffness adaptation schemes outlined in section 3.1.

(b) Contour tracking task

(c) Peg in the hole task

Figure 3.3: Experimental setup for the user study and designated tasks

The configuration of the virtual robot was estimated by attaching reflective markers to the user's shoulder and wrist and tracking their motions[1].

3.2.3 Execution

The interaction stage for each user consisted of three phases;

Warm-up phase: In this phase, the participants were asked to interact with the robot by holding its end-effector and moving it along the inner contour of a car door. This phase served two purposes. Firstly, it aimed at familiarizing the participants with the nature of interaction with robot and kinesthetic guidance, and help them to gain confidence for such tasks. Secondly, —and more importantly— it functioned as calibration phase based on the user specific parameters as follows.

Recall the users' manipulability limits $m_{min/max}$ from (3.2) and their force transmission ratio limits $ft_{min/max}$ from (3.4). While it is possible to calculate these values analytically from the users' physical measurements, the data was gathered based on the warm-up phase interactions. The rational is that each user works with the robot with certain individuality. One user might fully stretch their arm to reach a far point while another user may lean to reach there. By calibrating based on the warm-up data rather than analytically, some of these nuances are incorporated in the BR, even if ever so slightly.

Once the interactive partners' data during the warm-up phase was gathered, a relative frequency histogram for the manipulability and the corresponding normal distribution was computed. As shown in figure 3.2, the manipulability at inverse normal probability distribution of 98% was chosen as the manipulability limits empirically. The parameterization of force transmission ratio limits were done in a similar manner.

Contour following task: The first task was a contour following task where the user were asked to maintain the contact with the work piece throughout the task and had to care for the accuracy. This task requires high concentration and is physically demanding. This is a reoccurring task in industrial setups, for instance, applying a sealant or adhesive to an automobile part. With reference to figure 3.3b, the users were asked to move the robots' end-effector accurately along the black rubber, maintaining a light yet constant contact to the car body. This task was designed to have areas of varying manipulability in order to properly investigate the performance of the body regulation.

Peg in the hole task: In this assignment, the users were asked to perform a task similar to a non-continuous riveting task on the car body (cf. figure 3.3c). There are 10 drill holes in the door profile and users were required to approach them in an specific order. This task demanded the users' concentration toward the end of each goal.

[1]For the user study a 12-camera system by OptiTrack was used, although, the method itself is applicable without any specificity towards a particular hardware. It is even possible to use RGB cameras and track checker patterns in a similar fashion.

3.3 Empirical Evaluation

3.3.1 Evaluation Measures

Qualitative measures: The participants had four trials and after each interaction with the robot, they were asked to fill in the corresponding questionnaire. The questionnaire rated users' experience concerning *controllability* and *reliability* of the robot, *user satisfaction* and how *enjoyable* the task was during each trial. These criteria were selected from the sub-scales perceived ease of use, perceived enjoyment, and perception of external control from the Technology Acceptance Model [46], supplemented with items from the sub-scales reliability and system satisfaction [47]. The users were also queried about previous experiences with robots and other interactions with advanced technologies.

Quantitative measures: Using the robot and the tracking system feedback, alongside the interaction forces registered by the external sensor, five performance criteria were defined;

1. Time of completion: The time required to move the end-effector from the starting to the end point.

2. Arch-Length: The total length traversed while moving along the given trajectory. This measure is related to the accuracy in task completion: Larger arc length means that the user had more deviation from the intended path. The arc length is calculated as $\sum_{i=1}^{i=n} \sqrt{\Delta x_i^2 + \Delta y_i^2 + \Delta z_i^2}$.

3. Procrustes analysis: Procrustes is a rigid shape analysis that uses isomorphic scaling, translation and rotation to find the best fit between two or more landmarked shapes. It quantifies the similarities between the target path and the user's execution of it.

4. Trajectory smoothness: The smoothness of the traversed trajectory is measured by the number of peaks in the end-effector profile. The peaks in each axis are identified as the number of maxima in given trajectory. This criteria is used to determine the controllability of the system.

5. Force profile smoothness: Similarly the force profile is analyzed by studying the number of spikes in the measured interaction forces. A non-smooth force profile is the result of abrupt changes which signals low quality interactions and users' struggle with the robot.

3.3.2 Significant Results

Significant results of the conducted user study on stiffness adaptation relevant to the focus point of the thesis are presented here. Table 3.1 tabulates the ANOVA analysis of the results. The mean and standard deviation for all criteria are presented in table 3.3.

Analyzing the time of completion and trajectory smoothness, the directional adaptation is far superior to constant stiffness. The other two methods share similar performances and

Table 3.1: ANOVA results for different comparison criteria. F, p, and df are *F-ratio*, *p-value* and *degrees of freedom* in the ANOVA (not to be confused with DoF in robotics).

	Time	Smooth	Proc.	FSM	Arc.	Enjoy.	Cntrl.	Satis.	Ease.	Reliab.
df	3	3	3	3	3	3	3	3	3	3
F	4.04	19.3	4.15	2.24	12.04	4.99	1.86	3.66	6.64	3.20
p	0.009	<**0.001**	0.008	0.087	<**0.001**	**.003**	0.015	0.14	<**0.001**	0.26

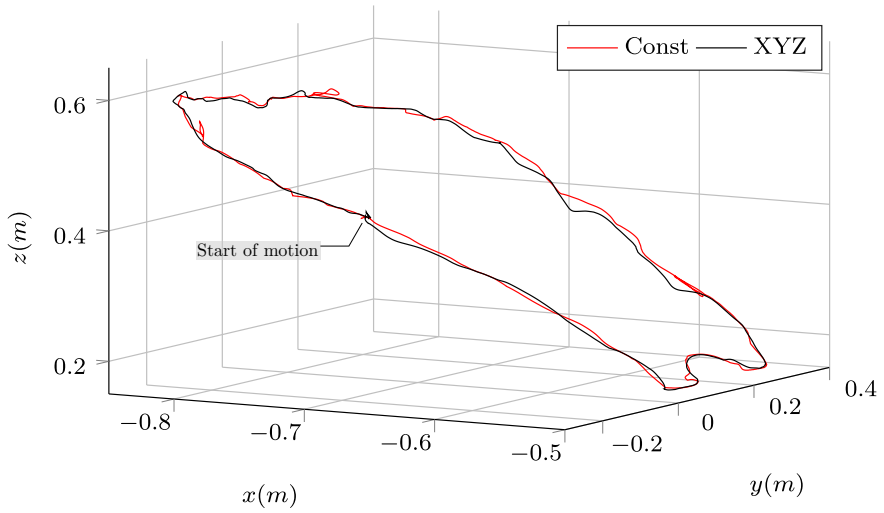

Figure 3.4: Trajectory profile of a user when performing in constant stiffness compared to directional stiffness adaptation. In constant stiffness, the profile not only appears shaky (indicating the user's struggle), it also demonstrates significant deviation in task precision. In this regards, body regulation in the form of stiffness adaptation has improved both the user experience and the task quality.

are both equally superior to constant stiffness. In the data set for trajectory smoothness, ANOVA shows a significant difference ($p < 0.001$).

The results of Procrustes are similar for all the three manipulability based modes, while the constant stiffness is slightly inferior in this measure. Similarly, the ANOVA of force profile smoothness shows no significant difference between three manipulability based modes but they are still better than the baseline method.

The result of Arc Length shows a significant difference ($p < 0.001$) between the control modes. The directional adaptation and the scalar adaptation performed identical, while the constant stiffness performance was the worst. Figure 3.4 shows the trajectory profile of a user performing in constant stiffness and directional adaptation modes. Alongside the traversed arc, note further the smoothness of trajectory for each mode.

In qualitative measures a similar trend is present. In most criteria directional adaptation out perform other schemes and in all criteria manipulability based methods perform better than the constant stiffness baseline. Particularly in the ease of use benchmark

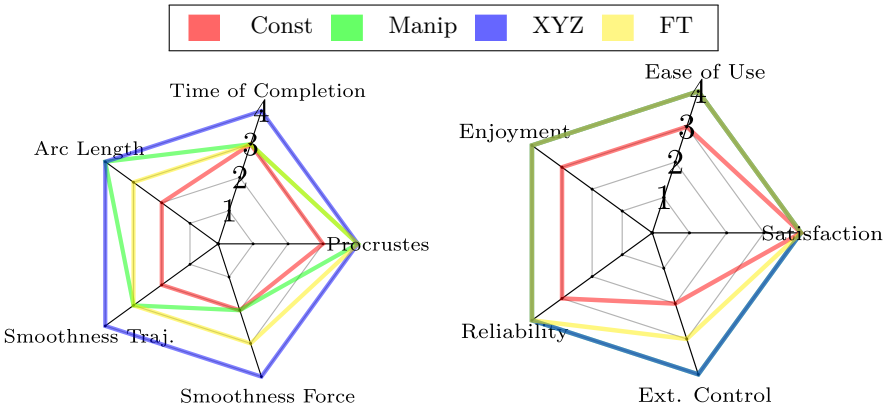

(a) Qualitative (b) Quantitative

Figure 3.5: Radar chart showings the ranking of the control modes for each performance criterion depending on their statistical significance, 4 is best rank and 1 is the worst. Note that the colors are additive, e.g., ■ + ■ = ■.

there is a significant difference ($p < 0.001$) between control schemes while the data set for enjoyment reports ($p < 0.003$).

The results for the peg in the hole task show an overall similar trend: both in approaching to, and withdrawing from the holes manipulability based adaptation schemes are favored in quantitative and qualitative criteria.

3.3.3 Peg in the Hole and Complementary Results

In the peg in the hole task the users start interacting with the robot at the parking configuration. They then approach to, and withdraw from 9 holes (h1 to h9) on the body of the car. Table 3.4 contains the user performance in these two phases.

From Figure 3.6 it is noticeable that the directional adaptation BR has an overall better performance. The performance of control modes in each hole are as follows:

h1: While approaching the hole 1, directional adaptation has a higher performance concerning the smoothness of force profile, trajectory and time of completion. Withdrawing from the hole, force transmission ratio has a better overall performance.

h2: Scalar adaptation works better in all criteria for withdrawing.

h3: Directional adaptation works well in hole 3 for approach, except for force smoothness.

h4: Directional adaptation performed better for force smoothness and time of completion.

h5: Directional adaptation had an overall better performance compared to other modes.

h6: While approaching, scalar and directional adaptation have similar performances in arc length. Directional adaptation is better regarding force smoothness and time

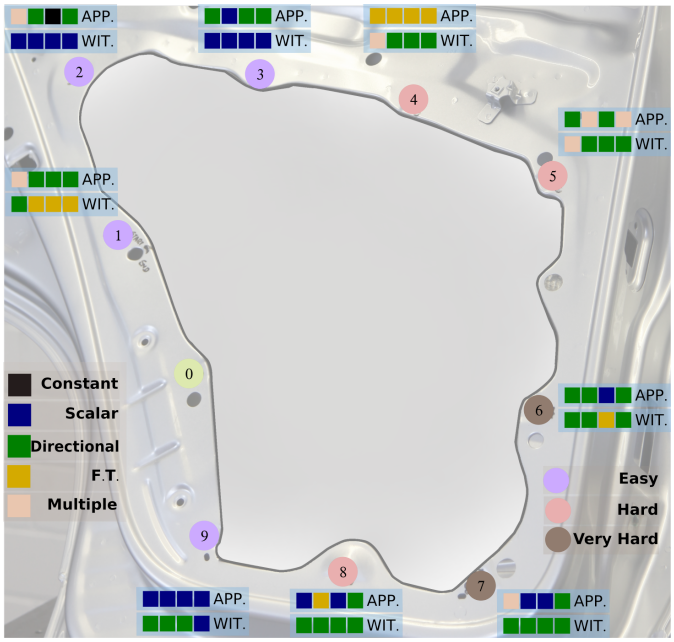

Figure 3.6: Best performing adaptation scheme per hole in different difficulty regions. The users start at point denoted by 0 and then traverse to the holes marked from 1 to 9. Each hole is associated with a difficulty level based on the sensor and users' feedback. Next to each hole 8 color-coded rectangles show the best performing scheme for both approach and withdraw phases.

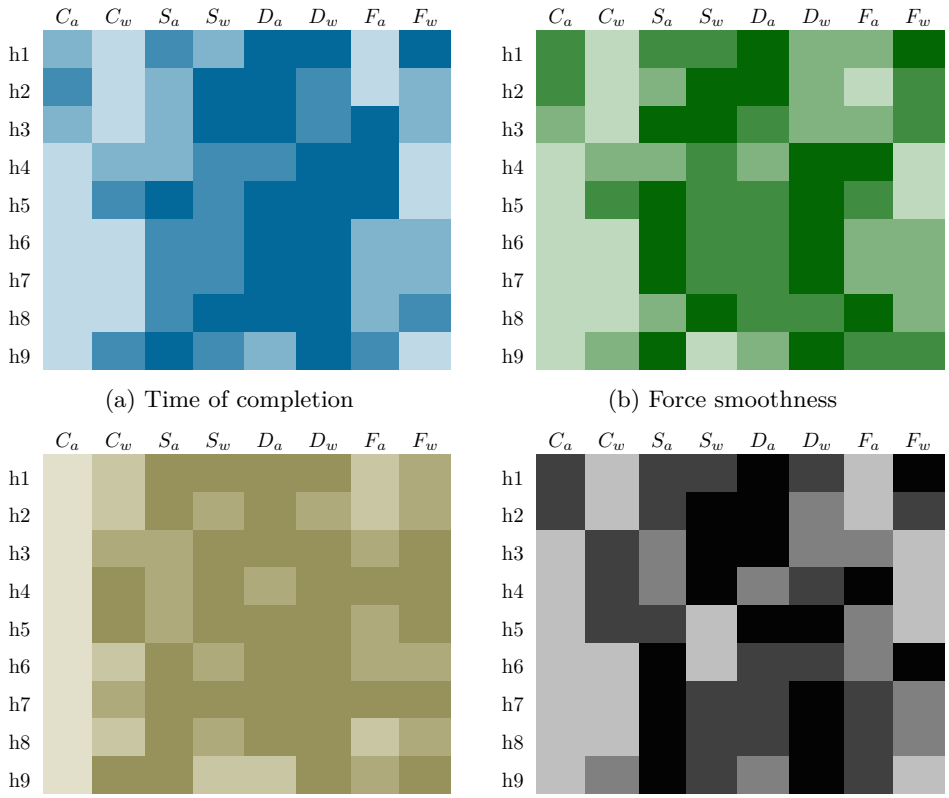

(a) Time of completion

(b) Force smoothness

(c) Arc length

(d) Trajectory Smoothness

Figure 3.7: Heat maps showing performance of the control modes in approach and withdraw for different comparison criteria. It is visible that the manipulability based approaches, especially Directional adaptation resulted in better performance. Subscripts 'a' and 'w' denote approach and withdraw for constant, scalar, directional, and force transmission adaptation schemes respectively.

of completion. During withdrawing, directional adaptation is better except for trajectory smoothness where force transmission based adaption is better.

h7: During approaching scalar adaptation is better for arc length, force/trajectory smoothness, while directional adaptation is better for the time of completion. While withdrawing, directional adaptation is preferred over all criteria.

h8: Considering approaching directional adaptation works better in terms of time of completion. During withdrawing, directional adaption works best for arc length, time of completion and trajectory smoothness.

h9: Scalar adaptation works best for the approach in all criteria and during withdrawing, directional adaptation is better.

Figure 3.7 demonstrates a heat-map of these results for all holes and control schemes in approaching and withdrawing maneuvers. Overall, the proposed BR mechanisms outperform the *Null Handling* in all holes, both in approaching and withdrawing phases.

3.4 Discussion

As the current trend in robotics shifts further towards collaborative and assistive interactions, taking the human factors and ergonomics into account becomes more crucial. In this chapter this question was addressed by stiffness adaption as body regulation based on manipulability criteria.

By analyzing the results in sections 3.3 it is evident that suitable adaptation schemes compared to constant stiffness (*Null Handling*) offers a superior experience for the users —a claim supported by the user study results with statistical significance. Furthermore these results proof the two hypotheses introduced at the beginning of this chapter (refer to page 32).

In terms of CABR, the three body regulation considered here were tested against the *Null Handling* and the results show the importance of handling the redundancy both for the user and the task. Nevertheless, there is an important question to answer and that is, what form of BR, among the three adaptation schemes, should be adopted in this context? By digging deeper, the answer can be deduced from the result.

From the users' feedback, task performance measures, and the force/torque sensor data it is possible to define regions of difficulty as shown in figure 3.8. Table 3.2 demonstrates performance of each regulation scheme in each region. Although not to the full extend, it is possible to choose a particular scheme when the user enters a specific difficulty zone. For instance, if the human counterpart is performing the task in the A4 zone, the directional adaptation denoted by 'XYZ' is expected to offer the best results both in terms of the human experience and regarding the task execution quality.

Identifying difficulty regions has major significance in industrial applications where humans safety and long term health is at risk. Furthermore, in the industry sector the improved task execution quality often has serious financial benefits. Both of these issues are addressed by systematically planning the suitable body regulations.

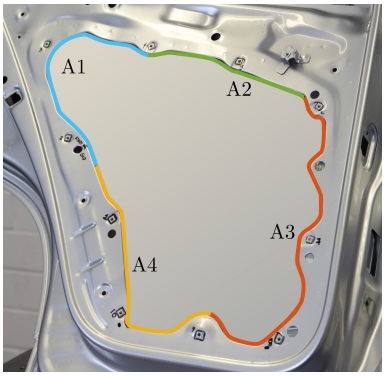

Figure 3.8: Difficulty regions are outlined by the domain experts based on the user feedback, interaction forces and other sensor data as well as the task execution quality. Alongside table 3.2, these result can be used to automatically trigger suitable BR when the users enter different difficulty regions. For instance, in A3 and A4, 'FT' and 'XYZ' clearly are the most suitable BR respectively. However, the best body regulation strategy in different regions cannot always be decided universally (e.g., in A2 the choice between 'Manip' and 'XYZ' is not easily made). Nonetheless, all the body regulation schemes beats the *Null Handling* in all regions.

Table 3.2: Users' performance in four areas of difficulty.Green and red colors highlight the best and the worst performing adaptation scheme in each criteria.

Areas	Creiteria	Const		Manip		FT		XYZ		p
		M	SD	M	SD	M	SD	M	SD	
A1	Time of Comp.	12.21	4.41	10.96	3.41	10.48	3.84	10.62	3.56	**0.002**
	ForceSmooth	68.31	28.36	59.66	23.61	56.14	23.63	57.57	23.32	**0.004**
	Traj Smooth	58.94	32.73	30.20	16.82	33.20	19.91	32.54	23.15	$<$ **0.001**
	Arc Length	0.391	0.023	0.383	0.015	0.385	0.026	0.384	0.018	**0.02**
	Procrustes	0.943	0.040	0.976	0.018	0.966	0.027	0.973	0.029	$<$ **0.001**
A2	Time of Comp.	6.63	3.18	6.83	2.65	6.62	2.87	6.52	2.55	0.82
	ForceSmooth	35.97	18.72	36.20	16.70	35.83	18.48	37.34	17.14	0.92
	Traj Smooth	19.17	17.32	15.89	9.47	16.49	11.26	14.80	11.73	0.16
	Arc Length	0.353	0.025	0.343	0.011	0.347	0.021	0.343	0.015	**0.006**
	Procrustes	0.985	0.012	0.989	0.011	0.986	0.018	0.987	0.009	0.54
A3	Time of Comp.	14.05	5.57	14.34	6.04	13.37	5.69	13.69	5.53	0.50
	ForceSmooth	73.44	36.69	73.41	42.48	69.24	32.72	73.18	37.00	0.76
	Traj Smooth	47.14	29.98	32.20	20.39	31.77	17.99	32.63	15.26	$<$ **0.001**
	Arc Length	0.502	0.071	0.460	0.027	0.458	0.026	0.461	0.026	$<$ **0.001**
	Procrustes	0.980	0.015	0.987	0.010	0.983	0.009	0.982	0.016	0.072
A4	Time of Comp.	11.00	4.03	10.31	3.58	9.48	3.47	9.33	3.55	**0.001**
	ForceSmooth	62.69	24.44	59.20	27.62	56.14	24.08	54.34	26.70	**0.02**
	Traj Smooth	43.46	28.00	26.77	16.63	26.71	15.60	23.00	12.32	$<$ **0.001**
	Arc Length	0.437	0.038	0.424	0.034	0.420	0.017	0.410	0.013	**0.01**
	Procrustes	0.942	0.069	0.977	0.028	0.964	0.040	0.981	0.020	$<$ **0.001**

Table 3.3: Table showing mean and standard deviation of all comparison criteria. Green and red colors highlight the best and the worst performing adaptation scheme in each criteria.

	Time [s]		Smooth *		Proc.		FSM		Arc. [m]		Enjoy.		Cntrl.		Satis.		Ease.		Reliab.	
	M	SD	M	SD	M	SD	M	SD	M	SD	M	SD	M	SD	M	SD	M	SD	M	SD
Const	45.74	18.35	164.09	68.71	0.95	0.04	248.56	99.96	2.10	0.17	3.71	0.74	3.55	0.79	3.70	0.44	3.63	0.70	3.74	0.67
Manip	44.75	16.70	113.94	59.19	0.97	0.01	244.25	101.80	2.00	0.06	3.95	0.68	3.88	0.60	3.78	0.50	4.00	0.56	3.97	0.55
XYZ	40.57	13.79	103.63	47.17	0.97	0.02	223.92	91.71	2.00	0.07	4.01	0.69	4.00	0.66	3.80	0.43	4.10	0.53	4.04	0.59
FT	43.05	18.35	118.80	63.87	0.96	0.02	232.44	99.85	2.02	0.10	3.90	0.68	3.75	0.79	3.65	0.48	3.94	0.60	3.92	0.67

*Smoothness and Force Smoothness are measure by the number of peaks.

Table 3.4: Approach and withdraw table. The results of the two phases alongside the 'p' value (statistical significance) are presented here. Green and red colors highlight the best and the worst performing adaptation scheme in each criteria.

Approach Table

	Arc Length					**Force Smoothness**					**Trajectory Smooth**					**Time of Completion**				
Hole	Const	Man	XYZ	FT	p	Const	Man	XYZ	FT	p	Const	Man	XYZ	FT	p	Const	Man	XYZ	FT	p
1	0.026	0.018	0.019	0.021	**0.01**	30.30	30.18	27.51	31.33	0.46	8.03	7.93	5.45	10.51	**0.01**	1.18	1.11	1.06	1.20	0.43
2	0.022	0.018	0.019	0.021	**0.00**	26.00	26.79	24.90	27.00	0.85	6.40	7.20	7.05	7.57	0.91	0.98	1.00	0.92	1.02	0.84
3	0.021	0.019	0.018	0.019	0.31	28.57	26.81	27.27	28.06	0.88	11.32	9.44	7.67	8.26	**0.03**	1.05	1.052	1.03	1.03	0.24
4	0.021	0.019	0.019	0.017	0.10	30.23	28.35	28.79	23.32	**0.02**	9.67	8.33	9.54	7.36	0.57	1.12	1.01	0.99	0.95	**0.03**
5	0.021	0.019	0.018	0.019	0.21	27.51	23.03	23.54	23.75	0.22	9.03	7.60	6.57	7.96	0.10	1.13	0.95	0.95	0.95	**0.04**
6	0.020	0.016	0.016	0.017	0.12	27.74	25.00	22.87	24.90	0.15	7.69	4.63	5.42	6.33	**0.02**	1.06	0.89	0.80	1.02	**0.02**
7	0.021	0.017	0.018	0.018	**0.03**	33.51	28.12	28.96	29.57	0.32	9.47	7.00	8.35	8.35	0.49	1.24	1.09	1.06	1.19	0.31
8	0.030	0.022	0.023	0.023	**0.04**	44.97	34.64	34.35	33.45	**0.04**	13.46	10.21	10.71	10.09	0.41	1.78	1.36	1.33	1.40	**0.04**
9	0.026	0.020	0.023	0.021	**0.02**	41.63	31.81	40.18	34.88	**0.00**	14.03	9.78	11.96	9.69	0.10	1.61	1.23	1.48	1.29	**0.03**

Withdraw Table

	Arc Length					**Force Smoothness**					**Trajectory Smooth**					**Time of Completion**				
Hole:	Const	Man	XYZ	FT	p	Const	Man	XYZ	FT	p	Const	Man	XYZ	FT	p	Const	Man	XYZ	FT	p
1	0.015	0.013	0.012	0.013	0.19	19.00	12.88	13.73	12.33	0.25	9.82	6.52	6.88	5.42	0.22	0.80	0.57	0.55	0.54	0.10
2	0.017	0.013	0.015	0.014	**0.00**	18.24	12.18	14.45	13.48	0.07	10.47	4.62	9.24	8.29	**0.00**	0.74	0.53	0.59	0.62	**0.03**
3	0.019	0.017	0.018	0.017	**0.03**	13.24	9.94	11.55	10.73	0.17	6.09	5.64	6.21	6.94	0.79	0.53	0.43	0.46	0.51	0.45
4	0.021	0.021	0.021	0.021	0.99	11.73	11.18	10.73	14.18	0.37	6.94	6.47	7.19	9.25	0.61	0.48	0.46	0.44	0.56	0.39
5	0.026	0.027	0.027	0.026	0.26	17.73	17.67	17.45	18.73	0.84	9.91	10.56	8.38	10.44	0.61	0.68	0.68	0.66	0.74	0.80
6	0.024	0.023	0.021	0.023	0.29	22.55	18.52	16.97	19.33	0.23	13.41	11.97	11.72	10.50	0.37	0.93	0.79	0.74	0.82	0.42
7	0.022	0.021	0.021	0.020	**0.03**	15.39	13.33	12.88	15.06	0.49	10.26	9.15	8.59	10.53	0.29	0.66	0.62	0.58	0.63	0.82
8	0.022	0.019	0.018	0.019	0.10	11.44	9.71	10.32	11.18	0.37	7.39	5.18	4.52	6.88	**0.04**	0.62	0.50	0.51	0.59	0.08
9	0.014	0.015	0.014	0.014	0.77	14.12	14.39	11.97	14.03	0.17	8.88	8.55	7.39	9.06	0.38	0.60	0.60	0.52	0.64	0.24

4 Body Regulation in Humanoids Contexts

Humanoid robotics studies perhaps has seen the most dedicated amount of research regarding the secondary tasks. This can safely be associated with the fact that humanoids offer the highest number of degrees of freedom among conventional robots (excluding soft and hyper-redundant manipulators). This high level dexterity in return makes them an interesting platform for the research on the hierarchy of multiple tasks. Besides, as will be shown in this chapter, performing even a single task with a humanoid requires proper handling of the robot's redundancies.

Being comprised of multiple kinematic chains (arms, legs, waist, head), naturally multiple tasks can be accomplished by a humanoid alongside the primary task which is often the whole-body motion. Furthermore, when there are more than two tasks and primary/secondary paradigm does not hold anymore, the priorities among the secondary tasks needs to be addressed. This demand has been dealt with by a supply of interesting research on hierarchy of prioritized tasks [51], [52]. The research has continued to current date, however, some implementations of the Stack of Tasks (SoT) have shifted towards the Quadratic Programming (QP) approaches [53]. This shift is in part due to the fact that QPs are more convenient in handling inequality and boundary constraints [54], and in part because of advances in numerical optimization techniques [55].

Operating in both velocity and acceleration levels, QP formalism has been extensively discussed and published in the humanoids field. However, in this chapter they are discussed as well (although at a surface level) on account of the following reasons: context aware body regulation in its core deals with handling of multiple tasks. Given a context, suitable BR must take into account the synergies among multiple tasks. That is, the tasks within a context not only should not interfere with each other, but also contribute to execution of one another. Furthermore, composability element mentioned in the introduction can benefit from the QP paradigm if it is attacked from particular angles. More concretely, context can be identified in terms of reoccurring tasks and suitable body regulation can be implemented in terms of hierarchy of tasks composed with soft and hard priorities. It is then necessary to discuss the SoT method based on the Inequality Hierarchical Quadratic Programming (iHQP) in the scope of CABR.

To this end, in the following sections a convenient task and constraint representation notation is introduced first. Based on this notation several *generic* and *input-agnostic*

The findings of this chapter is supported by [48]–[50]. Most sincere gratitude go to all the coauthor and colleagues for their contributions to the development of these works, particularly to Dr. Enrico Mingo Hoffman for his work on the stack of tasks formulation and the empirical evaluation.

Table 4.1: Specifications of COMAN and COMAN+ platforms.

		COMAN	COMAN+
DoF	Legs	6	6
	Arms	7	7
	Waist	3	2
	Neck	–	1
Modes		Position, Impedance, Voltage, Torque	Position, Impedance, Torque
Mass	(KG)	35	70
Height	(m)	0.95	1.7
Software		Orocos, ROS	XBotCore, Orocos, ROS
Sensors		IMU, 6Axis F/T sensors in wrists and ankles, Link&Joint side encoders, Joint torque sensors	IMU, 6Axis F/T sensors in wrists and ankles, Lidar Link&Joint side encoders, Joint torque sensors

tasks for the whole body of the humanoids are derived. These tasks are the building blocks of the SoT made of equality and inequality constraints. The BR of humanoids emerges as a particular SoT at a high level. At the same time, individual body regulations are applicable to each kinematic chain at a lower level. Hence, this chapter also briefly introduces an abstraction layer that encapsulates the kinematic chain details. The contents of the chapter are presented and tested on the COMAN and COMAN+ robots (real and simulated) depicted in figure 1.1c and their technical specifications in table 4.1.

4.1 Humanoids Body Regulation in the Literature

As was mentioned earlier, the humanoids field offers a very rich body of research and literature on the nature of secondary tasks. The CABR uses these works and builds upon them to deliver its message. Here some of these works are briefly mentioned.

The secondary tasks can be governed as a helper for the main task that is often locomotion, balance or both. In [56] for instance, 'centroidal momentum matrix' is introduced, its properties are derived and then it is exploited through SVD to improve locomotion capabilities of the robot. The dynamic balance ability of the robot was increased by leaning the robot's knees on the environment in [57], by merely touching the surrounding in [58], and by postural regulation for a very peculiar application in [59].

Alternatively, the secondary tasks can be studied standalone and not necessarily at the service of the primary task. Some examples include [60] where by analyzing the contact forces, the robot is able to respond to dynamic changes in the environment; pushing heavy objects with contact posture planning [61]; and in [62] where by combining the dynamic manipulability and reconfiguration, a gaze task is define in the residual redundancy of the primary task.

In most of the existing literature, however, the secondary tasks and body regulation are tailored to specific scenarios or walking/balancing applications. To fully capitalize on the potentials of humanoids, it is crucial to isolate the tasks, the applications, and the body regulation.

4.2 General Form of QP Problems and the Minimum Norm Solution

A QP problem with a constraint is defined as

$$\min_{\boldsymbol{y}\in\mathbb{R}^n} \frac{1}{2}\boldsymbol{y}^T\mathbf{H}\boldsymbol{y} + \boldsymbol{g}^T\boldsymbol{y} \tag{4.1}$$

$$\text{s.t.} \quad \mathbf{A}\boldsymbol{y} \leq \boldsymbol{b}, \tag{4.2}$$

where $\mathbf{H} \in \mathbb{R}^{n\times n}$ and $\boldsymbol{g} \in \mathbb{R}^n$, and the goal is to find a vector $\boldsymbol{y} \in \mathbb{R}^n$ that minimizes (4.1) while respecting (4.2). $\mathbf{A} \in \mathbb{R}^{m\times n}, \boldsymbol{y} \in \mathbb{R}^m$ define an n dimensional polytope in which the solution should reside.

The matrix $\mathbf{H}$ and the vector $\boldsymbol{g}$ are in fact the Hessian and the gradient with respect to the Newton step resolution [63]. This can be paralleled to the Taylor expansion of function $h(\boldsymbol{y})$

$$h(\boldsymbol{y}+\Delta\boldsymbol{y}) \approx h(\boldsymbol{y}) + \nabla h(\boldsymbol{y})^T\Delta\boldsymbol{y} + \frac{1}{2}\Delta\boldsymbol{y}^T\mathbf{H}(\boldsymbol{y})\Delta\boldsymbol{y}. \tag{4.3}$$

Indeed among the solutions of (4.1) are those based on the Newton-type methods that exploit the Taylor expansion.

Relate these equations to the relevant problems in robotic domain. Take the differential kinematic mapping between the robot's Cartesian and joint space velocities as $\dot{\boldsymbol{x}} = \mathbf{J}\dot{\boldsymbol{q}}$. Denote the desired task velocity by $\dot{\boldsymbol{x}}^*$, thus, computing the robot's input boils down to the following quadratic least square program [54]

$$\dot{\boldsymbol{q}} = \underset{\dot{\boldsymbol{q}}}{\operatorname{argmin}} \frac{1}{2}\|\mathbf{J}\dot{\boldsymbol{q}} - \dot{\boldsymbol{x}}^*\|^2. \tag{4.4}$$

This quadratic form can be expanded as follow

$$\begin{aligned}\|\mathbf{J}\dot{\boldsymbol{q}} - \dot{\boldsymbol{x}}^*\|^2 &= (\mathbf{J}\dot{\boldsymbol{q}} - \dot{\boldsymbol{x}})^T(\mathbf{J}\dot{\boldsymbol{q}} - \dot{\boldsymbol{x}}) \\ &= \dot{\boldsymbol{q}}^T\mathbf{J}^T\mathbf{J}\dot{\boldsymbol{q}} - \dot{\boldsymbol{q}}^T\mathbf{J}^T\dot{\boldsymbol{x}} - \dot{\boldsymbol{x}}^T\mathbf{J}\dot{\boldsymbol{q}} + \dot{\boldsymbol{x}}^T\dot{\boldsymbol{x}}.\end{aligned} \tag{4.5}$$

Given that $\dot{\boldsymbol{q}}^T\mathbf{J}^T\dot{\boldsymbol{x}} = (\dot{\boldsymbol{x}}^T(\mathbf{J}\dot{\boldsymbol{q}}))^T$, (4.5) can be expressed as

$$\|\mathbf{J}\dot{\boldsymbol{q}} - \dot{\boldsymbol{x}}^*\|^2 = \dot{\boldsymbol{q}}^T(\mathbf{J}^T\mathbf{J})\dot{\boldsymbol{q}} - 2(\dot{\boldsymbol{x}}\mathbf{J})\dot{\boldsymbol{q}} + \dot{\boldsymbol{x}}^T\dot{\boldsymbol{x}}. \tag{4.6}$$

Comparing (4.6) and (4.1) gives $\mathbf{H} = \mathbf{J}^T\mathbf{J}, \boldsymbol{g} = \mathbf{J}^T\dot{\boldsymbol{x}}$. Note that $\dot{\boldsymbol{x}}^T\dot{\boldsymbol{x}}$ does not contribute to the solution. Although this definition of the Hessian agrees with [63] and [53], some argue that $\mathbf{J}^T\mathbf{J}$ is not an exact approximation [64]. Nevertheless, using Taylor expansion of (4.4) it is possible to show that $\mathbf{J}^T\mathbf{J}$ suffices for humanoid control purposes [55], [65]. This approximation is almost universally used in the robotics domain.

Considering a full rank Jacobian matrix, among the solutions of (4.4) is

$$\dot{\boldsymbol{q}}^* = \mathbf{J}^+\dot{\boldsymbol{x}} \tag{4.7}$$

which minimizes $\|\mathbf{J}\dot{\boldsymbol{q}} - \dot{\boldsymbol{x}}\|^2$ on $\mathbb{R}^n$. It can be shown furthermore, that among all vectors in $\mathbb{R}^n$ that minimize the aforementioned equation, $\dot{\boldsymbol{q}}^* = \mathbf{J}^+\dot{\boldsymbol{x}}$ is the unique vector with minimal norm, a.k.a. the *the minimum norm solution*. This property, related to the pseudo-inverse approach (denote by +) plays an important role in body regulation.

Proofing the minimum norm solution consists of two steps, firstly to show that $\dot{\boldsymbol{q}}^* = \mathbf{J}^+\dot{\boldsymbol{x}}$ minimizes $\|\mathbf{J}\dot{\boldsymbol{q}} - \dot{\boldsymbol{x}}\|^2$; and secondly it is the *unique* vector with minimum norm. This proof is discussed in detail with all its aspects in [65] and here only its core concept is presented briefly for sake of completeness[1].

For any $\dot{\boldsymbol{q}} \in \mathbb{R}^n$,

$$\begin{aligned}\|\mathbf{J}\dot{\boldsymbol{q}} - \dot{\boldsymbol{x}}\|^2 &= \|\mathbf{J}(\dot{\boldsymbol{q}} - \dot{\boldsymbol{q}}^*) + \mathbf{J}\dot{\boldsymbol{q}}^* - \dot{\boldsymbol{x}}\|^2 \\ &= \|\mathbf{J}(\dot{\boldsymbol{q}} - \dot{\boldsymbol{q}}^*)\|^2 + \|\mathbf{J}\dot{\boldsymbol{q}}^* - \dot{\boldsymbol{x}}\|^2 + 2[\mathbf{J}(\dot{\boldsymbol{q}} - \dot{\boldsymbol{q}}^*)]^T(\mathbf{J}\dot{\boldsymbol{q}}^* - \dot{\boldsymbol{x}}).\end{aligned} \tag{4.8}$$

It can be shown (e.g., [65]) that $[\mathbf{J}(\dot{\boldsymbol{q}} - \dot{\boldsymbol{q}}^*)]^T(\mathbf{J}\dot{\boldsymbol{q}}^* - \dot{\boldsymbol{x}}) = 0$, hence

$$\|\mathbf{J}\dot{\boldsymbol{q}} - \dot{\boldsymbol{x}}\|^2 = \|\mathbf{J}(\dot{\boldsymbol{q}} - \dot{\boldsymbol{q}}^*)\|^2 + \|\mathbf{J}\dot{\boldsymbol{q}}^* - \dot{\boldsymbol{x}}\|^2. \tag{4.9}$$

Because $\|\mathbf{J}(\dot{\boldsymbol{q}} - \dot{\boldsymbol{q}}^*)\|^2 \geq 0$, then $\|\mathbf{J}\dot{\boldsymbol{q}} - \dot{\boldsymbol{x}}\|^2 \geq \|\mathbf{J}\dot{\boldsymbol{q}}^* - \dot{\boldsymbol{x}}\|^2$, consequently, $\dot{\boldsymbol{q}}^*$ minimizes $\|\mathbf{J}\dot{\boldsymbol{q}} - \dot{\boldsymbol{x}}\|^2$.

It is now sufficient to show that among all $\dot{\boldsymbol{q}} \in \mathbb{R}^n$, the solution $\dot{\boldsymbol{q}}^* = \mathbf{J}^+\dot{\boldsymbol{x}}$ is the unique vector with minimum norm. Consider an arbitrary solution $\tilde{\dot{\boldsymbol{q}}}$ that minimizes the quadratic form mentioned above. It is now enough to show that $\|\tilde{\dot{\boldsymbol{q}}}\| \geq \|\dot{\boldsymbol{q}}^*\|$.

$$\begin{aligned}\|\tilde{\dot{\boldsymbol{q}}}\| &= \|(\tilde{\dot{\boldsymbol{q}}} - \dot{\boldsymbol{q}}^*) + \dot{\boldsymbol{q}}^*\|^2 \\ &= \|\tilde{\dot{\boldsymbol{q}}} - \dot{\boldsymbol{q}}^*\|^2 + \|\dot{\boldsymbol{q}}^*\|^2 + 2\dot{\boldsymbol{q}}^{*T}(\tilde{\dot{\boldsymbol{q}}} - \dot{\boldsymbol{q}}^*).\end{aligned} \tag{4.10}$$

Based on properties of pseudo-inverse, as in [65] for instance, it is possible to derive $\dot{\boldsymbol{q}}^{*T}(\tilde{\dot{\boldsymbol{q}}} - \dot{\boldsymbol{q}}^*) = (\mathbf{J}^+\dot{\boldsymbol{x}})^T(\tilde{\dot{\boldsymbol{x}}} - \mathbf{J}^+\dot{\boldsymbol{x}}) = 0$. Therefore (4.10) reduces to

$$\begin{aligned}\|\tilde{\dot{\boldsymbol{q}}}\| &= \|\tilde{\dot{\boldsymbol{q}}} - \dot{\boldsymbol{q}}^*\|^2 + \|\dot{\boldsymbol{q}}^*\|^2 \\ \|\tilde{\dot{\boldsymbol{q}}} - \dot{\boldsymbol{q}}^*\| &> 0 \quad \text{for every } \tilde{\dot{\boldsymbol{q}}} \neq \dot{\boldsymbol{q}}^* \\ \|\tilde{\dot{\boldsymbol{q}}}\|^2 &> \|\dot{\boldsymbol{q}}^*\|^2,\end{aligned} \tag{4.11}$$

hence

$$\|\tilde{\dot{\boldsymbol{q}}}\| > \|\dot{\boldsymbol{q}}^*\|. \tag{4.12}$$

With this insight on the minimum norm solution, recall the example of the simple walk shown in section 1.1 and revisited here again. This was the case of *Null Handling* where the redundancy of the humanoid was remained uncontrolled. The implementation of the walk in figure 4.1 uses the support foot as the root of the kinematic tree and solves the motion generation problem by pseudo-inverse. Consequently, the right foot becomes the base of the chain at the beginning of the motion. The minimum norm joint velocities resulted from the pseudo-inverse of the Center of Mass (CoM) Jacobian creates twisted waist posture. Even though the base of the kinematic chain is switched at each step, the robot posture is never recovered. With an already twisted waist every step aggravates the problem.

[1] In page 62 of [63] an alternative proof based on the decomposition of $\dot{\boldsymbol{x}}$ into $R(\mathbf{J})\dot{\boldsymbol{x}}$ and $N(\mathbf{J}^T)\dot{\boldsymbol{x}}$,that are the range and the null space, is presented.

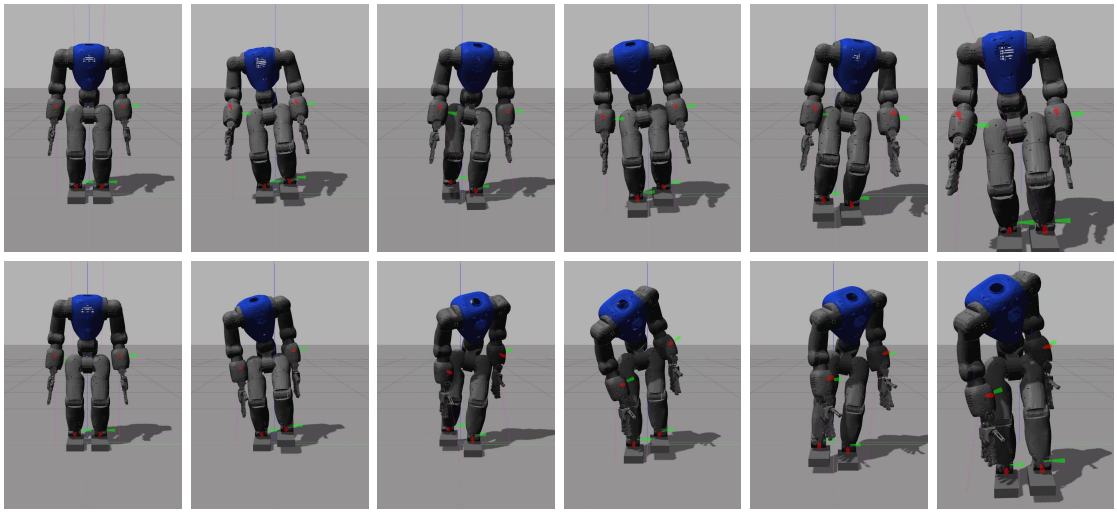

Figure 4.1: *Null Handling* of redundancy for humanoid walk revisited: On the top sequence of a very simple walk with naive joint space redundancy resolution for the waist. On the bottom the same walking implementation without any body regulation. Since the solver uses minimum norm solution and at the first step the base of the kinematic chain is at the right foot of the robot, without any BR the minimum norm solution generates unnatural waist rotations which propagate throughout, eventually resulting in a completely undesired configuration. Note that the execution of the primary task, however, is not impeded.

4.3 Inequality Hierarchical Quadratic Programming and the Stack of Tasks

The building blocks of the SoT are individual tasks. An iHQP governs the precedence of these blocks over each other. Since contexts and body regulations are defined in this paradigm, here the generic QPs are put into a suitable form for CABR and a suitable task notation is introduced. The notation is used to defined multiple tasks which form the SoT and the BR, yet they are context-agnostic. Furthermore, the synergies among the tasks need to be regulated and hard priorities of the stack of task might not suffice. This challenge is treated by introducing a soft priority scheme.

Consider the vector of generalized coordinates[2] of the humanoid as $\boldsymbol{q} \in \mathbb{R}^n$. Tracking the Cartesian position and orientation of an arbitrary frame $F \in \mathrm{SO}(3)$ attached to an arbitrary operational point of the robot can be achieved using (4.4). An error term $\boldsymbol{e} \in \mathbb{R}^6$ and a positive definite feedback gain matrix $\boldsymbol{\lambda}$ are added to close the control loop. Additionally, a regularization term ρ is required so that the solution remains bounded,

[2]It is possible, without the loss of generality, to consider a floating based notation with $\boldsymbol{q} \in \mathbb{R}^{6+n}$ where the first six coordinates represent the underactuated virtual chain, attached from the inertial frame to the floating base, while the remaining n are associated to the actuated joints. If this scheme is followed then $\mathbf{J}$ would be $\in \mathbb{R}^{6\times 6+n}$ and so on. However, to keep the notation light and independent of the presentation, $\boldsymbol{q}$ simply represents the generalized coordinates.

should the Jacobian becomes ill conditioned. When added to (4.4), these ingredients transform that quadratic form into:

$$\begin{aligned} \dot{\boldsymbol{q}} = \underset{\dot{\boldsymbol{q}} \in \mathcal{S}}{\operatorname{argmin}} \frac{1}{2} \left\| \mathbf{J}\dot{\boldsymbol{q}} - \dot{\boldsymbol{x}}^* - \boldsymbol{\lambda} \boldsymbol{e} \right\|^2 + \rho \left\| \dot{\boldsymbol{q}} \right\|^2, \\ \text{s.t. } \mathbf{A}\dot{\boldsymbol{q}} \leq \boldsymbol{b}. \end{aligned} \tag{4.13}$$

The set of all possible solutions of this equation [51] is defined as

$$\mathcal{S} = \left\{ \mathbf{J}^+ \dot{\boldsymbol{x}} + (\mathbf{I} - \mathbf{J}^+\mathbf{J})\boldsymbol{\omega}, \quad \boldsymbol{\omega} \in \mathbb{R}^n \right\}, \tag{4.14}$$

where $\boldsymbol{\omega}$ is an arbitrary vector orthogonally projected on to the null-space of the Jacobian defined as $\mathbf{I} - \mathbf{J}^+\mathbf{J}$.

As has been shown (for instance in [54], [66]) it is possible to form a hierarchy of quadratic programming problems with both equality and inequality constraints within this scheme. Regard the quadratic problem alongside its constraint in (4.13), at priority level i as

$$\begin{aligned} \mathrm{T}_i \coloneqq \quad & \dot{\boldsymbol{q}}_i = \underset{\dot{\boldsymbol{q}} \in \mathcal{S}_i}{\operatorname{argmin}} \tfrac{1}{2} \left\| \mathbf{J}_i\dot{\boldsymbol{q}} - \dot{\boldsymbol{x}}_i^* - \boldsymbol{\lambda} \boldsymbol{e} \right\|^2 + \rho \left\| \dot{\boldsymbol{q}} \right\|^2 \\ \mathrm{C}_i \coloneqq \quad & \mathbf{A}_i\dot{\boldsymbol{q}} \leq \boldsymbol{b}_i. \end{aligned} \tag{4.15}$$

$\mathcal{S}_i$ is the set of all possible solutions at this priority level and lies in the null-space of the task T_{i-1} at priority level $i-1$. Thus, the volume of $\mathcal{S}_i$ shrinks as i increases and the priority decreases. The task in (4.15) can be used to define a convenient notation for a variety of tasks as originally introduced in [66] and later reused in [49] . In such notation each task is defined as a Jacobian, desired task space quantities (e.g., motion, forces); and constraints that are expressed as a constraint matrix $\mathbf{A}$, and solution boundaries $\boldsymbol{b}$:

$$\mathrm{T}_i \coloneqq [\![\mathbf{J}_i, \dot{\boldsymbol{x}}_i^*]\!] \tag{4.16}$$

$$\mathrm{C}_i \coloneqq [\![\mathbf{A}_i, \boldsymbol{b}_i]\!]. \tag{4.17}$$

4.3.1 Hard/Soft Priorities and the Building Blocks of the SoT

For two tasks at two different priority levels, the solution of a T_j must reside in the null-space of T_i if $j > i$, which constitutes 'hard' prioritization among the two tasks. Alternatively it is possible that two tasks share the same priority level, hence forming a 'soft' priority tie. This is done by augmenting the Jacobian and Cartesian velocities of these tasks. Priority within the tasks can be achieved using a gain matrix $\boldsymbol{\psi}$ (cf figure 4.2). This concept is crucial for body regulation via stacks of tasks. Given that the BR is composed of prioritized tasks, it should possess a mechanism to regulate the synergies among individual parts and handle incompatibilities of constituting tasks. The soft prioritization system in general, and the relative priority gain $\boldsymbol{\psi}$ in particular, are among these mechanisms. The error of the task assigned to the left arm is also reduced compare to (b).

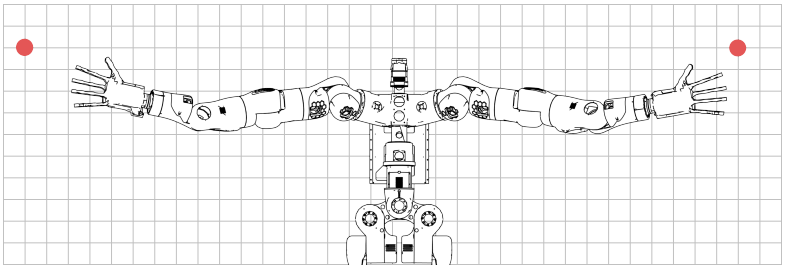

(a) Incompatible tasks with same priority $T_R = T_L$

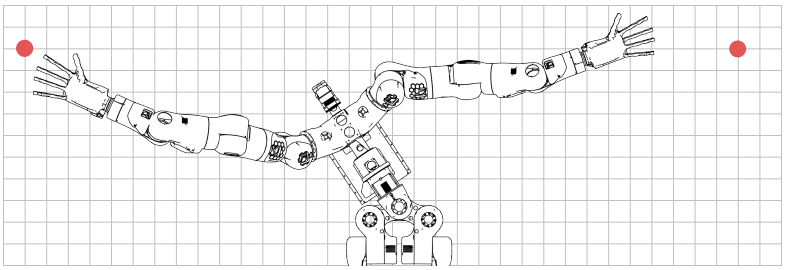

(b) Hard priority of $T_R < T_L$

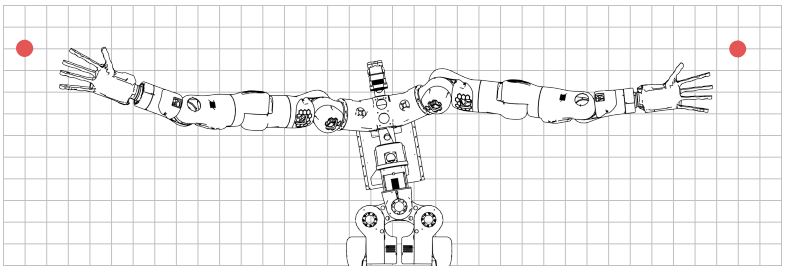

(c) Soft priority of $T_R \overset{\psi}{=} T_L$

Figure 4.2: Soft and hard priorities. The right and left arms are tasked (T_R, T_L) to reach the points highlighted in red on either side. In (a) the two tasks share the same hard priority so the robot is stuck in a stalemate situation between the two tasks. Instead in (b) the right arm task having a higher hard priority is executed properly while the left arm task suffers from increased error (Note that smaller task index indicates higher priority). Relative priority within the same hard level is enforced by ψ in (c) forming a soft priority scheme. Note in this case waist rotation is half-way between the two previous cases.

An example of these soft priority relationships are the tasks for the left and right sole (feet) of a humanoid.

$$\mathrm{T}_{\mathrm{SOLES}} \coloneqq \left[\!\left[[\boldsymbol{\psi}_{\mathrm{R}} \mathbf{J}_{\mathrm{RL}}, \psi_{\mathrm{L}} \mathbf{J}_{\mathrm{LL}}]^T,\ [\boldsymbol{\psi}_{\mathrm{R}} \dot{\boldsymbol{x}}^*_{\mathrm{RL}}, \boldsymbol{\psi}_{\mathrm{L}} \dot{\boldsymbol{x}}^*_{\mathrm{LL}}]^T \right]\!\right]. \tag{4.18}$$

$\boldsymbol{\psi}_{\mathrm{R}}$ and $\boldsymbol{\psi}_{\mathrm{L}}$ in (4.18) are the diagonal matrices that determine the relative, soft priority between left and right soles. The desired velocity vectors $\dot{\boldsymbol{x}}^*_{\mathrm{LL}}$ and $\dot{\boldsymbol{x}}^*_{\mathrm{RL}}$ are treated similar to Cartesian component of (4.20). Subscripts 'R/L' and 'RL/LL' denote right/left and right-leg/left-leg respectively.

The second task in the list of building blocks of the SoT is for the CoM

$$\mathrm{T}_{\mathrm{CoM}} \coloneqq \left[\!\left[\mathbf{J}_{\mathrm{CoM}},\ \dot{\boldsymbol{x}}^*_{\mathrm{CoM}} + \boldsymbol{\lambda}_{\mathrm{CoM}} (\boldsymbol{x}^*_{\mathrm{CoM}} - \boldsymbol{x}_{\mathrm{CoM}}) \right]\!\right], \tag{4.19}$$

where $\mathbf{J}_{\mathrm{CoM}}$ is the Jacobian of the CoM as partial derivatives relating the joint velocities to the CoM velocities. Note that the desired value for the velocity and the position of the CoM, namely $\dot{\boldsymbol{x}}^*_{\mathrm{CoM}}, \boldsymbol{x}^*_{\mathrm{CoM}}$ are independent of the SoT and based on the situation can be obtained from different sources. In walking for instance, a Walking Pattern Generator (WPG) dictates these values based on the Zero Moment Point (ZMP) [67] criterion while in push recovery Capture Point [68] governs the $\mathrm{T}_{\mathrm{CoM}}$. In other situations different criteria might be demanded. This form of agnosticity and separation of concern at the task level is an essential element of reusability and its impact is highlighted in the upcoming chapters.

Cartesian task for a frame F attached to an arbitrary point of the robot (e.g., EE of an arm) is expressed as

$$\mathrm{T}_{\mathrm{F}} \coloneqq \left[\!\left[\mathbf{J}_{\mathrm{F}},\ \dot{\boldsymbol{p}}^*_{\mathrm{F}} + \boldsymbol{\lambda}_{\mathrm{F}} (\boldsymbol{p}^*_{\mathrm{F}} - \boldsymbol{p}_{\mathrm{F}}) \right]\!\right], \tag{4.20}$$

where $\mathbf{J}_{\mathrm{F}}$ is the task Jacobian at the frame F, $\dot{\boldsymbol{p}}^*_{\mathrm{F}}$ is the desired twist of the frame, and $(\boldsymbol{p}^*_{\mathrm{F}} - \boldsymbol{p}_{\mathrm{F}})$ forms an error vector between the desired and the real pose of the end point F preventing error accumulation.

These three tasks, soles, CoM, and arbitrary Cartesian poses define the bare minimum for locomotion and manipulation scenarios. Given that many humanoids including the COMAN and COMAN+ robots have actuated waists (torso), it is beneficial to define a task for the waist. This task is expressed as a *Cartesian* orientation-only task that governs the rotations of the robots' waists

$$\mathrm{T}_{\mathrm{W}} \coloneqq \left[\!\left[\mathbf{J}^o_{\mathrm{W}},\ \boldsymbol{\lambda}^o_{\mathrm{W}} \delta\boldsymbol{\epsilon}_{\mathrm{W}} \right]\!\right], \tag{4.21}$$

where $\mathbf{J}^o_{\mathrm{W}}$ represents the rotational part of the waist Jacobian and $\delta\boldsymbol{\epsilon}_{\mathrm{W}}$ is the orientation error expressed as unit quaternions.

The overall joint motions and the residual redundancy can be governed by defining a desired joint behavior $\boldsymbol{q}^*_{\mathcal{N}}$ that functions analogously to the vector $\boldsymbol{\omega}$ in (4.14). Such a task is expressed as

$$\mathrm{T}_{\mathcal{N}} \coloneqq \left[\!\left[\mathbf{I}_n,\ \boldsymbol{\lambda}_{\mathcal{N}} (\boldsymbol{q}^*_{\mathcal{N}} - \boldsymbol{q}) \right]\!\right]. \tag{4.22}$$

The task uses the identity matrix as the Jacobian. Consequently the Hessian will equals identity matrix which respects the requirements on positive definiteness.

These tasks, particularly those of the Cartesian nature, are often accompanied by constraints that limit the robots' motion to certain bounds. Furthermore, two more constraints are always present as well, namely the joint position and velocity boundary constraints. Recall the constraint notation $\mathrm{C} \coloneqq [\![\mathbf{A}_i, \boldsymbol{b}_i]\!]$, the joint boundary constraints are defined by

$$\begin{aligned} \boldsymbol{b}_q &= (\mu(\boldsymbol{q}_{\downarrow} - \boldsymbol{q}_i), \mu(\boldsymbol{q}^{\uparrow} - \boldsymbol{q}_i)) \\ \boldsymbol{b}_{\dot{q}} &= (-\alpha_i \dot{\boldsymbol{q}}_{\downarrow} \Delta t, \alpha_i \dot{\boldsymbol{q}}^{\uparrow} \Delta t), \end{aligned} \tag{4.23}$$

where the vertical arrows denote lower and upper bounds. In (4.23), $\alpha_i \leq \alpha_{i+1}$ and μ implement a velocity allocation and integration scheme between priority levels. $\mathbf{A}_{q/\dot{q}}$ and $\boldsymbol{b}_{q/\dot{q}}$ are formed by aggregating the identity matrices and joint boundary vectors. The boundary conditions can be addressed in different ways, however, since [66] is used for the empirical evaluation of humanoid body regulation their notation and approach is adopted as well.

There are numerous other tasks and constraints that could be added here, e.g., minimum effort based on the gradient descent of the gravity vector [66]; regularization of centroidal linear and angular momentum [56]; or variety of tasks in the force domain [69]. All these possible additions can be regarded as BRs by adhering to the same task notation and defining appropriate Jacobians.

4.4 Whole-Body Regulation of Humanoids

Given a stack of tasks based on the inequality hierarchical quadratic programming, this section discusses multiple aspects of the whole-body regulation of humanoids in the view of previously mentioned generic tasks. Whole-body regulation of a humanoid robot uses these generic tasks by adapting and stacking a selection of them in a SoT for a given context.

Both contexts discussed in the previous chapters were applicable to the manipulators. Considering the substantially larger DoF size of a humanoid robot, the body regulation for humanoids in most contexts is multi-objective. Consequently, the privilege of "one context, one goal, one body regulation" that facilitated the BR planning phase previously, can no longer be enjoyed. Indeed, considering a typical humanoid scenario, multiple body regulation schemes come to mind. Without any specificity towards a particular application, some regulatory actions are listed.

A. Critical Body Regulation for the Balance

This form of body regulation favors the configurations where the robot has better equilibrium or capability to maintain or recover its balance [68]. In the SoT, the tasks for the soles and the CoM take the highest priorities to ensure the robot is stable. At lower priorities, other kinematic chains can also contribute to the balance. For instance, if an arm of the humanoid is unloaded, it could automatically pull back if the other arm is extending forward. This is due to the fact that the task for the CoM uses the Jacobian of the center of mass which is affected by all the joints of the robot, including those without

any explicit task. Alternatively, an explicit task that exploits the centroidal momentum can support the robot at kinematic chain level, or at the residual redundancy of the whole-body.

B. Critical Body Regulation for the Primary Task

Demanded by the main manipulation task, the body regulation in this case is generally governed by the next task after the balance in the SoT. An important aspect of the BR for the manipulation is the possibility of being deployed at kinematic chain level. Consequently, the BR policies defined for different contexts can be reused by considering the robot in terms of kinematic chains. On the other hand, there are certain considerations to be made when reusing the BR schemes, particularly if the reused BR internally relies on a minimum norm solution.

The minimum norm solution for a kinematic chain (for instance Kuka LWR-4+) affects the robot from the base to the EE. The importance of similarity between the source and the target kinematic chains structures must be taken into account when reusing them. The required similarity is not necessarily about the number of degrees of freedom, since kinematic chain abstraction encapsulates the DoF size differences. Instead, the joint-link topology, as well as the overall body structure[3] must be taken into account. Although this rarely causes any problem when reusing the BRs, should the problem occur the solution can be found in weighted pseudo-inverse.

In task oriented [70] or other direct pseudo-inverse approaches, a weighting matrix $\mathbf{W}$ tunes the minimum norm behavior toward arbitrary weighted norm:

$$\mathbf{J}_W^+ = \mathbf{W}^{-1}\mathbf{J}^T(\mathbf{J}\mathbf{W}^{-1}\mathbf{J}^T)^{-1}. \tag{4.24}$$

When opting for the QP approach, $\mathbf{W}$ can be integrated in the definition of QP problem. Considering that $\mathbf{W}$ is diagonal and $\forall i \in [1, \dots n], \mathbf{W}_{ii} > 0$, rewrite $\|\mathbf{J}\dot{\boldsymbol{q}} - \dot{\boldsymbol{x}}^*\|^2$ in (4.5) with a weighting matrix as

$$\begin{aligned} \|\mathbf{J}\dot{\boldsymbol{q}} - \dot{\boldsymbol{x}}^*\|^2 &= (\mathbf{J}\dot{\boldsymbol{q}} - \dot{\boldsymbol{x}})^T\mathbf{W}(\mathbf{J}\dot{\boldsymbol{q}} - \dot{\boldsymbol{x}}) \\ &= \|\mathbf{W}^{\circ\frac{1}{2}}(\mathbf{J}\dot{\boldsymbol{q}} - \dot{\boldsymbol{x}})\|^2 = \|(\mathbf{W}^{\circ\frac{1}{2}}\mathbf{J}\dot{\boldsymbol{q}} - \mathbf{W}^{\circ\frac{1}{2}}\dot{\boldsymbol{x}})\|^2. \end{aligned} \tag{4.25}$$

C. Whole-Body Human-Likeness

While hard to quantify, human-likeness can be viewed as a measure of resemblance to the way humans perform similar task. In case of walking, for instance, an upright torso with swinging arms is arguably a human-like motion. There are several elements contributing to this form of BR. Postural regulation is one of the most important factors that affects the human-like motions.

[3] As an example, COMAN and COMAN+ shown in figure 1.1c both have 7-DoF arms. However, COMAN employs a spherical joint for the wrists while COMAN+ does not. Instead, it has a double-elbow like structure. Consequently, the manner in which the two platforms handle an orientation task is different. BR of a Kuka LWR-4+, instead, is directly applicable to the COMAN arm.

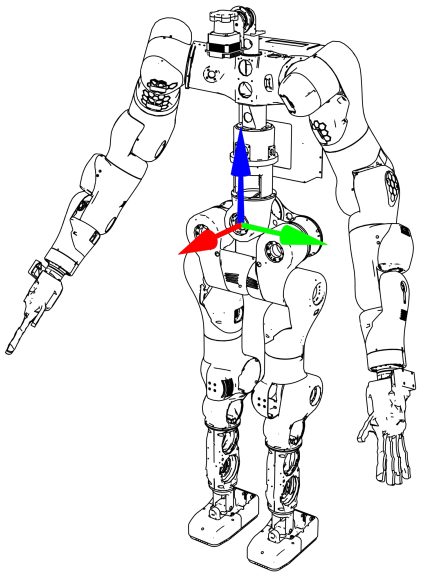

Figure 4.3: Coordinate frame convention in humanoid robots: red/green/blue $\longleftrightarrow$ $x/y/z$

Postural based BR describes the practice of regulating overall pose and figure of the robot. There are two major aspects to the postural regulation; first, the waist pose whether in Cartesian or joint space; and second, the overall redundancy resolution that dictate the robot's stance. Although, the former is more integral to an overall better posture.

Keeping the waist's configuration fixed, e.g, $\boldsymbol{q}_{\mathrm{W}} = [0, 0, 0]^T$, partially regulates the waist, however, does not fully address the issue as it is apparent in figure 4.1 (with the swing of the body the waist is also swinging which is not desirable). Instead, regulating the postural motion in the Cartesian space offers a more robust alternative. Recall the waist's equality constraint from (4.21) as $\mathrm{T}_{\mathrm{W}} \coloneqq [\![\mathbf{J}^o_{\mathrm{W}},\ \boldsymbol{\lambda}^o_{\mathrm{W}} \delta\boldsymbol{\epsilon}_{\mathrm{W}}]\!]$. The orientation error $\delta\boldsymbol{\epsilon}_{\mathrm{W}}$ can be expressed according to [71] as

$$\delta\boldsymbol{\epsilon}_{\mathrm{W}} = \eta^*_{\mathrm{W}}\boldsymbol{\epsilon}_{\mathrm{W}} - \eta_{\mathrm{W}}\boldsymbol{\epsilon}^*_{\mathrm{W}} + \begin{pmatrix} -\epsilon_y\epsilon^*_z + \epsilon_z\epsilon^*_y \\ \epsilon_x\epsilon^*_z - \epsilon_z\epsilon^*_x \\ -\epsilon_x\epsilon^*_y + \epsilon_y\epsilon^*_x \end{pmatrix}, \tag{4.26}$$

where η_{W}, $\boldsymbol{\epsilon}_{\mathrm{W}}$ are the scalar and the vector parts respectively. Hence, the BR is formed from an ideal waist orientation $\boldsymbol{o}^*_{\mathrm{W}}$ (w.r.t. standard coordinate frame in humanoids in figure 4.3) by imposing the scheme in (4.21),(4.26). Conveniently, $\boldsymbol{\lambda}^o_{\mathrm{W}}$ dictates how aggressively the robot regulates its body toward its optimal posture.

Apart from its impact on the human-like motions, postural regulation also has a significant influence on the overall whole-body regulation. Relaxing some of these constraints or imposing new ones, each tunes the robot's behavior in a specific fashion.

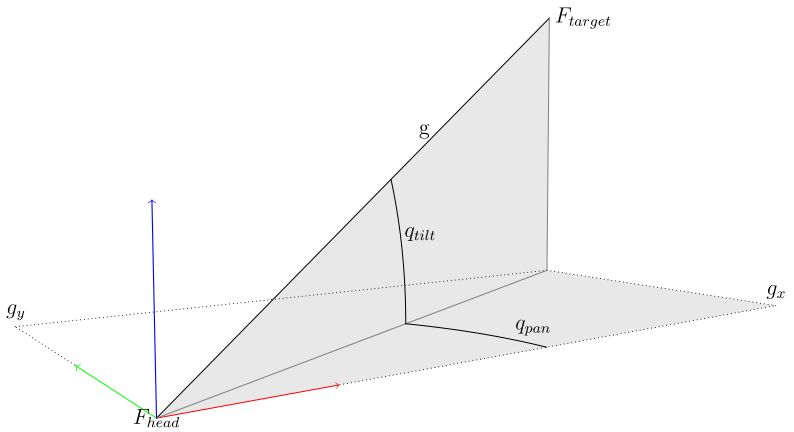

Figure 4.4: Pan/tilt configuration w.r.t. F_{head} for gaze tasks and head/neck regulation

Accordingly, the two contexts studied later exploit the postural regulation in different ways, both for achieving human-like motions and for contributing to the primary task.

D. Body Regulation for Unloaded Kinematic Chains

This criteria answers questions such as, what should the left arm do when the right one is performing the primary objective. If the stack of tasks contains any task for the CoM or other quantities that affect it, then unloaded kinematic chains (as well as the residual redundancy) will be exploited by the CoM task. As stated before, this is due to the nature of the Jacobian of the center of mass. Alternatively, these chains can be used to achieve other objectives. The neck chain for a robot with a head (e.g., COMAN+) demonstrates an example.

Consider a gaze task based on [72]. With reference to figure 4.4, frame F_{head} is attached to the robot's head; the gaze vector $\boldsymbol{g}$ points towards the target; and $\hat{\boldsymbol{g}} = \boldsymbol{g}\,\|\boldsymbol{g}\|^{-1}$. Considering a pan/title topology, the following assumption conveniently avoids all singularities of the head

$$\boldsymbol{q} = [q_0, \ldots, q_{n-2}, \boldsymbol{q}_{gaze}] \tag{4.27}$$

$$\boldsymbol{q}_{gaze} = [q_{pan}, q_{tilt}] \in (\frac{\pi}{2}, \frac{\pi}{2}) \times (\frac{\pi}{2}, \frac{\pi}{2}). \tag{4.28}$$

According to [72], the gaze direction and pan/tilt angles can be expressed as

$$\hat{\boldsymbol{g}} = \begin{pmatrix} g_x \\ g_y \\ g_z \end{pmatrix} = \begin{pmatrix} \cos(q_{pan})\cos(q_{tilt}) \\ \sin(q_{pan})\cos(q_{tilt}) \\ \cos(q_{tilt}) \end{pmatrix} \implies \tag{4.29}$$

$$q_{pan} = \operatorname{atan2}\left(\frac{g_y}{g_x}\right), \quad q_{tilt} = \operatorname{atan2}\left(\frac{g_z}{\sqrt{g_x^2 + g_y^2}}\right). \tag{4.30}$$

The results from (4.30) can be used in two ways; by considering a Cartesian task in the same scheme as (4.26); or as a joint space redundancy resolution sub-vector of $\boldsymbol{q}_{\mathcal{N}}^{*}$ from (4.22).

An interesting application of the head chain BR has emerged in the physiotherapeutic juggling [73]. Originating from the rehabilitation field, it is shown that in juggling exercises, where the patient and the therapist throw a light weight ball back and forth, if the therapist deceives the patient by looking at a direction unrelated to their throw, the patient could show improved rehabilitation performance. Similar practice can be implemented in humanoid assisted physiotherapeutic juggling [49].

E. Residual Redundancy Resolution

The residual redundancy of the humanoid governs the overall joint behavior for the rest of the body. Often at the lowest priority in the SoT, the residual redundancy is controlled at joint space using (4.22). For simple (stack of) tasks a naive yet effective way is to choose a suitable home configuration $\boldsymbol{q}_{H}$ and

$$\boldsymbol{q}_{\mathcal{N}}^{*}(t) = \boldsymbol{q}_{H}, t \in [0 \dots \mathtt{T}], \tag{4.31}$$

that is, for the duration of $\mathtt{T}$ seconds of the motion, the robot converges to the home configuration. Albeit this way of handling the joint space redundancy does not scale beyond maintaining the home posture. A more generic strategy would be to define a cost function that dictates the desired joint behavior, e.g., $\boldsymbol{q}_{\mathcal{N}}^{*}(t) = f_{\boldsymbol{q}_{\mathcal{N}}}(t, \mathrm{T}_i, \boldsymbol{q}_{S})$ where $\boldsymbol{q}_{S} = \{\boldsymbol{q}, \dot{\boldsymbol{q}}, \ddot{\boldsymbol{q}}, \boldsymbol{\tau}, \dots\}$ defines the robot state feedback and T_i is a task (or a constraint).

4.5 Exemplary Context: Whole-Body Standing

In the following, an illustrative context is considered and the outcomes of this chapter are used to perform CABR.

Whole-body standing embodies a reoccurring situation in humanoids research: a robot standing and maintaining its balance while performing a task with one or both hands. Throwing an object like a light weight ball is an example of a task that can be described by such a context. Throwing objects has different use cases, for instance, in rehabilitation and a real world example of such a scenario is presented in chapter 6. Furthermore, this context presents a basis that can be scaled up to accommodate related contexts.

Consider a SoT as shown in figure 4.5, implemented as an iHQP using [66]. The highest priority tasks for the soles ensure the robot does not slide. The CoM task brings the projection of the center of mass to the center point of the support polygon convex hull. With reference to the notation introduced in (4.16),(4.17) take the task and the

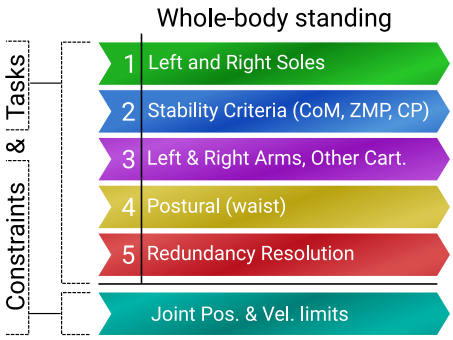

Figure 4.5: Stacks of tasks for humanoid whole-body standing context.

constraint for the center of mass at priority level 2 as

$$\mathrm{T}_2 \coloneqq [\![\mathbf{J}_{\mathrm{CoM}}, \dot{\boldsymbol{x}}^*_{\mathrm{CoM}}]\!]$$
$$\mathrm{C}_2 \coloneqq \left[\!\!\left[\begin{bmatrix} 1 & 0 & 0 \\ -1 & 0 & 0 \\ 0 & 1 & 0 \\ 0 & -1 & 0 \\ 0 & 0 & 1 \\ 0 & 0 & -1 \end{bmatrix}, \begin{bmatrix} 0.02 \\ 0.02 \\ 0.02 \\ 0.02 \\ 0.52 \\ -0.4 \end{bmatrix} \right]\!\!\right] \tag{4.32}$$

where C_2 defines a polytope that bounds the valid positions for CoM. $\dot{\boldsymbol{x}}^*_{\mathrm{CoM}}$ is controlled by a simple attractor that brings the CoM projection to the center point of the support polygon.

Due to the hierarchical structure of the SoT, the task for the arms (throwing in this case) is assigned without any negative influence on the robot's dynamic balance. This task —that exhibits its own sub-BR in the form of joint space redundancy resolution— can be viewed as follows: The EE of the arm first goes its current ($\boldsymbol{x}_{init}$) to a parking pose ($\boldsymbol{x}_{fin}$), for instance using a simple low jerk point to point motion:

$$\boldsymbol{x}(\tau)^* = \Delta\boldsymbol{x}\left[6\tau^5 - 15\tau^4 + 10\tau^3\right] + \boldsymbol{x}_{init} \tag{4.33}$$
$$\dot{\boldsymbol{x}}(\tau)^* = \Delta\boldsymbol{x}\left[30\tau^4 - 60\tau^3 + 30\tau^2\right] \tag{4.34}$$
$$\ddot{\boldsymbol{x}}(\tau)^* = \Delta\boldsymbol{x}\left[120\tau^3 - 180\tau^2 + 60\tau\right], \tag{4.35}$$
$$\Delta\boldsymbol{x} = \boldsymbol{x}_{fin} - \boldsymbol{x}_{init}, \quad \tau = \frac{t - t_{init}}{t_{fin} - t_{init}}. \tag{4.36}$$

From the parking pose, the arm performs the throwing motion trajectory. Such a trajectory can be obtained from the same equations or by using existing trajectory generation schemes for these types of tasks (e.g.,[74]). Alternatively it is possible to interpolate desired end-effector velocities between the parking, the throw and the stop points. In either case, the results are sent to the arm's QP task. Additionally, a suitable static posture or any other configuration of the arm must be provided as low level residual redundancy resolution for the BR purpose.

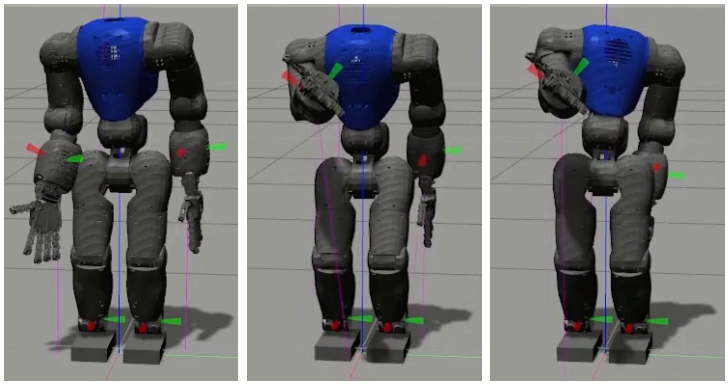

(a) Parking pose (b) Throw with BR (c) Throw without BR

Figure 4.6: Starting from same parking pose (a), the robot performs a throw. Snapshots (b) and (c) are the end pose of the robot with and without BR.

4.5.1 Constraining Waist Rotations

Body regulations of humanoids cannot be considered unilaterally since they could have conflicting side effects. It is shown that waist torsion plays a major role in humans' biomechanics [75]. The same applies to humanoids as well when they perform dynamic tasks such as throwing. Relaxing the constraint on the waist's rotation along the yaw (z-axis, the axis orthogonal to transverse plane, cf. figure 4.3) not only allows the robot to perform the task more efficiently, it also reduces the chance of conflict with other active BRs. A simple throw with postural Cartesian regulation is compared to a relaxed waist torsion in figure 4.6 to highlight this notion. Alternatively, when the task implies negotiation in environments cluttered with obstacles, or for complex manipulation tasks, all the constraints on the waist's Cartesian orientations can be relaxed to facilitate collision avoidance of the upper-body.

The body regulation for the whole-body standing context was evaluated in a dynamically consistent simulation. Throwing a ball is a relatively challenging task for a small size humanoid such as COMAN. Regardless, as shown in a series of snapshots in figure 4.7, COMAN was able to make the throw. Although these results are obtained from a realistic, dynamically consistent simulation, one might rightfully question their reproducibility on the real robot. There are two considerations to be made here: Firstly, the major contributing factor to a throw is the end-effector velocities and forces which in this case are generated based on the hardware specific joint limits. Secondly, with the current available technology, the robots' hands are too slow to release the ball in fractions of a second. This latter fact poses a challenge that cannot be resolved without the advent of faster articulated hands.

The human-likeness of the motion, as mentioned before, is hardly quantifiable. However, some metrics can be deduced regardless. In figure 4.6 for instance, comparing snapshots 'b' and 'c' shows the superiority of postural body regulation in generating natural looking

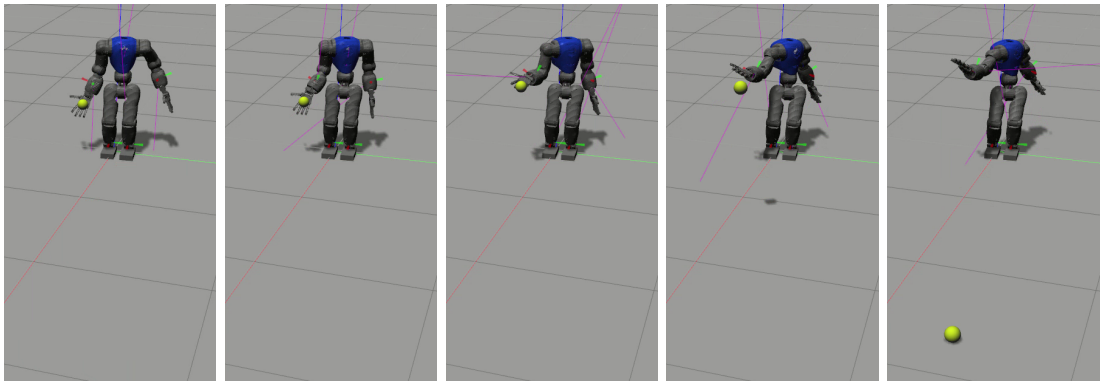

(a) (b) (c) (d) (e)

Figure 4.7: COMAN throw: (a) The robot starts at the parking configuration. The throw starts at (b), and by the time it is about to release the ball at (c), thanks to relaxed waist rotation along the z axis, it has gathered some momentum. After releasing the ball at (d), the robot's arm still continues its motion since instantaneous stopping would created instability. (e) The grid lines on the floor are 1m wide which means the robot has made a throw of approximately 2.5m which is impressive for a small size robot like COMAN.

motions. Another metric for the human-likeness of the motion is discussed later when the throwing is used in a physiotherapy application in chapter 6.

4.6 Discussion

This chapter addressed the formulation of humanoid BR based on QP formalism. By introducing a convenient notation, a number of tasks and constraints were defined which later formed the stacks of tasks. In the large scale, the SoTs define the body regulations for the contexts. On a smaller scale, each task within the SoT can exhibit sub-BR. It should be emphasized that there is no universal agreement on the correct hierarchy of tasks, however, what was proposed for the whole-body standing context follows a straightforward logic: first the stability and locomotion via the feet and the CoM tasks, then the manipulation by adding the arms tasks, and eventually postural regulation and residual redundancy resolution at the lowest levels. Such a SoT structure scales up well in locomotion contexts as it will be discussed later.

The theoretical and empirical aspects of this chapter are derived and conducted keeping in mind two important considerations. Firstly, the definition of contexts follows an inheritance scheme that mimics that of software engineering. Building the contexts from abstract to specific facilitates the body regulation planning, and accordingly the execution and deployment in terms of reusing. The second consideration is the distinction between CABR process and scenario specific inputs.

Take the task for the center of the mass as an example. The definition of the task makes no assumption about the governing input. It can be a simple attractor as it was the case

in the whole-body context, or it can be a complex scheme such as a stabilized walking pattern generator. In both cases, the task for the CoM is exactly identical and the SoT can be reused with no modifications. Similar argument is valid for the postural regulation tasks. For the presented context the yaw angle was allowed to change and contribute to the throwing motion. A different motion might need the explicit control of all degrees of freedom of the waist. Regardless, exactly the same task can be reused as *the QP tasks definitions do not make any assumption about the nature, type or the implementation of the body regulations*. If the context identification and/or body regulation planning are not task-agnostic, the reusability, scalability and composability of the tasks and body regulation can be compromised.

5 Deployment and Execution

The message that this thesis communicates is the need for systematic handling of secondary tasks and body regulation. So far, multiple contexts were identified and suitable body regulations for each context derived. These steps however, address two parts of context aware body regulation, namely, context identification and BR planning. The next step is implementing, deploying, and using (or rather, reusing) the regulation schemes when different contexts arise.

To *just implement and run them* would immediately falls back into the disorderly fashion that CABR tries to distance itself from. Instead, by adhering to software engineering principles that promote modularity and separation of concerns, the deployment and execution of body regulations can be elevated to a higher tier.

In section 1.3 three features —that are mostly a concern in software engineering— were pointed out that CABR attempts to achieve, namely reusability, scalability and composability. In all of the previously reported cases, the identification of the contexts and planning the body regulations have been performed keeping these goals in mind. Transforming these notions from theoretical into practical factors is accomplished by a component based software architecture. This software architecture named CoSimA [76], [77] is developed through the European project CogIMon [78] with the efforts of numerous developers including the author of the thesis. The CABR uses CoSimA as its underlying framework at the software level.

CoSimA promotes a systematic, model-based [79] approach to control architecture design that facilities achieving the aforementioned goals. Its design follows the principles of modularity and separation of concerns from software engineering to integrate functionality in a real-time safe environment with the aim to provide a blueprint for a reusable, hardware independent systems. It features transparent switching between robot and simulation, between different hardware or control paradigms, and the assimilation of non real-time components. It thereby supports a flexible yet systematic application development, while accommodating diverse and changing technologies.

The contents of this chapter and the effectiveness of the component based software architecture are supported by [49], [76], [77]. Special thanks go to all the coauthors for their contributions and to the developers of the architecture. In particular, to the lead development team, Joshua Smith, Dennis Leroy Wigand, and Dr. Enrico Mingo Hoffman.

5.1 Requirements

A sensible system architecture that alleviates the complexity, facilitates the development and grants scalability, is no easy feat given the complexities and difficulties of robotic experiments (or contexts, in the scope of this work). Furthermore, the nature of each context dictates certain requirements and specifications that the architecture should comply with. For instance, when there is direct interactions with humans, the users' safety is of utmost importance.

A number of such requirements are listed in this section. While these requirements do not holistically represent all robotic contexts, they are nonetheless applicable to many of them and most applications could benefit from these requirements and specifications.

R0. Safety

The system must be safe for the users at all times and under all conditions. The implementation (in the general meaning of the word) of this requirement often is not limited to the scope of software engineering. For instance in real world situations safety is mostly achieved by cages and harnesses. Its inclusion in the requirement list is motivated by multiple considerations. Firstly, a good architecture automatically reduces unforeseen circumstances, some of which potentially hazardous to the human counterparts. For example, real-time capabilities (cf. R1) are paramount to safely responding to measured interaction forces. Secondly, the architecture allows assimilation of non real-time components in to a real-time system. Among these non real-time components is the Virtual Reality (VR). In a VR experiment there is no direct interaction between the human and the robot. The use of VR furthermore allows the developers to test their controllers and algorithms in a test bed before exposing them to the users. Last but not least, a properly designed system architecture facilitates unit tests which in turn reveal edge cases that could become potentially hazardous.

R1. Real-Time

Real-Time (RT) requirements in robot experiments are well-known to be crucial. For standard manipulators the system become unstable if the response time of controllers violate the hard deadlines. Even though many robot software and controllers are Non Real-Time (NRT) yet fictional in some applications, unpredictability of response times makes them unsuitable for certain applications, particularly in torque control domain.

In humanoid robots, real-timeness is paramount in two major respects in addition to what was stated above: i) when the control scheme relies on timely communication between different components and ii) dynamic stability criteria of humanoid robots dictates sensing of the robot state (e.g., encoders, inertial measurement units, force/torque sensors, etc.) to be done at precise time intervals.

To highlight the significance of predictable response time, consider the example of COMAN walking on a straight line in simulation. Figure 5.2a,b depict snapshots of such an experiment once when all components respond on time (a), and once when

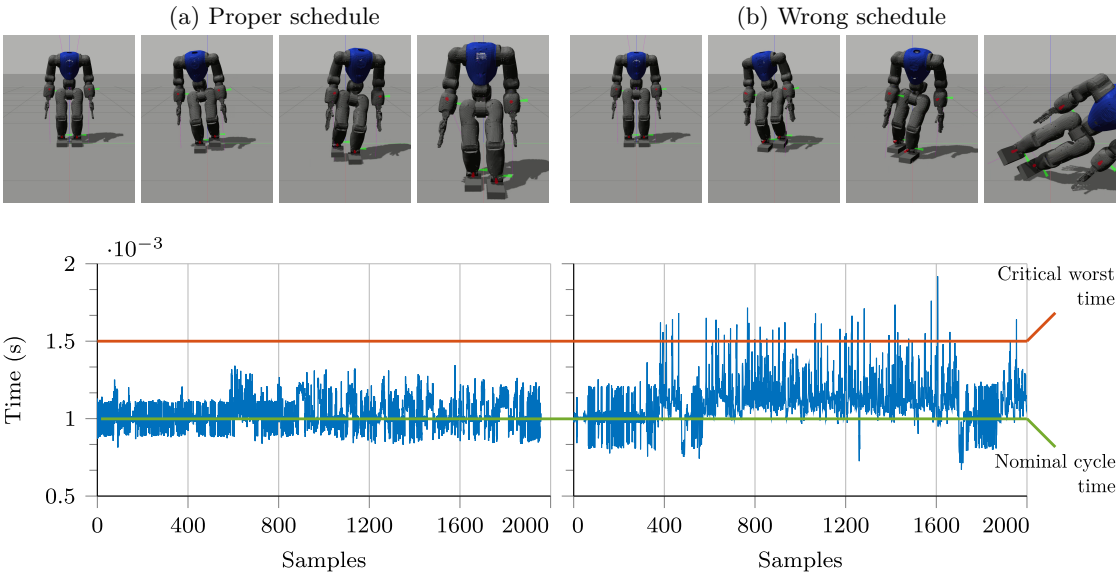

Figure 5.2: (a) All components meet their timing requirements according to the specification. (b) `CoMPrimitive` is intentionally slowed at 300th sample by introducing a constant delay of $\frac{1}{3}$ms. This causes the CoM to receive the desired values ($\boldsymbol{x}^*_{\text{CoM}}$) that are old and out of sync with respect to the real CoM values ($\boldsymbol{x}_{\text{CoM}}$) from the robot's feedback (cf. equation (4.19)). The critical worst time indicates at what stage the out of sync and old data causes failure, defining the hard real-time deadline.

the execution of a single component is impeded so that it misses its deadline (b). As seen in the figure, by its very first step (second snapshot) the robot is diverging from the path and loosing its stability. By the third step the robot is already about to fall. The figure 5.2 also shows the response time of `CoMPrimitive`, the impeded component, when it works properly and when it malfunctions. The difference is rather minute. To fully understand the effect of a single component on the whole network of connected components an introspection mechanism should be in place. Such introspection tools are described in detail in [77] and briefly in the next section.

Another aspect of real-time control of humanoids is isolation of non real-time components of the system so that their lack of reliable response time would not impede the execution of RT components.

R2. Secondary Requirements

Apart from R0 and R1 which are fundamental to proper execution of the robotic tasks, there are certain requirements which are not necessarily critical but highly desirable. Given the amount of engineering effort dedicated to design and implementation of these systems, it is worthwhile to make them flexible and reusable as long as they remain conformant to R0 and R1. Below, a number of general secondary requirements are listed, however, different contexts might demand further specifications and considerations.

System Transparency: It allows switching between different robots with minimum programming efforts. While there are platform specific parameters to be tuned (e.g., control gains), proper model-based abstractions can relieve the burden of switching by a considerable degree. The transparency also includes switching between the real and the simulated robots and reduces it to a simple plug-and-play of components.

Reusability: Among different applications, similar functionalities are required. For example, when dealing with dynamic balance of the humanoids, often times a stabilizer is necessary. The ability to deploy and reuse already existing components can drastically reduce the cost and complexity of the development process. Intrinsic properties of component-based solutions facilitate this aspect to a considerable degree. The reusability of components, furthermore, implies the ability to deploy third party algorithms which also facilitates the development, provided they adhere to the principles of component based design.

Adaptability to emerging technology: An often overlooked aspect of reusability is adaptability to new and emerging technologies. Improved algorithms, faster and more reliable solvers, and new middleware become available frequently, hence, a modern architecture must be able to integrate them with reasonable effort. The initial investment of time and development in respective architecture design will eventually pay off when it can be migrated to keep up with the changing technology demands.

5.2 Architecture

The context aware body regulation goals and the software requirements laid down above are addressed by a software architecture which is described in the following. Such an architecture should not only consider these explicit requirements, it also should be scalable to handle other demands as more complex tasks and contexts emerge.

5.2.1 A Component Based Approach

A component based environment, namely Orocos [80], acts as the underlying framework of the architecture. Component-Based Software Engineering (CBSE) has become a serious alternative to traditional methods of software development [81]. Similarly, component based robotics engineering has gained some attention in the past decade [82]. To truly appreciate the advantages of CBSE it is necessary to investigate the meaning of the "component"[1] and contrast it with object/class paradigm. While the definition is debated

[1] A classical example that is not strictly accurate but quite informative is a toolbar. A toolbar can be seen as a dynamic library that is loaded at run-time for different software (a word processor and a spreadsheet program for instance). The individual buttons (new, load, save, etc.) can be seen thematically as classes or single units that standalone cannot be deployed, however, they become deployable in the greater context of a component that offers a coherent set of functionalities (i.e., a file management toolbar).

among sources, the following notions for components are generally agreed upon, for instance in [81], [83], [84]:

- Components are binary (pre-compiled) units of computation that are deployed while objects are source codes that exist at run-time. Components could be made of objects though.
- Components implement well-defined interfaces. These interfaces and their behaviors should be well documented allowing procedure calls, and enforcing inter-component communications.
- The interfaces provide access to functionalities at a higher granularity level compared to classes. Furthermore, all the functionalities offered by the components are inter-related in a clearly outlined scope.
- Without access to the source code, components should be customizable allowing the user/developer to tailor them to their needs. This aspect further alleviates the reusability concern.

From these points it is clear that a component based system intrinsically lessens the complexity of reusability goal since the components —as opposed to classes— are self-sustained deployable units of computation in their own nature. In CABR's architecture, reusability is tackled by Orocos Component Library (OCL) while the deployment is handled by the *Orocos Deployment Component* and the *Deployer Application*.

5.2.2 Addressing the Real-Time Requirements

The RT requirements are handled by Real-Time-Toolkit (RTT) which is an integral part of Orocos. The RTT allows the exposure of ports[2], handles their communication and provides tools to create new typekits which permit transfer of custom data over the ports.

Some technologies (e.g., ROS [85]), hardware (e.g., certain sensors) and protocols (e.g., TCP/IP) are inherently non real-time. To orchestrate their execution alongside the real-time components, it is crucial to isolate them such that they do not compromise the execution of the RT units. At the same time, this isolation should allow synchronicity of the two units, i.e., any delay should be measured and handled. This challenge is resolved by Robotics Service Bus (RSB) [86]. RSB is a middleware that provides transport plug-ins for the RT and the NRT components, allowing them to communicate even if some components could be running on completely different machines or operating systems. It also keeps track of the network delays and latencies. Alternatively, if there are ROS nodes or stacks in the NRT unit, it is possible to use RTT-ROS-Integration as the communication channel between the two units. This is an example of transparency towards different technologies.

[2]Ports are RTT's communication channels that allow 1-to-1 and 1-to-n connections, as oppose to ROS for instance which opts for publisher/subscriber scheme. Ports furthermore, grant a wide range of functionalities for queuing of the messages.

Although the Orocos/RTT framework offers a RT environment, it still remains to ensure the system behaves according to the developers' intentions, both in terms of sequencing and the orchestration of many components in complex scenarios, and in terms of identification of faulty components, should errors occur. To this end, CoSimA extends the Orocos framework by introducing an introspection mechanism. Introspection function is two fold. Firstly, by extending RTT's `TaskContext`, it gathers information about specific ports, as well as the life-cycle state of the introspected components. The collected samples are then sent over specific transports depending on the used marshallers. Secondly, the introspection produces visualization and analysis toolbox that offer an enhanced timing diagram enriched with data-flow information. Figure 5.3 demonstrates an example of these visualizations for the simple walking experiment that was previously shown in figure 5.2. The details of introspection mechanism and other RT related intricacies of the architecture can be found in [77].

5.2.3 Addressing the Secondary Requirements

To address the secondary requirements, a larger number of functional components are provided at different granularity levels and classified based on their operational objective.

1. Robot Models and Interfaces

Low level components wrap around the robot drivers and their simulated versions. The exposure of identical interfaces and ports across real hardware and simulation, as well as between different robots, is achieved through a model-based approach that resorts to common abstractions.

The task to read and write from/to the robots' low-level drivers, and to mediate and broadcast the hardware related information, is implemented in a single component named *rtt_robot* (cf. figure 5.4). It is parametrized w.r.t. to the URDF and SRDF (Unified/Semantic Robot Description Format) files and is the only part of the system that needs to be implemented according to the specific robot driver protocol or simulation environment. Therefore, switching from simulation to the real robot or between robots, reduces to switching a single component and adjusting control parameters or actuator gains. It should be emphasized that adhering to identical interfaces when designing robot specific driver wrappers could be challenging. The structure of *rtt_robot* for COMAN+ is briefly described in [48]. It presents examples of the challenges that the developers face and considerations that they make when creating reusable robot components that follow these standards.

2. Kinematic Chain Abstraction

Kinematic chain abstraction was briefly mentioned in section 4.4. Concretely, kinematic chain abstraction, as shown in figure 5.4, is based on the robots' URDF and SRDF information. The URDF describes the kinematics and dynamics information of the robot such as inertia matrices, joint locations and limits, etc. SRDF instead, encapsulates all

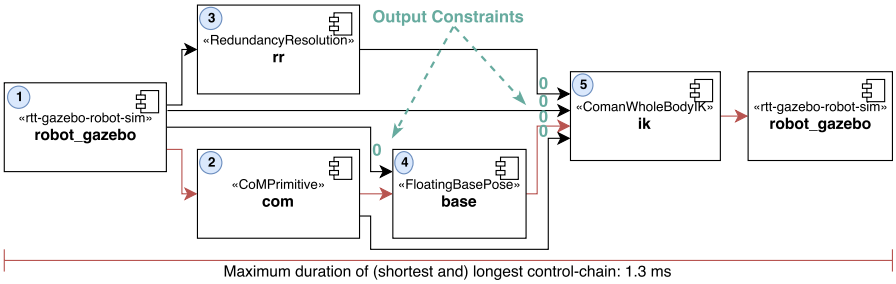

(a) The data-flow of simple walking in figure 5.2 and its introspection below. 1) The simulation component of the robot, 2) Suitable trajectories for the CoM and the feet required for walking, 3) Naive redundancy resolution, 4) Floating based estimation required for walking, 5) The inverse kinematics of the humanoid that generates walking motion provided CoM and feet trajectories.

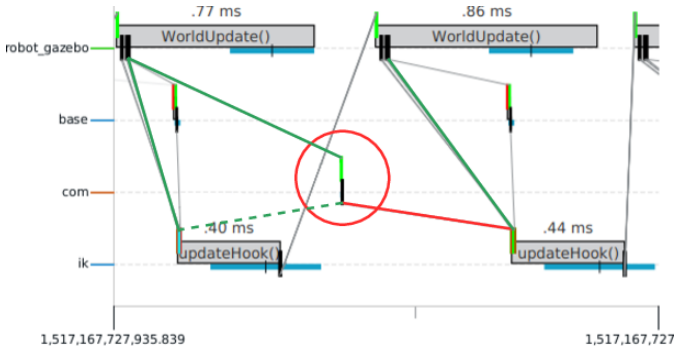

(b) This diagram shows a wrong specification, in which `CoM` is running in a separate activity and is slightly misaligned to `base` and `ik`. Here, `CoM` is executed after `ik` by means of artificial impediment, so it sends its data to the *next* iteration of `ik`. This means that `ik` operates on "old" data, which causes the behavior seen in figure. 5.2. The green lines indicate the correct data-flow, whereas the red lines indicate the actual but wrong data transfer.

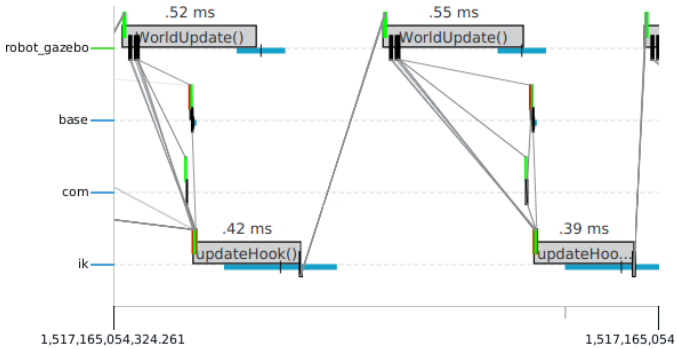

(c) Time diagram with data-flow information of the correct specification. `CoM`, `base`, and `ik` are deployed in the same activity. The components are executed in the right order and `ik` only receives input data that is based on the current cycle. Short vertical lines represent output (black) and input ports with (green ≡ new, cyan ≡ old, red ≡ no) data.

Figure 5.3: Introspectio of proper and wrong scheduling of the walking components in figure 5.2.

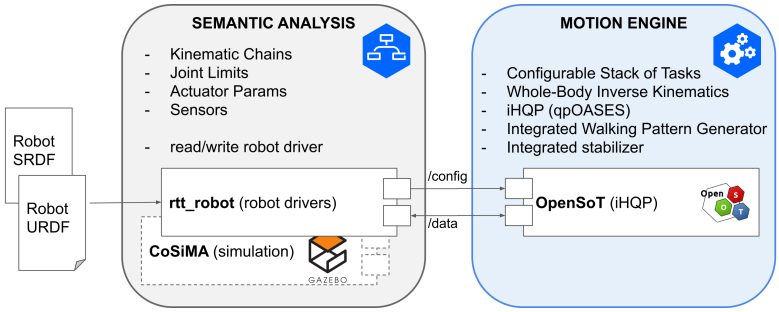

Figure 5.4: Semantic analysis and kinematic chain abstraction of robot models: kinematic and dynamic information for joints and links from URDF and semantic information like kinematic chains from SRDF are parsed, grouped, and exposed as interfaces to different components including the control side. Likewise, the motion engine is configured according to the information broadcasted by the components in the semantic analysis block. For instance, the SoT is pre-configured with suitable joint position, velocity and torque (effort) limits extracted from the URDF. Furthermore, default tasks for the kinematic chains extracted from SRDF can be generated on the fly, courtesy of [66], [87]. These abstractions are shared among all components.

necessary information regarding kinematic chain structure, available sensors, and actuator PID gains. At configuration time, these description files are parsed and appropriate interfaces are exposed to the users (components, drivers, etc.) automatically. Resorting to this abstraction mechanism, the developers can operate the robot based on conceptual entities such as the *right-arm* instead of dealing with an $n-$vector of the whole body configuration. This design paradigm not only alleviates the reusability in general, it also complies with reusability in the scope of context aware body regulation.

3. Functional and Control Components

Leveraging on the OCL and Orocos deployment tools, a large number of components operating on a wide range of functionalities have been developed by numerous developers and researchers throughout the course of the CogIMon project. This includes, but is not limited to, walking pattern generators, stabilizers and trajectory planners as well as loggers and helper tools. These components are deployed in real or non real-time units depending on their internal implementation.

The centerpiece of functional components is the *motion engine*. At its core, motion engine implements the iHQP based SoT that was described in section 4.3 and is utilized in humanoids body regulation evaluations. Bilateral bound constraints (such as joint limits) are extracted from the URDF model of the robot and automatically integrated in the solver. Furthermore, the kinematic chain definitions from the SRDF description are used to create Cartesian tasks for all the robot chains. This accelerates the development process considerable as the roboticists need not to deal with the derivation of Jacobians and operations at joint level.

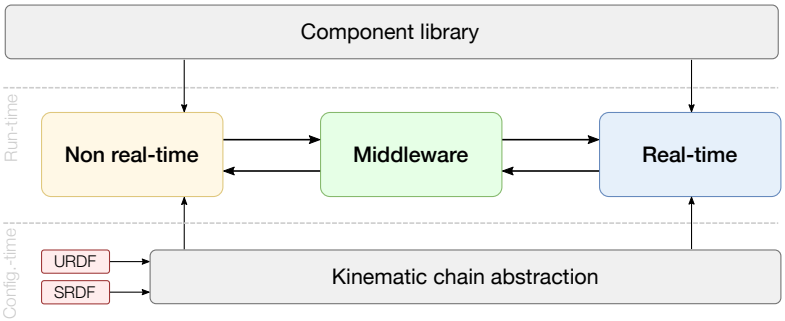

Figure 5.5: A bird's-of eye of the overall architecture

Motion engine implementation is not necessarily limited to the QP formulation. It is possible, for instance, to use the projection-based approach as well. In this regards and with an emphasis on transparency towards the technology, an alternative motion engine implementation is available based on a novel dynamically consistent null-space projections [88] that even allow a smooth rearrangement of the task hierarchy at runtime. This setup, however, requires somewhat extra manual work as integration of bilateral constraints in projection based schemes are not as straight forward as in iHQP.

5.2.4 The Architecture as a Whole

Putting all pieces together, the main concepts of the software architecture are presented in figure 5.5. At the configuration time the semantic analysis performed over the robot description files create the kinematic chains. The component library provides building blocks of the real and non real-time units. These components can be configured using the kinematic chain abstractions (e.g., default tasks for the arms as well as automatic generation of bilateral constrains such as joint limits). The communication between RT and NRT is strictly performed using a middleware. Figure 6.3 in the next chapter demonstrates a finer granularity of this structure in the scope of a real world application.

This chapter ends by mentioning an important fact. Developing wrapper components, robot interfaces, controllers, etc. can be challenging. The problem gets further complicated when these components have to adhere to unified interfaces. However, these difficulties are rewarded by exceptionally straightforward integration process. For instance, in the simulation environment for the assessment of the transparency requirements, it was possible to deploy a walking controller on the COMAN robot even though it was originally designed for the COMAN+ platform. For this test, the switching was merely a matter of connecting Orocos ports to different inputs. All aspects, including different DoF-size and structure, were handled automatically thanks to suitable abstractions, exposure of identical interfaces and a modular design.

6 Real World Applications of CABR

Chapter 4 discussed the theoretical background for humanoids body regulation and chapter 5 addressed the practical implementation concerns. With that background, this part of the thesis studies two real world case examples of CABR. First, the whole-body standing context that was introduced previously alongside the humanoids BR in chapter 4 is used directly in a physiotherapeutic juggling application. The same context is then scaled up to accommodate an assisted walking/joint object carrying scenario. Both of these experiments have uses in rehabilitation with important implications for the general public. After this small introduction, a brief motivation for humanoid assisted rehabilitation is presented to highlight these implications.

6.1 Humanoids Assisted Rehabilitation

At the time of writing, many countries in the world are facing an aging problem and a demographic shift. According to a report by the European Union [89], by 2020 a quarter of the EU population will be above the age of 60. This demographic shift puts a burden on the social service workers and the tax payers. Additionally, the same aging problem will impact the healthcare providers themselves which in turn aggravates further the issue.

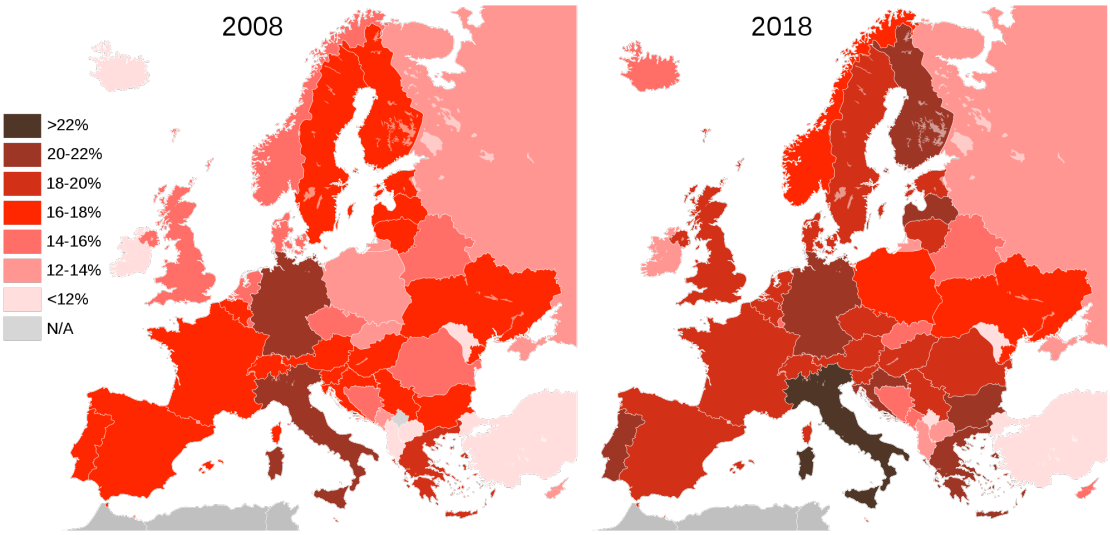

Figure 6.1: The growth of the EU population over the age of 65 between 2008 and 2018. This trend is expected to continue and it is not necessarily limited to the EU (e.g., Japan).

In parallel, thanks to advances in medical science, there are increasing number of patients surviving medical emergencies, such as stroke, who are left with minor to severe functional motor impairments, and other patients with motor impairments like cerebellar ataxia. The changing demographics and increased number of patients surviving emergencies, together, heighten the demand for case specific physiotherapy procedures that aim to enhance their functional ability and renew their involvement in daily life.

Among the treatments for age related complications are physiotherapeutic juggling [90] where the patient and the therapist throw a light weighted ball back and forth. These exercises are shown to be motivating, challenging and can induce brain plasticity [91], [92]. They also have positive impact for brain stroke patients and those suffering from Parkinson's disease [93].

To be effective, such physiotherapy procedures have to employ an intensive intervention, which is demanding, task-specific and motivating and is primarily based on rote exercise. Often such rehabilitation therapy involves daily one-on-one interactions with the therapist and can last for extended periods of time. Overall, the physiotherapy process places a significant load on the therapists and the healthcare providers.

A possible solution to mediate this problem is using robots in the rehabilitation field. However, in the particular case of physiotherapeutic juggling practice, the direct use of humanoids poses several challenges. The current humanoids are not yet cost effective, and more importantly, nor are they reliable enough to be deployed, particularly to the members of the society with the need for special care. Virtual reality is an intermediate solution that lessens the burden on the therapists and exploit the humanoid potentials. In VR, the robot is reliable, predictable and never suffers from overheating or other complications related to excessive use of hardware. Furthermore, the VR headsets are becoming more affordable on daily basis as a result of a large scale use in the entertainment industry. It is crucial though that the dynamics and physics of the robot motions are consistent and they are rendered to the patients with no perceivable delay.

There are already some ongoing research on adoption of VR in physiotherapy with human avatars [94]. Using a simulated robot instead of a human avatar is based on three considerations. Firstly, the uncanny valley [95] problem remains an unsolved issue when human face and body is depicted. For a humanoid robot on the other hand, mechanical motions and unhuman postures are perfectly acceptable. Secondly, there are some studies that suggest in certain cases, children respond positively towards robots compared to humans (avatars) [96]. Lastly, using humanoids constitutes an intermediate steps towards more prominent application of robots in rehabilitation. VR in this regards, acts as a test bed to identify potential problems and assess applicability of humanoids.

While the physiotherapeutic juggling in VR is at a stage that can be used by real patients, there are other possibilities to exploit humanoids for rehabilitation that are not still at a readiness level to be deployed to the general public. However, there are intermediate steps being made towards such applications [76]. An example of these early stage scenarios are assisted walking and joint object carrying.

They are motivated similarly by the increased demand in the domestic care domain. In assisted walking the robot should be able to understand and detect the human

counterpart's intention and react accordingly by making suitable motion, often in the form of taking steps. Although exposing the elderly to humanoids is not yet reasonable due to safety concerns, the research in this field is justified as it provides insight about the nature of non-verbal communications, interactions, and intention detection.

Intention detection and reaction in loco-manipulation has been approached from two distinct angles: i) focusing on the locomotion by designing specific walking pattern generators; ii) addressing the problem from the interaction quality point of view.

In the first group there are most notably the works in which a walking pattern generator is tailored to respond to human intentions by performing suitable steps [97]–[99]. In this camp the intention detection is often achieved by measuring the interaction forces from wrist mounted force/torque sensors. Thus, the interactions must occur downstream of the sensors.

In the second camp, where the focus is more inclined toward interaction and intention detection, the problem is often tackled by using external sensors. For instance, the human counterpart's motive is interpreted using verbal communication in [100], by exploiting computer vision in [101], and by designing a cost effective tactile sensor [102]. Although, the last work is mostly intended for industrial manipulators. Alternatively, the humans' intents can be recognized by machine learning and classification techniques, for instance, in [103]. Later in this chapter, a new context named whole-body loco-manipulation is presented by scaling up the whole-body standing context. This new context incorporates another form of intention detection that falls into the second group and is based on the aggregated manipulabilities of the humanoid's arms.

6.2 Case Study 1: Whole-Body Standing Context and Physiotherapeutic Juggling in VR

Recall the whole-body standing context where a humanoid is standing still, maintaining its dynamic balance and attends to Cartesian tasks with its either or both arms. In section 4.5 this context was used to throw a light weight ball. The stack of task for such a motion is revisited in figure 6.5.

The same SoT can be used for physiotherapeutic juggling. This fact, demonstrates one of the fundamental aspects of context abstraction: a single context present multiple applications of similar nature. This observation, however, is dependent on another fact. For the new juggling application, the trajectories for the throwing arm is no longer provided from a trajectory generation module. Instead, the trajectories for the therapeutic juggling were obtained by tracking professional therapists throws first, and then reshaping and retargeting [104] them for humanoids. Regardless of the input source of the throwing trajectories, the SoT is remained unchanged, which once more signifies the importance of separation of concerns and input agnosticity.

The retargeting phase ensures that desired end-effector trajectories mapped from the human, respect the robot's workspace limits (cf. figure 6.2). Moreover, the actual recordings from the therapist can be used for low level joint space redundancy resolution input of (4.22) as sub-BR to mimic a human-like motion.

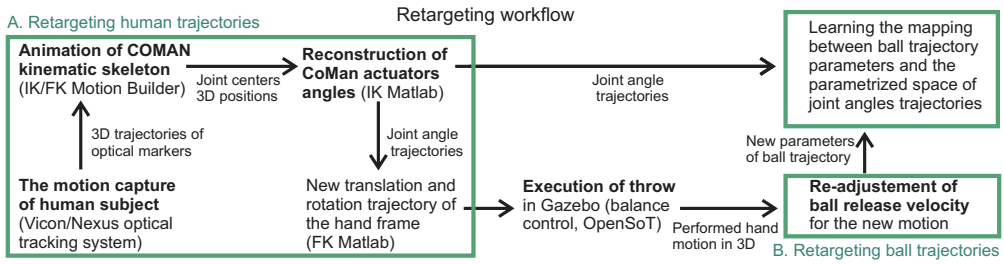

Figure 6.2: Trajectory retargeting workflow consists of three major steps: A. Human captured kinematic trajectories for the robot; B. Offline reevaluation of motion using robot constraints and the retargeting of the ball trajectory; and C. Machine learning of the mapping from ball trajectory parameters to parametric space of kinematic motion primitives for generative motion synthesis.

In order to keep the users engaged, the interactions with the simulated robot via virtual reality goggles should be natural and physically consistent. This requirement implies that the robot needs to be dynamically simulated which in turn, as it was shown in figure 5.2, demands real-time communication among the components. However, the communication with the VR headset is inherently non real-time. This challenge is resolved by the transparent software architecture described in the previous chapter. Figure 6.3 depicts the CoSimA setup for the physiotherapeutic juggling.

6.2.1 Integration of VR

A bird's-eye view of the architecture by considering a single iteration of the throwing of a ball in the physiotherapy application is seen as follow. Depending on the specific needs of the patient based on their physique and the nature of their therapy, the therapist selects a throw point for the ball via the *VR agent* in the non real-time unit. The RSB middleware communicates this point to the *trajectory generation* component in the real-time unit. Note the strict separation of RT and NRT loops. This component computes an end-effector trajectory for the arm of the robot (or any other appropriate kinematic chain for that matter) which determines the desired interception point of the ball by the patient, and sends its results to the *Motion Engine* over Orocos/RTT ports. The *motion engine*, equipped with the kinematic chain abstraction information, solves the differential kinematics problem taking into account the joint position and velocity limits of the chain provided by URDF/SRDF, and Cartesian constraints gathered by the context and the task specifications. Solving the SoT, the desired joint motions are sent to the robot drivers, or in this case to the simulator which exhibits the same kinematic chains interfaces. All components within the RT unit receive the robot's feedback state ($\boldsymbol{q}_s$) directly. The simulation time or the robot's internal clock is considered as the reference clock and other components synchronize their execution with it using RTT's `TimeService`. Concurrently the robot's feedback and clock are sent to the NRT components indirectly, via RSB where the robot motions are rendered for the patient by the VR headset. The robot service bus tracks all the network latencies and delays, and informs the components

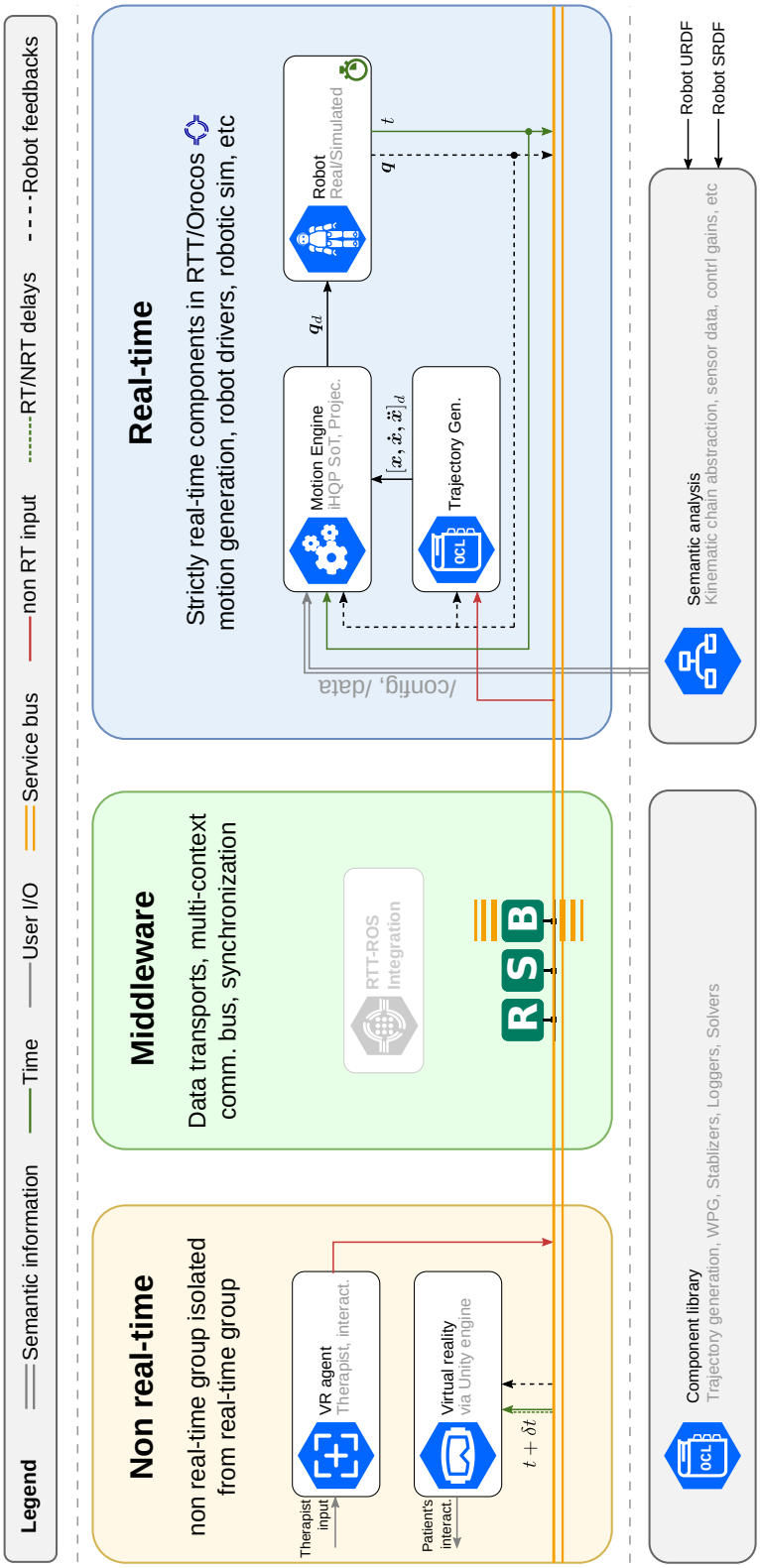

Figure 6.3: The component based architecture in a real world application: The system comprises three major units; real-time and non real-time units as well as a middleware that handles the communication, synchronization and data-transport between the two. In the case of physiotherapy application, the robot service bus plays the middleware role, while in other contexts RTT-ROS-Integration or other middleware could be used. Building blocks of RT and NRT units are components which constitute a component library and are deployed by Orocos' deployment mechanism and environment. Semantic analysis (cf. figure 5.4) provides inputs to different components including the *motion engine*. (cf. figure 5.5)

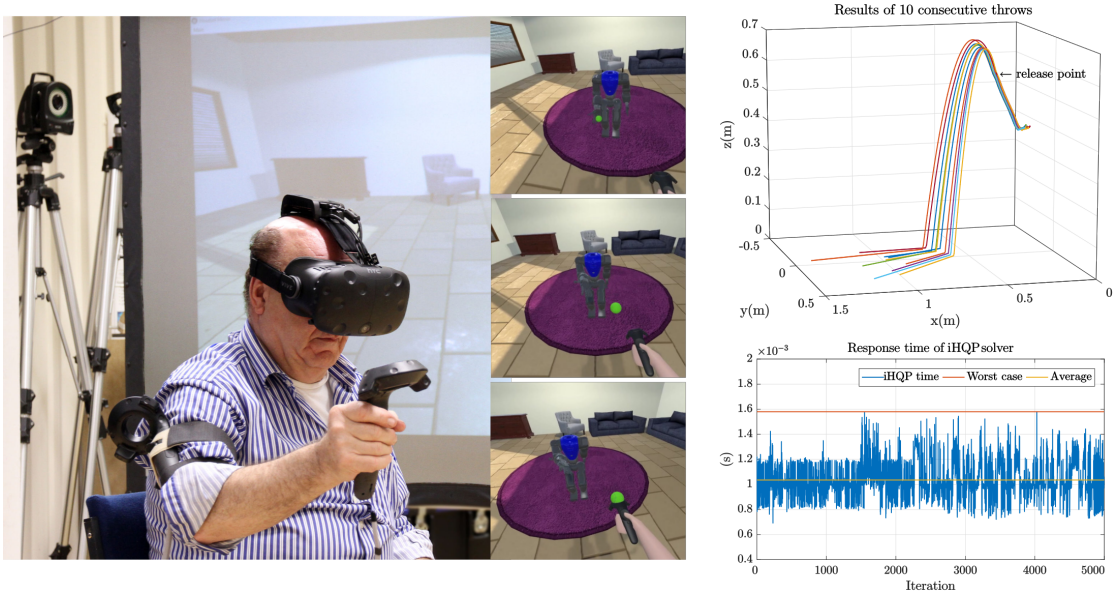

Figure 6.4: Experimental results from physiotherapeutic juggling in VR: Left: a volunteer patient performing the catching exercise alongside snapshots of the view through the VR goggles. On the right, the results of 10 consecutive throws on the top, and the response time of the iHQP solver on the bottom, are depicted. Note that these trajectories are different from those of figure 4.7. They are substantially shorter in range to accommodate the physiotherapy demands.

on either side if their functions might be affected by imprecise NRT responses. RTT's port system offers mechanisms that enables the components to conditionally act if the received data is old, new or buffered.

6.2.2 Physiotherapeutic Juggling with Patients

With this setup, the whole experiment was first conducted with healthy laboratory staff to gather their feedback regarding VR-assisted robot interactions. This phase aimed at assessing the quality of the body regulation, comfort level when using virtual reality googles, and evaluating the feasibility of the throwing/catching exercise before exposing the setup to the real patients. Upon the positive feedback from the healthy users, a volunteer patient was introduced to the training as shown in figure 6.4. The volunteer had performed similar juggling exercise in VR before, however, with a human avatar. Despite not being acquainted with a humanoids previously, the patient quickly became familiar and comfortable with the setup after only few throws. Although, the impact of previous experience with the human avatar on the success rate cannot be disregarded.

The repeatability test as seen in figure 6.4 shows reliability of the control scheme. Small deviations in the landing point of the ball are due to the variations in the physics engine randomness and its impact on the robot's spawn location and the simulated release

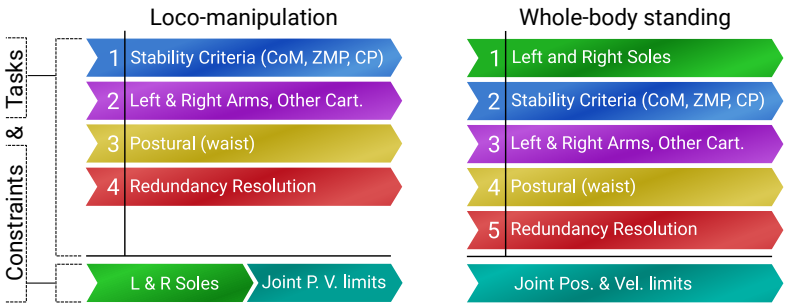

Figure 6.5: Stacks of tasks for humanoid contexts. In loco-manipulation, the sole tasks are inserted as constraints in order to achieve better computational performance, although this is an implementation specific optimization.

mechanism —which for the purpose of therapy practice is a welcomed side-effect since it mimics human throws' imperfections.

6.3 Case Study 2: Whole-Body Loco-Manipulation Context and Assisted Walking

A more realistic, technically challenging case is the BR in whole-body loco-manipulation context.This context is distinguished by the humanoid walking while performing a manipulation task with hands and possibly attending to other objectives. As shown in figure 6.5 the SoT is quite similar to the previous context. Indeed, this SoT is obtained by scaling and reusing the BR from the whole-body standing context.

Many human-humanoid interactions can be presented by this context, e.g., cooperative bi-manipulation, hand-in-hand movements, and so on. This setup presents another similar application. Consider the robot and the human, that instead of their hands, are connected by a rigid object such as a table top. This can be viewed as an application in joint object carrying. Note how the same context presents different applications. The hand-in-hand motion is studied here as an intermediate step towards the realization of assisted walking with humanoids.

Given that this context involves walking, it is convenient to reconsider the generalized coordinates of the humanoid robot. Hence, the generalized coordinates of a humanoid robot with n degrees of freedom can be defined as the vector of joint values $\boldsymbol{q}_\mathrm{j}$ and the position and the orientation of another link or body. This does not create any conflict or inconsistencies with previously introduced notation. Indeed, all aspects of the iHQP and the SoT hold in this notation, however, it is necessary to introduced a selection matrix that isolates the actuated joints when commanding the robot. Consider the configuration space notation proposed in [105] as

$$\boldsymbol{q} = \begin{pmatrix} \boldsymbol{q}_\mathrm{CoM} \\ \boldsymbol{q}_\mathrm{j} \end{pmatrix}, \tag{6.1}$$

where $\boldsymbol{q}_{\text{CoM}} \in \text{SE}(3)$ is the pose of a frame attached to the center of the mass of the robot and $\boldsymbol{q}_{\text{j}} \in \mathbb{R}^n$ are the actuated joints. The configuration space of the robot, hence, is $\boldsymbol{q} \in \mathbb{R}^{6+n}$.

The notation laid out so far is conveniently independent of the desired input for all kinematic chains. This serves CABR well since different WPGs can be employed in the loco-manipulation context. Consider the motion scheme of a *generic* WPG as

$$\hat{x}_{k+1} \leftarrow \text{WPG}(\hat{x}_k) \leftarrow \dot{\boldsymbol{x}}^*_{\text{CoM}}, \tag{6.2}$$

$$\dot{\boldsymbol{x}}^*_{\text{CoM}} = f(\boldsymbol{q}_S), \tag{6.3}$$

where $\hat{x}_k$ is the current system state as described, for instance in [106], [107]. The latter work is used in the experiment of this context. The WPG takes the desired walking direction in forms of the velocity of the center of CoM input and computes the next system state $(k+1)$.

6.3.1 Intention Detection in Human Interactions

Both joint object carrying and assisted walking depend on i) assessing the interactions, ii) detecting the human's intention and iii) reacting accordingly [48]. Previous section named few approaches of intention detection such as verbal communication or relying on additional sensors. Here, the impedance properties of COMAN+ are exploited to handle intention detection in a new fashion. Furthermore, tackling this problem using intrinsic characteristics of the robot at a kinematic or dynamic level, not only allows seamless integration of any humanoid regardless of its structure, it also eliminates the dependency on external sensors which might not be offered by some platforms.

The heuristic used here is inspired by humans' behavior in similar situation. Consider two persons carrying a table top, one assuming the leader role and the other the follower. Also consider there are no verbal or visual communications. Thus, the only way of responding to the leader's intentions are by interpreting their interactions. If the follower has fully stretched arms, probably it is necessary to make a step forward. Similarly, when the follower's arms push inwards, or pulled to the sides, it signals the leader's movement towards the follower or to the sides respectively.

The function f in (6.3) maps the robot's state $\boldsymbol{q}_S = \{\boldsymbol{q}, \dot{\boldsymbol{q}}, \ddot{\boldsymbol{q}}, \boldsymbol{\tau}, \ldots\}$ into suitable inputs for the WPG. The problem of detecting and reacting to the human's intentions and interactions then reduces to obtaining a suitable definition of f, which is related to the singular values and the left singular vectors of the robot's arms Jacobians, obtained from

their SVD. Recall the SVD of a kinematic chain from (1.2) as

$$\begin{aligned}
\mathbf{J}^{\text{arm}} &= \mathbf{U}\mathbf{\Sigma}\mathbf{V}^{*}, \\
\mathbf{U} &= [\boldsymbol{u}_1, \boldsymbol{u}_2, \ldots, \boldsymbol{u}_m], \\
\mathbf{V} &= [\boldsymbol{v}_1, \boldsymbol{v}_2, \ldots, \boldsymbol{v}_n], \\
\mathbf{\Sigma} = [\text{diag}(\sigma_1, \ldots, \sigma_m)|0] &= \left[\begin{array}{cccc|c} \sigma_1 & & & & \\ & \sigma_2 & & & \\ & & \ddots & & 0 \\ & & & \sigma_m & \end{array}\right],
\end{aligned} \tag{1.2 revisited}$$

and the volume of the velocity manipulability ellipsoid as

$$v = c_v \cdot \prod_{i=1}^{m} \sigma_i, \tag{1.5 revisited}$$

$$c_v = \begin{cases} (2\pi)^{m/2} \cdot (2 \cdot 4 \cdots m)^{-1} & \text{if } m \text{ is even,} \\ 2(2\pi)^{(m-1)/2} \cdot (1 \cdot 3 \cdots m)^{-1} & \text{if } m \text{ is odd.} \end{cases}$$

Take the motions on transverse (horizontal) plane by considering the first two rows of the Jacobian ($m = 2$, $c_v = \pi$). The left singular vector ($\boldsymbol{u}_m$) associated with the smallest singular value (σ_m) signals the direction where the robot is least capable of generating velocities on the XY plane. The $\boldsymbol{u}_m$, σ_m of each arm, as well as the volume of the manipulability ellipsoid v, are utilized to compute suitable velocities for the CoM as control input for the WPG according to (6.2).

For many anthropomorphic arm mechanisms with shoulder-elbow-wrist structure — which includes common humanoid arms— one of the singular configurations is a fully stretched arm. Consider the robot with almost fully stretched arms. Such near singularity configurations could be handled by a suitable forward step that decreases the condition number ($\frac{\sigma_1}{\sigma_m}$) of the Jacobian.

With this consideration, the function f in (6.3) can be verbally described as follow: Observe the manipulability v of each arm and when it hits a threshold v_d, command the WPG to take a step based on $\boldsymbol{u}_m, \sigma_m$ in a direction that brings v back into a safe range and decreases the condition number of the Jacobians. Or more formally:

$$\dot{\boldsymbol{x}}^{*}_{\text{CoM}} = \begin{cases} \frac{\boldsymbol{u}^{\text{L}}_m}{\sigma^{\text{L}}_m} + \frac{\boldsymbol{u}^{\text{R}}_m}{\sigma^{\text{R}}_m}, & \text{if} \quad (v^{\text{R}} \leq v_d) \vee (v^{\text{L}} \leq v_d), \\ 0, & \text{if} \quad (v^{\text{R}} > v_d) \wedge (v^{\text{L}} > v_d). \end{cases} \tag{6.4}$$

In (6.4), super-scripts 'L' and 'R' denote the left and the right arms. This concept is depicted in figure. 6.6b.

6.3.2 Considerations on Intention Detection Function

Alternative definition of f: It is tempting to define the function f as the distance between the robot's waist (or other suitable points) and the bisection point of an imaginary

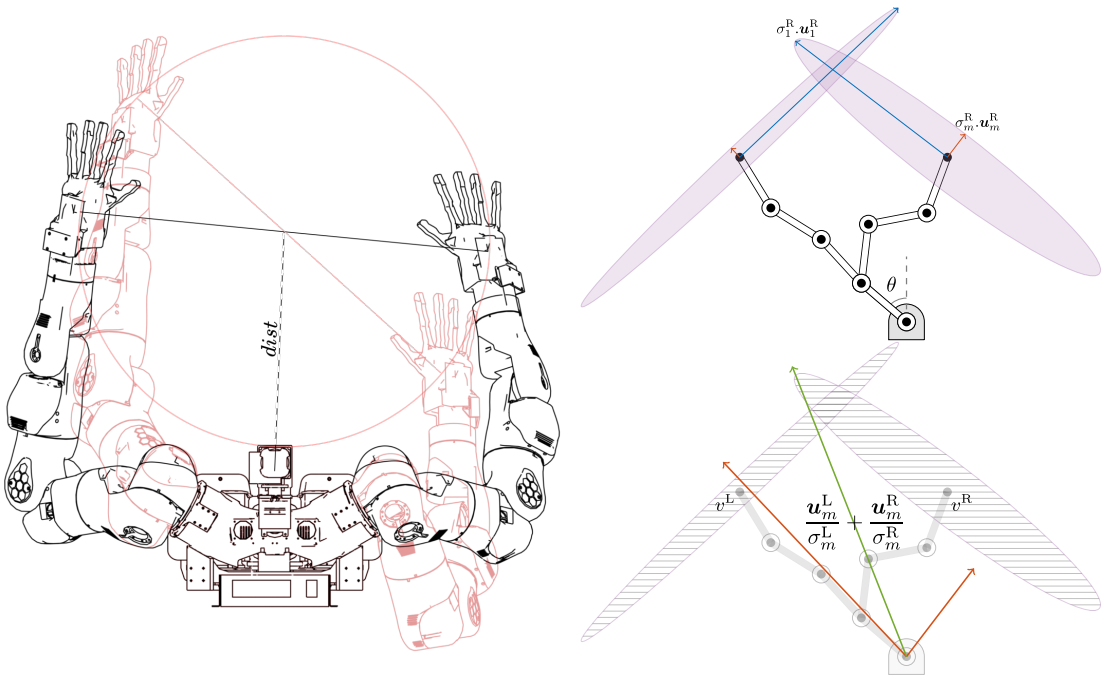

(a) Incompleteness of distance as heuristic (b) Simplified representation of f

Figure 6.6: (a) Infeasibility of distance as f: the configurations shown in black and red are within the same distance to the torso, however, the red configuration clearly requires a forward step to the left while the robot in black configuration should remain unmoved. (b) On top, manipulability ellipsoid of a simplified model of the robot arms alongside the semi-axes are shown. The red axes show the singular vectors related to the smallest singular values. On the bottom, these axes are scaled by the inverse of σ_m (projected at the base). The sum of the two shows the walking direction indicated by the green arrow.

line connecting the arms' end-effectors. As is shown in figure. 6.6a, this is an incomplete measure as it fails to distinguish between vastly different configurations.

Exploiting the arms' manipulability offers another advantage compared to the use of wrist-mounted sensors. Relying on the wrist sensors implies that the interaction must happen downstream of the sensors, however, the arms' manipulability as the basis of the intention detection function allows the interactions to happen at any point on the arms.

Relationship to joint velocity limits: An important implication of (6.4) is in its relationship to joint velocities. Consider two configurations $\boldsymbol{q}_1$ and $\boldsymbol{q}_2$, the first one with suitable manipulability ($v_1 > v_d$) and the second one with significantly smaller manipulability $v_2 \ll v_d$. If reacting to human interaction requires certain joint velocities, it is possible to show that $\|\dot{\boldsymbol{q}}_2\| \gg \|\dot{\boldsymbol{q}}_1\|$ and in near singular configurations $\|\dot{\boldsymbol{q}}_2\|$ will most likely violate the joint velocity limits. Choosing v_d in (6.4) conservatively makes sure that robot will take a step before it reaches a state that would result in joint velocity violation. Indeed, v_d dictates the robot's agility in reacting to the interactions (large

values mean the robot reacts sooner while with smaller values, the robot will linger before committing to a step).

Addressing the backward steps: An important issue to address is the problem of detecting the necessity of backward steps. This problem is tackled by exploiting the volume of the *force* manipulability ellipsoid $(\boldsymbol{\sigma}_1 \cdot \boldsymbol{u}_m)^{-1}$ according to (1.7). The rationale is that with arms stretched away from the body (which requires a forward step) the robot has a higher force transmission factor while at configurations with similar velocity manipulability but closer to the body, the arms have a smaller force transmission characteristics. Force manipulability index is not directly used here, rather it is exploited as an indicator for deciding whether to step forward or backwards. Alternatively, it is possible to use the time derivative and the rate of change of singular vectors, taking into consideration the orthogonality constraints of the components [108].

6.3.3 Postural Regulation

Similar to the previous context, postural regulation governs the waist's Cartesian orientation. However, in this case a low level postural task attempts to align the lower and the upper body of the robot by explicitly regulating the yaw angle of the waist. This angle, denoted by θ in figure 6.6b is controlled by

$$\omega = \dot{\boldsymbol{x}}^*_{\text{CoM}} - \langle \dot{\boldsymbol{x}}^*_{\text{CoM}}, \hat{\boldsymbol{n}} \rangle \cdot \hat{\boldsymbol{n}}, \tag{6.5}$$

$$\boldsymbol{q}_{\text{W}}[z] = \text{atan2}(\omega_y, \omega_x), \tag{6.6}$$

where ω is the projection of the CoM desired velocities on the horizontal plane denoted by $\hat{\boldsymbol{n}} = (0, 0, 1)^T$ and the waist's yaw is regulated by (6.6).

The significance of keeping the angle θ under control results from the hybrid nature of interaction and locomotion. That is, the robot is under interaction continuously, however, the stepping reaction takes place discretely at step-duration intervals. Regulation of the waist in (6.6) allows the robot to respond to the interactions continuously and its upper/lower body alignment is recovered within multiple steps. Being included as a low priority task ensures the convergence happens at a slow pace, imitating the humans' response in similar situations.

6.3.4 Stabilization of the CoM

The WPG in this context generates desired trajectories for the CoM as well as the swing feet, however, given the uncertainties arising from the nature of human interactions, the unstructured environment, and the simple model assumption it is necessary to add a stabilization term to the CoM trajectories.

Consider the linear inverted pendulum model [109] of a humanoid. Since the motion of the CoM is restricted to the XY plane by the WPG, the model reduces to the cart table model [106] depicted in figure 6.7. By introducing a spring-damper mechanism some of the problems resulting from the uncertainties can be alleviated. The ZMP is computed based on [110] from the readings of the ankle mounted force/torque sensors.

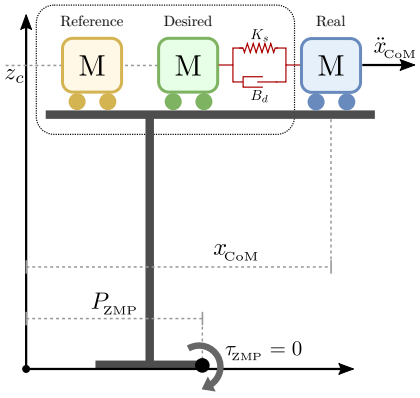

Figure 6.7: Cart table model with stabilization. First consider the classical model without the stabilizer denoted by the black dotted box. If the CoM remains fixed, the table (robot) will tip over. However, if the cart is accelerating fast enough, the table remains stable even though the projection of the CoM is outside of the support polygon. The stabilizer adds a spring damper system that regulates the system according to real, desired, and reference CoM coming from the WPG to handle simplified point mass model inconsistencies as well as imperfections resulted from human interactions.

The derivation of the stabilizer and its mathematical analysis are not relevant to this thesis and their details can be found in [111]. It is mentioned here to point out once more the significance of the separation of concerns in CABR. The context identification *and* body regulation planning should be done independent of the implementation. In this case for instance, the body regulation is independent of the techniques governing the CoM. Reusing the scaled context of previous section would have been impossible if the task and control scheme were entangled.

6.3.5 Empirical Evaluation of the Loco-Manipulation Context

The evaluation of BR for loco-manipulation context involves close interaction between the robot *follower* and the human *leader*. The test platform was COMAN+ controlled in real-time. Details of the software architecture in charge of this and the previous scenario, alongside the robot hardware interfaces are detailed in section 5.2. The iHQP based SoT was implemented in OpenSoT [66] which internally uses qpOASES [112] as the QP solver. This solver employs an online active set strategy to solve model predictive control problems [113].

Figure 6.8a depicts the hand-in-hand locomotion scenario setup. The robot's arms are in joint impedance mode and comply with user's motion. At each control cycle, the function f computes walking parameter and sends them to the stack of tasks. The scenario involves the human counterpart moving and the robot following by performing suitable forward or backward steps. The block-diagram of this scheme is shown in figure 6.9. The threshold of each arm in (6.4) is selected as $v_d = 0.5$. As mentioned previously, selecting a less conservative value makes the robot less reactive and vice versa. The evolution of manipulability of the arm throughout the experiment is depicted in figure 6.10. The user interactions change the robot's manipulability and when the manipulability of either arms (in this case the right arm is shown) hits the threshold v_d, the robot makes a step. It is clear from the figure how the steps constantly brings the manipulability above the threshold, consequently responding to human's intentions. Moreover the steps ensure the arms' Jacobian degeneracy is avoided. The performance of the iHQP based SoT can be

observed in figure 6.8c. Despite the constant disturbances by the human counterpart, the error of the CoM position shows excellent tracking performance.

6.4 Discussion of the Results

This chapter demonstrated the CABR in real world applications and tested its claims in practice.

The whole-body standing context presented a physiotherapeutic juggling application, demonstrating the notion of "contexts present multiple applications" in action. The BR of this context was based on the optimization of the posture to allow better throws while maintaining an overall human-like motion. As was stated before, human-likeness is not easily quantifiable, however, the user experience reported by the patients could shed some light on this corner.

The overall patients' feedback were highly positive, they were able to catch balls frequently and showed the desired training effects. The positive user experience regarding the interaction —at least indirectly— signals reasonable human-likeness on the robot side. This claim is supported by the fact that most of the people tend to negatively react towards unnatural and/or uncanny visual elements [95]. These results, moreover, encourage further research in humanoid based physiotherapeutic juggling. Moving towards this goal, more validation is being made [50] as the first step in order to eventually conduct a comprehensive user study of many patients.

In assisted walking and joint object carrying, other aspects of CABR were put into the test likewise. The whole-body standing context was scaled up well to the whole-body loco-manipulation context, and the stack of task was reused with minimum effort. The reusability was achieved, in part thanks the separation of concerns that makes no assumption regarding the tasks (e.g., same tasks but controlled from completely different inputs). Kinematic chain abstraction also had a major role in the smooth reusing experience. Note that the reused stacks of tasks are in fact shared among two different robots, However, the differences between the two platforms are encapsulated from the users' views.

The deployment of the second scenario also highlights some of the strengths of the CoSimA framework. COMAN+ robot uses XBot [87] to control its actuators. CoSimA's component library is mainly consists of Orocos components and the computation of arms' manipulability could be[1] non real-time. The reasons that roboticists have to find themselves in situations like this where they have to deal with a mixture of potentially incompatible solutions is not relevant to the scope of this thesis[2]. What is relevant, however, is the fact that CoSimA is able to provide mechanisms to integrate all these assets and compose a working setup in a very short amount of time. The physical interaction with the robot is predictable and mimics the behavior of a human in similar situation, although, there is still some room to improve the backward steps.

[1] Some implementations of SVD are real-time but most of them are in fact not real-time.
[2] There are indeed serious efforts to mitigate this problem, e.g., [114]

(a) Assisted walking with COMAN+

(b) Stabilized WPG

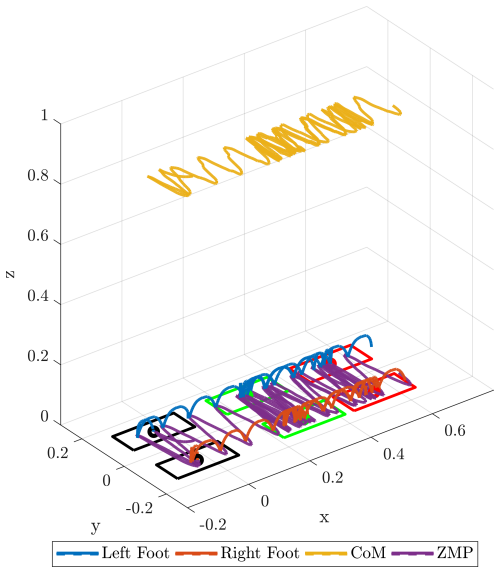

(c) Error of Position of CoM

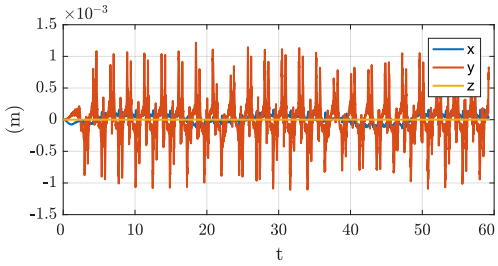

Figure 6.8: Loco-manipulation context experiment. (a) Experimental setup where the user's intention is detected based on the robot's arms manipulability; (b) The stabilized trajectories from the WPG; (c) Tracking error of CoM demonstrate the performance of iHQP based SoT. The double excursions on the y-axis is a natural occurrence in humanoids walking motion resulted from the lateral swings of the body.

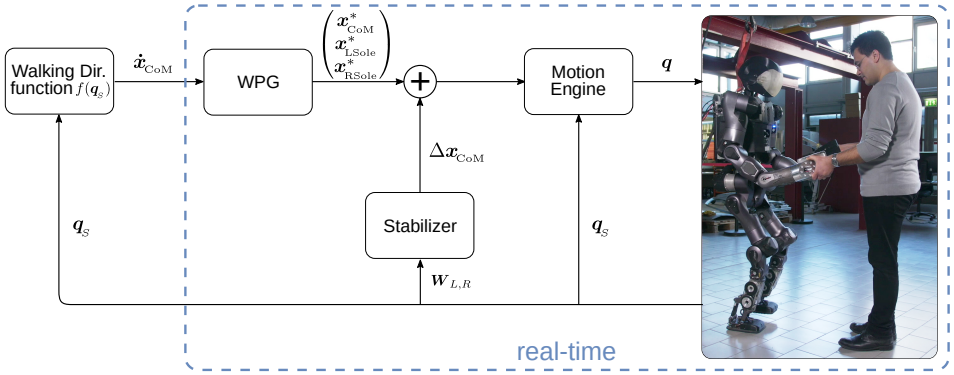

Figure 6.9: Feedback from the robot consists of joint positions and velocities, as well as wrenches computed from ankle mounted force/torque sensors. The former is used to compute the desired walking direction where the outcome is sent to the WPG while the latter is fed to the stabilizer which corrects the WPG output.

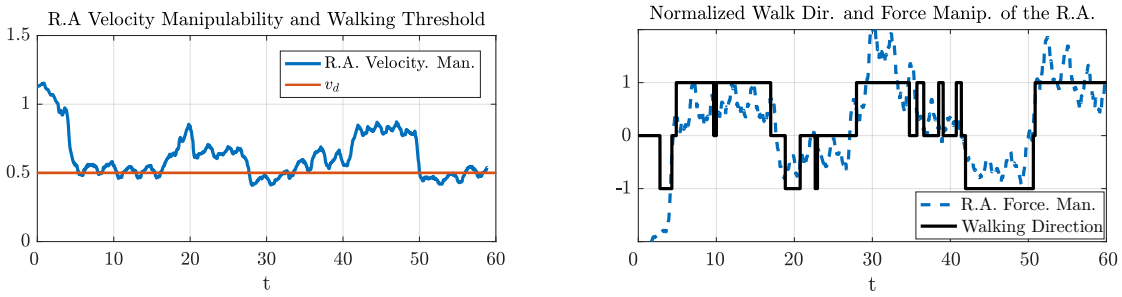

Figure 6.10: Evolution of manipulability of the right arm (R.A.) during the loco-manipulation experiment. Left: Manipulability and v_d threshold during the walk. This figure demonstrates how a sequence of steps increases the manipulability and keeps the Jacobian away from degeneracy. Right: forward, backward and in-place steps (indicated by $+1, -1$ and 0) are selected based on the force manipulability of the arm. Note that the blue dashed line has a different range and here is scaled and shifted to demonstrate its effect.

7 Conclusion

Advancements in hardware, software and control have enabled the emergence of redundant manipulators and highly dexterous humanoids capable of handling multiple task simultaneously. As most of the attention in academia and industry has been attracted by the primary tasks, resolving the secondary and lower level tasks has often been done in application specific and tailored fashions. This thesis argued that the tailored approach can no longer serve the needs of the modern era of robotics and called for an alternative strategy for handling the secondary tasks, namely, context aware body regulation.

The thesis introduced the concept of contexts in the robotics domain as a collection of abstract tasks that present reoccurring robotic situations semantically. It also studied four contexts that were selected to highlight some of its features. Furthermore, for all the introduced contexts several body regulation schemes were derived and the whole scheme was tested in several real world applications with state of the art manipulators and humanoids. The derived body regulations not only served the CABR, but they are also fully applicable stand-alone outside the scope of the thesis.

On Reusability, Scalability and Composability

CABR not only is scalable, it also features reusability and composability of body regulations and contexts. The scalability was exhibited throughout the thesis in several situations where the contexts and body regulations were based on existing ones. For instance, the postural regulation in the whole-body standing context required a relaxed constraint for one Cartesian rotation of the waist while the loco-manipulation context scaled the same policy to govern the same orientation by adding a low level task. The SoT itself was the scaled version of a simpler stack of task. Additionally, the scalability reflects an important aspect of the CABR in a bigger picture. The paradigm as a whole, thanks to its abstractions and the complementary software architecture, is very adaptable and easily adjustable for accommodating new contexts, body regulations and applications.

The reusability criterion was demonstrated empirically in several cases throughout this dissertation. The stack of tasks was shared (reused) between the whole-body standing and loco-manipulation contexts. At a finer level, the individual BR for the tasks also benefited from the reusability. In the humanoids contexts, for instance, the body regulation for the balance was identical among the two stacks of tasks. This was indeed possible due to an application-agnostic definition of the tasks. Furthermore, the kinematic chain abstraction allows the body regulation of a manipulator to be applied to a humanoid's arm. For instance, the stiffness adaptation based on the manipulability index (used in chapter 3 in a pHRI-like context) can be directly applied to the COMAN+'s arms in the loco-manipulation context involving assisted walking similar to figure 7.1. That is,

the arms get stiffer when the manipulability is reducing and the robot takes steps when necessary. This mimics similar reactions when two humans are engaging in joint object carrying and the follower cannot catch up and signals the leader with resistance to their moves.

Composability principal is also evident in the stacks of tasks as formulated in humanoids' body regulation. In chapter 4, a set of generic tasks without any specificity for a particular platform or application were defined. These tasks were then composed to form the stacks of tasks. Note that these tasks can be composed in any other meaningful fashion and still be applicable since they are not tailored. Another aspect of composability is in using two body regulations for one task. For instance, in the physiotherapeutic juggling, the rotation constraint of the waist was relaxed so that it can contribute to better throws. Additionally, the actual throws by the human were composed on the top of that as a low level joint space redundancy resolution to mimic the motions of the human arm.

There is a delicate balance between the three features of the CABR and the applicability of the whole scheme in real world applications. This balance is dictated by the abstraction level that a context exhibits alongside its granularity level. If a context is too abstract it can be easily extended to more specific contexts, however, it no longer fits in any meaningful scenario. Conversely, a context that is defined too concretely accommodates a specific application easily but it cannot be shaped to address similar situations.

The Component Based Software Architecture

Context aware body regulation alone cannot offer any of its features if not paired with a suitable software solution. To this end, an accompanying component based software architecture was also introduced. The architecture, thanks to the inherent properties of the component based systems, facilitates the reusability and accelerates the development. The transparency and reusability aspects were lifted to a higher tier by providing semantic abstractions that present the robot in terms of kinematic chains, encapsulating underlying structures. The architecture is not solely useful in the scope of this thesis. In fact, CoSimA has been used in numerous robotic applications within the CogIMon project[1] and CABR is one of its many users. Its toolset contains many robots, motion engines, and components and it is growing constantly.

Component-based software engineering had another contribution to CABR. The contexts, being composed of multiple tasks describing a functionality larger than individual constituting tasks, resembles the higher operational level of components compared to their internal classes and objects. This is no coincidence since some of the aspects of CABR were inspired by the component based software engineering, most notably the context definitions and the reusability of regulations.

Future Research and Possible Extensions

The CABR can be extended by following multiple future research paths. The contexts and the body regulations of humanoids in the force/torque control domain remained

[1] `https://cogimon.eu/biblio` contains these works and other CogIMon publications.

Figure 7.1: Potential scaled up SoT for loco-manipulation context: Leveraging on the existing assets such as reuse of the stiffness adaptation schemes, composition of body regulations and kinematic chain abstraction, it is possible to scale up the body regulation of loco-manipulation context to include impedance adaptation to further emulate a human like behavior.

untouched in this thesis. Given that the humanoids field offers a rich body of research in iHQP and SoT in the torque domain, extending the catalog of contexts and their appropriate BR to the torque and acceleration levels is the most immediate extensions of this work.

Another interesting research question revolves around the body regulation planning phase. So far, this was done based on the expert knowledge and analysis. However, the study of body regulations for the four contexts reveal some facts that can facilitate the planning phase. In three contexts the manipulability, an instantaneous measure, formed the basis of the BR. Note that in all the three cases, the nature of the context was dominated by the instantaneous motions. This hints that the nature of the context could point towards the appropriate BR. Similarly, for the environmental contact context, the prominent task within the context was about exerting forces by the EE. Consequently, the appropriate body regulation was revealed through analysis of the forces acting on the body. Whether the nature of the context can predict/hint the essence of the suitable body regulation or not, is a question that demands further investigations.

Context awareness is a concept borrowed from computer science and here it was altered to a definition that suits the purposes of this thesis. However, there are some notions in the original definition that could benefit the presented concepts. For instance, the context awareness in mobile communication automatically changes the behavior of devices when the context changes. In a similar fashion, a possible extension of the current framework is to be able to transition from a context to another smoothly and adjust the body regulation accordingly.

The software architecture's extensions are along two paths. CoSimA itself as a standalone framework will expand its component library and the list of integrated robots. It was mentioned this thesis benefits from and contributes to CoSimA. Hence, the additions to the BR library are extensions of CoSimA and vice versa. The second future branch for both CABR and CoSimA is in direction of domain specific languages and stronger focus on the model base approach. Leveraging on the features of models

in a domain specific language, certain aspects of CABR can be improved and some challenges can be mitigated. Consider the case of compatibility check when composing body regulation schemes. This is one of the shortcomings of the CABR in its current shape and form. Take the second priority level in figure 7.1-right as an example. Here two body regulation schemes are aggregated together forming a composed BR, however, how does one ensures about the compatibility of the two individual tasks?

For well established problems there are relatively clear composition rules. For instance, composing the manipulation task at a higher priority over the balance tasks in a humanoid context is problematic and the users can be notified about it (in such a hierarchy the manipulation task could compromise the balance). Furthermore, CoSimA (in general and not specific to this work) deals with other forms of compatibility checks thanks to its integrated data-structures. That is, by defining model based data-types it ensures the component composition sanity at a software level. For instance, instead of an array of size 6, CoSimA uses Wrenches which consist of Forces and Torques. A component that exposes a port which writes out Wrenches cannot be connected to a component that accepts Twists. If standard array type were used, such composition would have been possible. The third way that compositions can be checked which is part of the future works is to deploy a data-sheet alongside each BR component. Deploying data-sheets is a common practice in model based approaches [115]. Such data-sheets can be patched to contain composition rules which prohibit or provide early feedback to the system engineers should they attempt to make error prone compositions. This will be most useful when the other two approaches mentioned above are not applicable or fail to notify the users (i.e., there are no clear rules and the types do match). Nonetheless, the expert knowledge should be injected when drafting composition and reusability guidelines within these data-sheets. Consequently, identifying criteria and patterns of compatibility and synergy among body regulations is vital.

Final Notes

CABR heavily invest in abstractions, in-depth analysis of body regulations, and principles of modularity and separation of concerns. The initial investment in time and analysis will eventually pay off by reducing the development time, by creating robust systems that respond predictably and by offering a path to exploitation of the full potentials of the humanoids and redundant robots.

For the environmental contact context, the dissipation of reaction forces was analyzed in detail. In the process, it was discovered for the first time, that not every secondary contact is a good contact. In stiffness adaptation user study, the detailed analysis of users, robot, and sensor feedback revealed difficulty regions of the work-piece, a knowledge that has important implication for humans' physical health. As the proverb goes: "the devil is in the detail". CABR subscribes to a methodology that practices rigour, diligence, and attention to the detail. Although CABR offers many advantages and benefits it still has room to improve. Nonetheless, discovering these new facts and gaining new knowledge about such interesting phenomenon makes the Context Aware Body Regulation of Redundant Robots worthwhile.

Related References by the Author

This thesis is based on a number of peer reviewed papers by the author during the doctoral research. In the following, these papers alongside the contribution of each publication to this thesis are briefly described. Furthermore, the candidate has coauthored two more publications during the master's studies. Provided that these two papers establish notations that are reused in the humanoids body regulation in chapter 4, they are listed here with their contributions likewise.

Additionally, another journal paper is currently prepared and is ready to be submitted. This paper contains the results of the user study and different aspects of impedance adaptation as described in chapter 3. The prepared manuscript is expected to be published in a journal or a special issue on physical human robot interaction.

[76] P. Mohammadi, E. M. Hoffman, N. Dehio, M. S. Malekzadeh, M. Giese, N. G. Tsagarakis, and J. J. Steil, "Compliant humanoids moving toward rehabilitation applications, Transparent integration of real-time control, whole-body motion generation and virtual reality for compliant humanoids", *IEEE Robotics & Automation Magazine*, vol. 26, no. 4, pp. 83–93, Dec. 2019. DOI: 10.1109/MRA.2019.2940970

This journal paper is the cumulative result of humanoids in rehabilitation field research. The empirical evaluation of the whole-body standing and whole-body loco-manipulation contexts, physiotherapeutic juggling, and assisted walking are presented in this paper. The author had major contribution in writing, performing theoretical analysis and conducting the experiments.

[48] P. Mohammadi, E. M. Hoffman, L. Muratore, N. G. Tsagarakis, and J. J. Steil, "Reactive walking based on upper-body manipulability: An application to intention detection and reaction", *International Conference on Robotics and Automation*, pp. 4991–4997, May 2019. DOI: 10.1109/icra.2019.8794309

The contribution of this paper and the author is the mathematical derivation and implementation of the intention detection in assisted walking and joint object carrying scenarios. This work creates the foundation that the whole-body loco-manipulation's BR is based upon. The intention detection function is used with an existing walking pattern generator on the COMAN+ robot to empirically prove the validity of the analysis. Furthermore, this paper formalized the notion of kinematic chain abstraction.

[11] P. Mohammadi, D. Kubus, and J. J. Steil, "Exploiting environment contacts of serial manipulators", *IEEE International Conference on Robotics and Automation*, pp. 197–203, May 2019. DOI: 10.1109/icra.2019.8794027

In this paper the concept of contact exploitation is introduced. It is the foundation of the body regulation scheme introduced in chapter 2. By rigorous physical and mathematical analysis of the forces acting on the robot in dual contact situations, this paper proved for the first time that the intuitive assumption that every contact is a good contact, is wrong. The author contributed to both theoretical analysis and real robot experiments.

[50] J. Kodl, A. Mukovskiy, P. Mohammadi, M. Malekzadeh, N. Taubert, A. Christensen, T. Dijkstra, J. Steil, and M. Giese, "Online planning and control of ball throwing by the humanoid robot COMAN and validation exploiting VR in rehabilitation scenarios with ataxia patients", in *In Proc. of CYBATHLON Symposium on Assistive and Wearable Robotics*, May 2019

The results of VR assisted physiotherapeutic juggling with ataxia patients are validated in this paper. The author's contribution to this work is limited to providing a working prototype of the full setup that was used in the validation process.

[77] D. L. Wigand, P. Mohammadi, E. M. Hoffman, N. G. Tsagarakis, J. J. Steil, and S. Wrede, "An open-source architecture for simulation, execution and analysis of real-time robotics systems", *IEEE International Conference on Simulation, Modeling, and Programming for Autonomous Robots*, pp. 93–100, May 2018. DOI: 10.1109/simpar.2018.8376277

The simulation and timing aspects of CoSimA framework are introduced in this paper. The author implemented a walking simulation that was used for as the test bed for CoSimA. Furthermore, the author was also heavily involved in the implementation of the whole framework as one of the lead developers. This paper has a major contribution to the thesis as it is the basis of the whole software architecture. Most notably, the introspection mechanisms, the timing aspects, separation of concerns and the transparency are all addressed in this work.

[**49**] P. Mohammadi, M. Malekzadeh, J. Kodl, A. Mukovskiy, D. L. Wigand, M. Giese, and J. J. Steil, "Real-time control of whole-body robot motion and trajectory generation for physiotherapeutic juggling in vr", *IEEE/RSJ International Conference on Intelligent Robots and Systems*, pp. 270–277, Oct. 2018. DOI: 10.1109/iros.2018.8593632

In this paper the physiotherapeutic juggling in VR as an alternative form of rehabilitation is introduced. The contribution of this work to the thesis is two fold. Firstly, it studies suitable body regulations (e.g., waist constraints, cf. section 4.5.1) for throwing motion. Secondly, it outlines the basic structure of an architecture which incorporate real and non real time components. The author contributed to the implementation of the stack of tasks for throwing, different body regulations and integration of the COMAN simulation and the rest of the system architecture.

[**34**] S. Gopinathan, P. Mohammadi, and J. Steil, "Improved human-robot interaction: A manipulability based approach", IEEE Workshop on Ergonomic Physical Human-Robot Collaboration, Jun. 2018

In this workshop submission the primary concepts of stiffness adaptation schemes are outlined theoretically. The effectiveness of these approaches were then tested in the user study mentioned in section 3.3. The results of the user study will be published in a journal paper and a manuscript is already prepared.

[**27**] Z. Shareef, P. Mohammadi, and J. Steil, "Improving the inverse dynamics model of the KUKA LWR IV+ using independent joint learning", *IFAC-PapersOnLine*, vol. 49, no. 21, pp. 507–512, 2016, ISSN: 2405-8963. DOI: 10.1016/j.ifacol.2016.10.653

Exchanging contact wrenches with the environment requires accurate dynamic models which are often not provided by the robot vendors. Consequently, the roboticists often have to resort to inaccurate models which in turn compromise the quality of the final results. This paper leverages on the concept of independent joint learning [116] to improve a reverse engineered dynamic model [26] of the Kuka LWR-4+. This improved model is used in conducting the experiments related to the body regulation in secondary contact context. The author's contribution to this paper is in conducting the real robot trajectory planning and motion generation for data collection required for the independent joint learning process.

[105] M. Cognetti, P. Mohammadi, and G. Oriolo, "Whole-body motion planning for humanoids based on CoM movement primitives", *IEEE-RAS International Conference on Humanoid Robots*, pp. 1090–1095, Nov. 2015. DOI: 10.1109/humanoids.2015.7363504

This paper introduced the notion of CoM movement primitives. The paper contributed to this thesis in multiple places. Its walking pattern generation was used as the test bed for the introspection of the architecture. Furthermore, the generalized coordinate notation proposed by this paper was used for the whole-body loco-manipulation context. The author had contribution to both theoretical derivation and empirical aspects of this paper.

[70] M. Cognetti, P. Mohammadi, G. Oriolo, and M. Vendittelli, "Task-oriented whole-body planning for humanoids based on hybrid motion generation", *IEEE/RSJ International Conference on Intelligent Robots and Systems*, pp. 4071–4076, Sep. 2014. DOI: 10.1109/iros.2014.6943135

The contribution of this paper is to promote a hybrid motion generation scheme which uses random motion planning in the task space to create stepping motion for humanoids. The base of the kinematic chain in this work switches between the feet of the robot. This concept has been reused in certain experimental aspects of the thesis. The contribution of the author to this work, similar to the previous item, was both in theoretical and empirical aspects.

References

[1] B. Schilit, N. Adams, and R. Want, "Context-aware computing applications", *IEEE Workshop on Mobile Computing Systems and Applications*, pp. 85–90, Dec. 1994. DOI: 10.1109/wmcsa.1994.16.

[2] F. Miranda, T. Cabral Ferreira, J. P. Pimentão, and P. Sousa, "Review on context classification in robotics", in *Rough Sets and Intelligent Systems Paradigms*, Springer International Publishing, 2014, pp. 269–276. DOI: 10.1007/978-3-319-08729-0_26.

[3] J. Quintas, P. Menezes, and J. Dias, "Cloud robotics: Toward context aware robotic networks", Nov. 2011. DOI: 10.2316/P.2011.752-062.

[4] T. Yoshikawa, "Manipulability of robotic mechanisms", *The International Journal of Robotics Research*, vol. 4, no. 2, pp. 3–9, Jun. 1985. DOI: 10.1177/027836498500400201.

[5] ——, "Dynamic manipulability of robot manipulators", *IEEE International Conference on Robotics and Automation*, vol. 2, pp. 1033–1038, 1985. DOI: 10.1109/robot.1985.1087277.

[6] D. S. Bernstein, *Matrix Mathematics: Theory, Facts, and Formulas*, 2nd ed. Princeton University Press, Jul. 2009, ISBN: 978-0691140391.

[7] P. Chiacchio, S. Chiaverini, L. Sciavicco, and B. Siciliano, "Reformulation of dynamic manipulability ellipsoid for robotic manipulators", *IEEE International Conference on Robotics and Automation*, vol. 3, pp. 2192–2197, Apr. 1991. DOI: 10.1109/robot.1991.131955.

[8] P. Chiacchio, Y. Bouffard-Vercelli, and F. Pierrot, "Force polytope and force ellipsoid for redundant manipulators", *Journal of Robotic Systems*, vol. 14, no. 8, pp. 613–620, Aug. 1997. DOI: 10.1002/(sici)1097-4563(199708)14:8<613::aid-rob3>3.0.co;2-p.

[9] M. Sasaki, T. Iwami, K. Miyawaki, I. Sato, G. Obinata, and A. Dutt, "Higher dimensional spatial expression of upper limb manipulation ability based on human joint torque characteristics", *Robot Manipulators New Achievements*, Apr. 2010. DOI: 10.5772/9344.

[10] T. Yoshikawa, "Translational and rotational manipulability of robotic manipulators", *IEEE International Conference on Industrial Electronics, Control and Instrumentation*, vol. 2, pp. 1170–1175, 1991. DOI: 10.1109/iecon.1991.239275.

[11] P. Mohammadi, D. Kubus, and J. J. Steil, "Exploiting environment contacts of serial manipulators", *IEEE International Conference on Robotics and Automation*, pp. 197–203, May 2019. DOI: 10.1109/icra.2019.8794027.

[12] O. Khatib, "Real-time obstacle avoidance for manipulators and mobile robots", *Proceedings. 1985 IEEE International Conference on Robotics and Automation*, vol. 2, pp. 500–505, 1985. DOI: 10.1109/robot.1985.1087247.

[13] S. Kockara, T. Halic, K. Iqbal, C. Bayrak, and R. Rowe, "Collision detection: A survey", *IEEE International Conference on Systems, Man and Cybernetics*, pp. 4046–4051, Oct. 2007. DOI: 10.1109/icsmc.2007.4414258.

[14] S. M. Khansari-Zadeh and A. Billard, "A dynamical system approach to realtime obstacle avoidance", *Autonomous Robots*, vol. 32, no. 4, pp. 433–454, Mar. 2012. DOI: 10.1007/s10514-012-9287-y.

[15] M. Cefalo and G. Oriolo, "A general framework for task-constrained motion planning with moving obstacles", *Robotica*, vol. 37, no. 3, pp. 575–598, Oct. 2018. DOI: 10.1017/s0263574718001182.

[16] A. De Luca and F. Flacco, "Integrated control for phri: Collision avoidance, detection, reaction and collaboration", *IEEE-RAS International Conference on Biomedical Robotics and Biomechatronics*, pp. 288–295, Jun. 2012. DOI: 10.1109/biorob.2012.6290917.

[17] C. Eppner, R. Deimel, J. Álvarez-Ruiz, M. Maertens, and O. Brock, "Exploitation of environmental constraints in human and robotic grasping", *The International Journal of Robotics Research*, vol. 34, no. 7, pp. 1021–1038, Apr. 2015. DOI: 10.1177/0278364914559753.

[18] T. Kröger, B. Finkemeyer, and F. M. Wahl, "Manipulation primitives — a universal interface between sensor-based motion control and robot programming", *Robotic Systems for Handling and Assembly*, pp. 293–313, 2010. DOI: 10.1007/978-3-642-16785-0_17.

[19] A. Muxfeldt and J. Steil, "Fusion of human demonstrations for automatic recovery during industrial assembly", *IEEE International Conference on Automation Science and Engineering*, pp. 1493–1500, Aug. 2018. DOI: 10.1109/coase.2018.8560388.

[20] N. Hogan, "Impedance control: An approach to manipulation: Part i – theory", *Journal of Dynamic Systems, Measurement, and Control*, vol. 107, no. 1, p. 1, 1985. DOI: 10.1115/1.3140702.

[21] S. Tittel, M. Malekzadeh, and J. Steil, "Full 6-dof admittance control for the industrial robot stäubli tx60", in *IEEE International Conference on Automation Science and Engineering*, Aug. 2019, pp. 1450–1455. DOI: 10.1109/COASE.2019.8843128.

[22] R. Anderson and M. Spong, "Hybrid impedance control of robotic manipulators", *IEEE Journal on Robotics and Automation*, vol. 4, no. 5, pp. 549–556, 1988. DOI: 10.1109/56.20440.

[23] K. Harada, H. Hirukawa, F. Kanehiro, K. Fujiwara, K. Kaneko, S. Kajita, and M. Nakamura, "Dynamical balance of a humanoid robot grasping an environment", vol. 2, pp. 1167–1173, Sep. 2004. DOI: 10.1109/IROS.2004.1389554.

[24] H. Audren, A. Kheddar, and P. Gergondet, "Stability polygons reshaping and morphing for smooth multi-contact transitions and force control of humanoid robots", *IEEE-RAS International Conference on Humanoid Robots*, pp. 1037–1044, Nov. 2016. DOI: 10.1109/humanoids.2016.7803399.

[25] J. Swevers, W. Verdonck, and J. De Schutter, "Dynamic model identification for industrial robots", *IEEE Control Systems Magazine*, vol. 27, no. 5, pp. 58–71, Oct. 2007. DOI: 10.1109/MCS.2007.904659.

[26] C. Gaz, F. Flacco, and A. De Luca, "Identifying the dynamic model used by the KUKA LWR: A reverse engineering approach", *IEEE International Conference on Robotics and Automation*, pp. 1386–1392, May 2014. DOI: 10.1109/icra.2014.6907033.

[27] Z. Shareef, P. Mohammadi, and J. Steil, "Improving the inverse dynamics model of the KUKA LWR IV+ using independent joint learning", *IFAC-PapersOnLine*, vol. 49, no. 21, pp. 507–512, 2016. DOI: 10.1016/j.ifacol.2016.10.653.

[28] E. Schwartz, R. Manseur, and K. Dot, "Noncommensurate systems in robotics", *International Journal Of Robotics And Automation*, vol. 17, pp. 86–92, Jan. 2002.

[29] J. C. Trinkle, J.-S. Pang, S. Sudarsky, and G. Lo, "On dynamic multi-rigid-body contact problems with coulomb friction", *ZAMM - Journal of Applied Mathematics and Mechanics / Zeitschrift für Angewandte Mathematik und Mechanik*, vol. 77, no. 4, pp. 267–279, 1997. DOI: 10.1002/zamm.19970770411.

[30] A. Naylor and G. Sell, *Linear Operator Theory in Engineering and Science*, ser. Applied Mathematical Sciences. Springer New York, 2000, ISBN: 9780387950013.

[31] J. Angeles, "Fundamentals of robotic mechanical systems", *Mechanical Engineering Series*, 2014. DOI: 10.1007/978-3-319-01851-5.

[32] C. Meyer, *Matrix Analysis and Applied Linear Algebra*, ser. Other Titles in Applied Mathematics. Society for Industrial and Applied Mathematics (SIAM, 3600 Market Street, Floor 6, Philadelphia, PA 19104), 2000, ISBN: 9780898719512.

[33] S. L. Chiu, "Task compatibility of manipulator postures", *The International Journal of Robotics Research*, vol. 7, no. 5, pp. 13–21, Oct. 1988. DOI: 10.1177/027836498800700502.

[34] S. Gopinathan, P. Mohammadi, and J. Steil, "Improved human-robot interaction: A manipulability based approach", IEEE Workshop on Ergonomic Physical Human-Robot Collaboration, Jun. 2018.

[35] N. Hogan, "Impedance control: An approach to manipulation: Part ii – implementation", *Journal of Dynamic Systems, Measurement, and Control*, vol. 107, no. 1, p. 8, 1985. DOI: 10.1115/1.3140713.

[36] ——, "Impedance control: An approach to manipulation: Part iii – applications", *Journal of Dynamic Systems, Measurement, and Control*, vol. 107, no. 1, p. 17, 1985. DOI: 10.1115/1.3140701.

[37] V. Duchaine and C. Gosselin, "Safe, stable and intuitive control for physical human-robot interaction", *IEEE International Conference on Robotics and Automation*, pp. 3383–3388, May 2009. DOI: 10.1109/robot.2009.5152664.

[38] C. Ott, R. Mukherjee, and Y. Nakamura, "Unified impedance and admittance control", *IEEE International Conference on Robotics and Automation*, pp. 554–561, May 2010. DOI: 10.1109/robot.2010.5509861.

[39] J. De Schutter, H. Bruyninckx, W.-H. Zhu, and M. W. Spong, "Force control: A bird's eye view", *Control Problems in Robotics and Automation*, pp. 1–17, 1998. DOI: 10.1007/bfb0015073.

[40] R. Alami, A. Albu-Schaeffer, A. Bicchi, R. Bischoff, R. Chatila, A. De Luca, A. De Santis, G. Giralt, J. Guiochet, G. Hirzinger, F. Ingrand, V. Lippiello, R. Mattone, D. Powell, S. Sen, B. Siciliano, G. Tonietti, and L. Villani, "Safe and dependable physical human-robot interaction in anthropic domains: State of the art and challenges", *IEEE/RSJ International Conference on Intelligent Robots and Systems*, pp. 1–16, Oct. 2006. DOI: 10.1109/iros.2006.6936985.

[41] F. Flacco and A. De Luca, "Safe physical human-robot collaboration", *IEEE/RSJ International Conference on Intelligent Robots and Systems*, pp. 2072–2072, Nov. 2013. DOI: 10.1109/iros.2013.6696635.

[42] M. Linsinger, M. Sudhoff, K. Lemmerz, P. Glogowski, and B. Kuhlenkötter, "Task-based potential analysis for human-robot collaboration within assembly systems", *Tagungsband des 3. Kongresses Montage Handhabung Industrieroboter*, pp. 1–12, 2018. DOI: 10.1007/978-3-662-56714-2_1.

[43] C. Thomas, B. Matthias, and B. Kuhlenkötter, "Human-robot collaboration – new applications in industrial robotics", Jan. 2016.

[44] L. Peternel, N. Tsagarakis, and A. Ajoudani, "Towards multi-modal intention interfaces for human-robot co-manipulation", *IEEE/RSJ International Conference on Intelligent Robots and Systems*, pp. 2663–2669, Oct. 2016. DOI: 10.1109/iros.2016.7759414.

[45] P. Biernacki and D. Waldorf, "Snowball sampling: Problems and techniques of chain referral sampling", *Sociological Methods & Research*, vol. 10, no. 2, pp. 141–163, Nov. 1981. DOI: 10.1177/004912418101000205.

[46] V. Venkatesh and H. Bala, "Technology acceptance model 3 and a research agenda on interventions", *Decision Sciences*, vol. 39, no. 2, pp. 273–315, May 2008. DOI: 10.1111/j.1540-5915.2008.00192.x.

[47] B. H. Wixom and P. A. Todd, "A theoretical integration of user satisfaction and technology acceptance", *Information Systems Research*, vol. 16, no. 1, pp. 85–102, Mar. 2005. DOI: 10.1287/isre.1050.0042.

[48] P. Mohammadi, E. M. Hoffman, L. Muratore, N. G. Tsagarakis, and J. J. Steil, "Reactive walking based on upper-body manipulability: An application to intention detection and reaction", *International Conference on Robotics and Automation*, pp. 4991–4997, May 2019. DOI: 10.1109/icra.2019.8794309.

[49] P. Mohammadi, M. Malekzadeh, J. Kodl, A. Mukovskiy, D. L. Wigand, M. Giese, and J. J. Steil, "Real-time control of whole-body robot motion and trajectory generation for physiotherapeutic juggling in vr", *IEEE/RSJ International Conference on Intelligent Robots and Systems*, pp. 270–277, Oct. 2018. DOI: 10.1109/iros.2018.8593632.

[50] J. Kodl, A. Mukovskiy, P. Mohammadi, M. Malekzadeh, N. Taubert, A. Christensen, T. Dijkstra, J. Steil, and M. Giese, "Online planning and control of ball throwing by the humanoid robot COMAN and validation exploiting VR in rehabilitation scenarios with ataxia patients", in *In Proc. of CYBATHLON Symposium on Assistive and Wearable Robotics*, May 2019.

[51] B. Siciliano and J.-J. Slotine, "A general framework for managing multiple tasks in highly redundant robotic systems", *IEEE International Conference on Advanced Robotics 'Robots in Unstructured Environments*, vol. 2, pp. 1211–1216, 1991. DOI: 10.1109/icar.1991.240390.

[52] C. Samson, M. Borgne, and B. Espiau, *Robot control: the task function approach*, ser. Oxford engineering science series. Clarendon Press, 1991, ISBN: 9780198538059.

[53] A. Escande, N. Mansard, and P.-B. Wieber, "Hierarchical quadratic programming: Fast online humanoid-robot motion generation", *The International Journal of Robotics Research*, vol. 33, no. 7, pp. 1006–1028, May 2014. DOI: 10.1177/0278364914521306.

[54] O. Kanoun, F. Lamiraux, and P.-B. Wieber, "Kinematic control of redundant manipulators: Generalizing the task-priority framework to inequality task", *IEEE Transactions on Robotics*, vol. 27, no. 4, pp. 785–792, Aug. 2011. DOI: 10.1109/tro.2011.2142450.

[55] J. Nocedal and S. Wright, *Numerical Optimization*, ser. Springer Series in Operations Research and Financial Engineering. Springer New York, 2006, ISBN: 9780387400655.

[56] D. Orin and A. Goswami, "Centroidal momentum matrix of a humanoid robot: Structure and properties", *IEEE/RSJ International Conference on Intelligent Robots and Systems*, pp. 653–659, Sep. 2008. DOI: 10.1109/iros.2008.4650772.

[57] B. Henze, A. Dietrich, M. A. Roa, and C. Ott, "Multi-contact balancing of humanoid robots in confined spaces: Utilizing knee contacts", *IEEE/RSJ International Conference on Intelligent Robots and Systems*, pp. 697–704, Sep. 2017. DOI: 10.1109/iros.2017.8202227.

[58] M. Azad, J. Babic, and M. Mistry, "Dynamic manipulability of the center of mass: A tool to study, analyse and measure physical ability of robots", *IEEE International Conference on Robotics and Automation*, pp. 3484–3490, May 2017. DOI: 10.1109/icra.2017.7989398.

[59] S. Xin, Y. You, C. Zhou, C. Fang, and N. Tsagarakis, "A torque-controlled humanoid robot riding on a two-wheeled mobile platform", *IEEE/RSJ International Conference on Intelligent Robots and Systems*, pp. 1435–1442, Sep. 2017. DOI: 10.1109/iros.2017.8205945.

[60] L. Sentis, J. Park, and O. Khatib, "Compliant control of multicontact and center-of-mass behaviors in humanoid robots", *IEEE Transactions on Robotics*, vol. 26, no. 3, pp. 483–501, Jun. 2010. DOI: 10.1109/tro.2010.2043757.

[61] M. Murooka, S. Nozawa, Y. Kakiuchi, K. Okada, and M. Inaba, "Whole-body pushing manipulation with contact posture planning of large and heavy object for humanoid robot", *IEEE International Conference on Robotics and Automation*, pp. 5682–5689, May 2015. DOI: 10.1109/icra.2015.7139995.

[62] K. Shen, X. Li, H. Tian, D. Izawa, M. Minami, and T. Matsuno, "Application and analyses of dynamic reconfiguration manipulability shape index into humanoid biped walking", *IEEE International Conference on Robotics and Biomimetics*, Dec. 2016. DOI: 10.1109/robio.2016.7866529.

[63] N. Mansard, *Numerical Methods for Robotics*. Laboratory for Analysis and Architecture of Systems - LAAS, 2015.

[64] K. Erleben and S. Andrews, "Inverse kinematics problems with exact hessian matrices", *Proceedings of the Tenth International Conference on Motion in Games - MIG '17*, 2017. DOI: 10.1145/3136457.3136464.

[65] E. Chong and S. Zak, *An Introduction to Optimization*, ser. Wiley – Interscience Series in Discrete Mathematics and Optimi. Wiley, 2004, ISBN: 9780471654001.

[66] A. Rocchi, E. M. Hoffman, D. G. Caldwell, and N. G. Tsagarakis, "Opensot: A whole-body control library for the compliant humanoid robot coman", *IEEE International Conference on Robotics and Automation*, pp. 6248–6253, May 2015. DOI: 10.1109/icra.2015.7140076.

[67] M. Vukobratović and B. Borovac, "Zero-moment point — thirty five years of its life", *International Journal of Humanoid Robotics*, vol. 01, no. 01, pp. 157–173, Mar. 2004. DOI: 10.1142/s0219843604000083.

[68] J. Pratt, J. Carff, S. Drakunov, and A. Goswami, "Capture point: A step toward humanoid push recovery", *IEEE-RAS International Conference on Humanoid Robots*, pp. 200–207, Dec. 2006. DOI: 10.1109/ichr.2006.321385.

[69] K. Bouyarmane, K. Chappellet, J. Vaillant, and A. Kheddar, "Quadratic programming for multirobot and task-space force control", *IEEE Transactions on Robotics*, vol. 35, no. 1, pp. 64–77, Feb. 2019. DOI: 10.1109/tro.2018.2876782.

[70] M. Cognetti, P. Mohammadi, G. Oriolo, and M. Vendittelli, "Task-oriented whole-body planning for humanoids based on hybrid motion generation", *IEEE/RSJ International Conference on Intelligent Robots and Systems*, pp. 4071–4076, Sep. 2014. DOI: 10.1109/iros.2014.6943135.

[71] J. Yuan, "Closed-loop manipulator control using quaternion feedback", *IEEE Journal on Robotics and Automation*, vol. 4, no. 4, pp. 434–440, 1988. DOI: 10.1109/56.809.

[72] G. Milighetti, L. Vallone, and A. De Luca, "Adaptive predictive gaze control of a redundant humanoid robot head", *IEEE/RSJ International Conference on Intelligent Robots and Systems*, pp. 3192–3198, Sep. 2011. DOI: 10.1109/iros.2011.6094417.

[73] A. Maselli, A. Dhawan, B. Cesqui, M. Russo, F. Lacquaniti, and A. d'Avella, "Where are you throwing the ball? i better watch your body, not just your arm!", *Frontiers in Human Neuroscience*, vol. 11, Oct. 2017. DOI: 10.3389/fnhum.2017.00505.

[74] D. M. Lofaro, R. Ellenberg, P. Oh, and J. Oh, "Humanoid throwing: Design of collision-free trajectories with sparse reachable maps", *IEEE/RSJ International Conference on Intelligent Robots and Systems*, pp. 1519–1524, Oct. 2012. DOI: 10.1109/IROS.2012.6385987.

[75] E. Anson, P. Agada, T. Kiemel, Y. Ivanenko, F. Lacquaniti, and J. Jeka, "Visual control of trunk translation and orientation during locomotion", *Experimental Brain Research*, vol. 232, no. 6, pp. 1941–1951, Mar. 2014. DOI: 10.1007/s00221-014-3885-1.

[76] P. Mohammadi, E. M. Hoffman, N. Dehio, M. S. Malekzadeh, M. Giese, N. G. Tsagarakis, and J. J. Steil, "Compliant humanoids moving toward rehabilitation applications, Transparent integration of real-time control, whole-body motion generation and virtual reality for compliant humanoids", *IEEE Robotics & Automation Magazine*, vol. 26, no. 4, pp. 83–93, Dec. 2019. DOI: 10.1109/MRA.2019.2940970.

[77] D. L. Wigand, P. Mohammadi, E. M. Hoffman, N. G. Tsagarakis, J. J. Steil, and S. Wrede, "An open-source architecture for simulation, execution and analysis of real-time robotics systems", *IEEE International Conference on Simulation, Modeling, and Programming for Autonomous Robots*, pp. 93–100, May 2018. DOI: 10.1109/simpar.2018.8376277.

[78] *Cognitive interaction in motion - CogIMon*, https://cogimon.eu/, H2020-ICT-2014-1, Grant Agreement ID: 644727.

[79] D. Wigand, A. Nordmann, N. Dehio, M. Mistry, and S. Wrede, "Domain-specific language modularization scheme applied to a multi-arm robotics use-case", *Journal of Software Engineering for Robotics*, vol. 8, pp. 45–64, Dec. 2017. DOI: 10.6092/JOSER.

[80] H. Bruyninckx, "Open robot control software: The Orocos project", *IEEE International Conference on Robotics and Automation*, vol. 3, pp. 2523–2528, 2001. DOI: 10.1109/robot.2001.933002.

[81] A. Brooks, T. Kaupp, A. Makarenko, S. Williams, and A. Oreback, "Towards component-based robotics", *IEEE/RSJ International Conference on Intelligent Robots and Systems*, pp. 163–168, 2005. DOI: 10.1109/iros.2005.1545523.

[82] D. Brugali and P. Scandurra, "Component-based robotic engineering (part i) [tutorial]", *IEEE Robotics & Automation Magazine*, vol. 16, no. 4, pp. 84–96, Dec. 2009. DOI: 10.1109/mra.2009.934837.

[83] M. Collins-Cope, "Component based development and advanced oo design",

[84] C. Szyperski, *Component Software: Beyond Object-Oriented Programming*, 2nd ed. Addison-Wesley Professional, Nov. 2002, ISBN: 978-0321753021.

[85] M. Quigley, K. Conley, B. Gerkey, J. Faust, T. Foote, J. Leibs, R. Wheeler, and A. Ng, "Ros: An open-source robot operating system", vol. 3, Jan. 2009.

[86] J. Wienke and S. Wrede, "A middleware for collaborative research in experimental robotics", *IEEE/SICE International Symposium on System Integration*, pp. 1183–1190, Dec. 2011. DOI: 10.1109/sii.2011.6147617.

[87] L. Muratore, A. Laurenzi, E. M. Hoffman, A. Rocchi, D. G. Caldwell, and N. G. Tsagarakis, "Xbotcore: A real-time cross-robot software platform", *IEEE International Conference on Robotic Computing*, pp. 77–80, Apr. 2017. DOI: 10.1109/irc.2017.45.

[88] N. Dehio and J. J. Steil, "Dynamically-consistent generalized hierarchical control", *International Conference on Robotics and Automation*, pp. 1141–1147, May 2019. DOI: 10.1109/icra.2019.8793553.

[89] A. Chłoń-Domińczak, I. Kotowska, J. Kurkiewicz, M. Stonawski, and A. Abramowska - Kmon, *Population ageing in Europe. Facts, implications and policies.* Jan. 2014. DOI: 10.13140/2.1.5039.6806.

[90] S. T. Rodrigues, P. F. Polastri, G. C. Gotardi, S. A. Aguiar, M. R. Mesaros, M. B. Pestana, and F. A. Barbieri, "Postural control during cascade ball juggling", *Perceptual and Motor Skills*, vol. 123, no. 1, pp. 279–294, Aug. 2016. DOI: 10.1177/0031512516660718.

[91] C. Sampaio-Baptista, N. Filippini, C. J. Stagg, J. Near, J. Scholz, and H. Johansen-Berg, "Changes in functional connectivity and gaba levels with long-term motor learning", *NeuroImage*, vol. 106, pp. 15–20, Feb. 2015. DOI: 10.1016/j.neuroimage.2014.11.032.

[92] B. Draganski, C. Gaser, V. Busch, G. Schuierer, U. Bogdahn, and A. May, "Changes in grey matter induced by training", *Nature*, vol. 427, no. 6972, pp. 311–312, Jan. 2004. DOI: 10.1038/427311a.

[93] N. Norouzi-Gheidari, P. S. Archambault, and J. Fung, "Effects of robot-assisted therapy on stroke rehabilitation in upper limbs: Systematic review and meta-analysis of the literature", *Journal of rehabilitation research and development*, vol. 49, no. 4, p. 479, 2012.

[94] H.-I. Ma, W.-J. Hwang, C.-Y. Wang, J.-J. Fang, I.-F. Leong, and T.-Y. Wang, "Trunk–arm coordination in reaching for moving targets in people with parkinson's disease: Comparison between virtual and physical reality", *Human Movement Science*, vol. 31, no. 5, pp. 1340–1352, Oct. 2012. DOI: 10.1016/j.humov.2011.11.004.

[95] M. Mori, K. MacDorman, and N. Kageki, "The uncanny valley [from the field]", *IEEE Robotics & Automation Magazine*, vol. 19, no. 2, pp. 98–100, Jun. 2012. DOI: 10.1109/mra.2012.2192811.

[96] N. A. Malik, H. Yussof, F. A. Hanapiah, R. A. A. Rahman, and H. H. Basri, "Human-robot interaction for children with cerebral palsy: Reflection and suggestion for interactive scenario design", *Procedia Computer Science*, vol. 76, pp. 388–393, 2015. DOI: 10.1016/j.procs.2015.12.315.

[97] D. J. Agravante, A. Sherikov, P.-B. Wieber, A. Cherubini, and A. Kheddar, "Walking pattern generators designed for physical collaboration", *IEEE International Conference on Robotics and Automation*, pp. 1573–1578, May 2016. DOI: 10.1109/icra.2016.7487296.

[98] A. Bussy, P. Gergondet, A. Kheddar, F. Keith, and A. Crosnier, "Proactive behavior of a humanoid robot in a haptic transportation task with a human partner", *IEEE International Symposium on Robot and Human Interactive Communication*, pp. 962–967, Sep. 2012. DOI: 10.1109/roman.2012.6343874.

[99] O. Stasse, P. Evrard, N. Perrin, N. Mansard, and A. Kheddar, "Fast foot prints re-planning and motion generation during walking in physical human-humanoid interaction", *IEEE-RAS International Conference on Humanoid Robots*, pp. 284–289, Dec. 2009. DOI: 10.1109/ichr.2009.5379563.

[100] K. Yokoyama, H. Handa, T. Isozumi, Y. Fukase, K. Kaneko, F. Kanehiro, Y. Kawai, F. Tomita, and H. Hirukawa, "Cooperative works by a human and a humanoid robot", *IEEE International Conference on Robotics and Automation*, vol. 3, pp. 2985–2991, DOI: 10.1109/robot.2003.1242049.

[101] A. Tavakkoli, R. Kelley, C. King, M. Nicolescu, M. Nicolescu, and G. Bebis, "A vision-based architecture for intent recognition", *Lecture Notes in Computer Science*, pp. 173–182, DOI: 10.1007/978-3-540-76856-2_17.

[102] J. N. Haus, A. Muxfeldt, and D. Kubus, "Material comparison and design of low cost modular tactile surface sensors for industrial manipulators", *IEEE International Conference on Emerging Technologies and Factory Automation*, pp. 1–7, Sep. 2016. DOI: 10.1109/etfa.2016.7733553.

[103] J. Lanini, H. Razavi, J. Urain, and A. Ijspeert, "Human intention detection as a multiclass classification problem: Application in physical human–robot interaction while walking", *IEEE Robotics and Automation Letters*, vol. 3, no. 4, pp. 4171–4178, Oct. 2018. DOI: 10.1109/lra.2018.2864351.

[104] M. A. Giese, A. Mukovskiy, A.-N. Park, L. Omlor, and J.-J. E. Slotine, "Real-time synthesis of body movements based on learned primitives", *Statistical and Geometrical Approaches to Visual Motion Analysis*, pp. 107–127, 2009. DOI: 10.1007/978-3-642-03061-1_6.

[105] M. Cognetti, P. Mohammadi, and G. Oriolo, "Whole-body motion planning for humanoids based on CoM movement primitives", *IEEE-RAS International Conference on Humanoid Robots*, pp. 1090–1095, Nov. 2015. DOI: 10.1109/humanoids.2015.7363504.

[106] S. Kajita, F. Kanehiro, K. Kaneko, K. Fujiwara, K. Harada, K. Yokoi, and H. Hirukawa, "Biped walking pattern generation by using preview control of zero-moment point", *IEEE International Conference on Robotics and Automation*, vol. 2, pp. 1620–1626, DOI: 10.1109/robot.2003.1241826.

[107] A. Herdt, H. Diedam, P.-B. Wieber, D. Dimitrov, K. Mombaur, and M. Diehl, "Online walking motion generation with automatic footstep placement", *Advanced Robotics*, vol. 24, no. 5-6, pp. 719–737, Jan. 2010. DOI: 10.1163/016918610x493552.

[108] A. Edelman, T. A. Arias, and S. T. Smith, "The geometry of algorithms with orthogonality constraints", *SIAM Journal on Matrix Analysis and Applications*, vol. 20, no. 2, pp. 303–353, Jan. 1998. DOI: 10.1137/s0895479895290954.

[109] S. Kajita, O. Matsumoto, and M. Saigo, "Real-time 3d walking pattern generation for a biped robot with telescopic legs", *IEEE International Conference on Robotics and Automation*, vol. 3, pp. 2299–2306, 2001. DOI: 10.1109/robot.2001.932965.

[110] S. Kajita, H. Hirukawa, K. Harada, and K. Yokoi, "Introduction to humanoid robotics", *Springer Tracts in Advanced Robotics*, 2014. DOI: 10.1007/978-3-642-54536-8.

[111] C. Zhou, Z. Li, X. Wang, N. Tsagarakis, and D. Caldwell, "Stabilization of bipedal walking based on compliance control", *Autonomous Robots*, vol. 40, no. 6, pp. 1041–1057, Nov. 2015. DOI: 10.1007/s10514-015-9507-3.

[112] H. J. Ferreau, C. Kirches, A. Potschka, H. G. Bock, and M. Diehl, "qpOASES: A parametric active-set algorithm for quadratic programming", *Mathematical Programming Computation*, vol. 6, no. 4, pp. 327–363, Apr. 2014. DOI: 10.1007/s12532-014-0071-1.

[113] H. J. Ferreau, H. G. Bock, and M. Diehl, "An online active set strategy to overcome the limitations of explicit MPC", *International Journal of Robust and Nonlinear Control*, vol. 18, no. 8, pp. 816–830, 2008. DOI: 10.1002/rnc.1251.

[114] *Composable models and software for robotics systems - RobMoSys*, https://robmosys.eu/, H2020-ICT-2016-1, Grant Agreement ID: 732410.

[115] H. Bruyninckx, "Composable, adaptive, and explainable systems-of-systems: Knowledge-based modelling and best practicesto build resilient holonicdata, information, task and software architecturesfor robotics and other cyber-physical systems", Apr. 2020.

[116] K. Caluwaerts and J. J. Steil, "Independent joint learning in practice: Local error estimates to improve inverse dynamics control", pp. 643–650, Nov. 2015. DOI: 10.1109/humanoids.2015.7363439.

Image Copyrights and Courtesies

Some of the images, figures, and illustrations are kind courtesies or copyright of the followings.

Figures	**Copyright/Courtesy**
1.1a	Stanford university
1.1b	Kuka GmbH
3.2	Dr. Sugeeth Gopinathan
6.2	Albert Mukovskiy
Image of the patient in figure 6.4	Thomas Müller, FRG
Figure 6.7 is *inspired by*	Zhou et al. [111]
5.3	Dennis Leroy Wigand
6.1	Mayugo - Own work, CC BY-SA 4.0, `https://commons.wikimedia.org/w/index.php?curid=85444565`
COMAN+ CAD model	Italian Institute of Technology